6-2014

A Comparative Study of the Low Speed Performance of Two Fixed Planforms versus a Variable Geometry Planform for a Supersonic Business Jet

Aaron C. Smelsky
Embry-Riddle Aeronautical University - Daytona Beach

A COMPARATIVE STUDY OF THE LOW SPEED PERFORMANCE OF TWO FIXED PLANFORMS VERSUS A VARIABLE GEOMETRY PLANFORM FOR A SUPERSONIC BUSINESS JET

by

Aaron C. Smelsky

A Thesis Submitted to the College of Engineering, Department of Aerospace Engineering in Partial Fulfillment of the Requirements for the Degree of Master of Science in Aerospace Engineering at Embry-Riddle Aeronautical University 2014

Embry-Riddle Aeronautical University
Daytona Beach, Florida
June 2014

A COMPARATIVE STUDY OF THE LOW SPEED PERFORMANCE OF TWO FIXED PLANFORMS VERSUS A VARIABLE GEOMETRY PLANFORM FOR A SUPERSONIC BUSINESS JET

by

Aaron C. Smelsky

This thesis was prepared under the direction of the candidate's Thesis Committee Chair, Dr. Luis Gonzalez-Linero, Professor, Daytona Beach Campus, and Thesis Committee Members Dr. Reda Mankbadi, Distinguished Professor, Daytona Beach Campus, and Dr. Laksh Narayanaswami, Professor, Daytona Beach Campus, and has been approved by the Thesis Committee. It was submitted to the Department of Aerospace Engineering in partial fulfillment of the requirements for the degree of Master of Science in Aerospace Engineering.

Thesis Review Committee:

Luis Gonzalez-Linero, Ph.D.
Committee Chair

Reda Mankbadi, Ph.D.
Committee Member

Laksh Narayanaswami, Ph.D.
Committee Member

Yi Zhao, Ph.D.
Graduate Program Chair,
Department of Aerospace Engineering

Robert Oxley, Ph.D.
Associate Vice President of Academics

7-30-14
Date

Acknowledgements

Without the tremendous amount of time and effort put forth by Dr. Gonzalez with this project it would not have been possible. A great deal of gratitude is owed to him for the help editing this document. I am thankful for the quick office visits to the hours spent in his office. I not only appreciate his advice and energy during the analysis phase but also his time in the editing stage.

In addition, many thanks go to Dr. Narayanaswami with all of the time he took out of his busy days to assist with the manuscript. Without his knowledge and effort this thesis would have lacked the background and focus it required. His knowledge and guidance was a staple in this research effort.

Dr. Mankbadi was instrumental with his guidance, offering great direction and leadership in our meetings. Without his input this project would not have progressed to what it is now.

In addition, many thanks are owed to Dr. Mirmirani and Dr. Lyrintzis for assisting in the forward progress of this paper.

Lastly, but certainly not least, this paper would not have been possible without the love and support of my wife Amanda. Without her compassionate care and encouragement the long hours would have been tremendously more difficult.

Table of Contents

List of Tables

Page

Table

List of Figures

Page

Figure

Definition of Terms

Augmented Planform	Any of the fixed planforms (fixed sweep or delta) where high lift devices are added to the trailing edge and or leading edge of the wing.
Clean Planform	Any of the three planforms (variable geometry, fixed sweep or delta) where no high lift devices are added
Fixed Planforms	The planforms which cannot vary the sweep angle. In this case, they are the fixed swept and delta planforms.
Lift to Flap Weight Ratio	A created ratio which compares the increment in maximum lift coefficient to the weight of the flap mechanisms.
Unswept Wing	The case where the variable geometry planforms wings are in the forward most swept position.

List of Acronyms and Variables

BFL	Balanced Field Length
CFD	Computational Fluid Dynamics
FAA	Federal Aviation Administration
HISAC	High-Speed Aircraft
LEVF	Leading Edge Vortex Flap
LEX	Leading Edge Extension
MLW	Maximum Landing Weight
MTOW	Maximum Takeoff Weight
OEW	Operational Empty Weight
NACA	National Advisory Committee for Aeronautics
NASA	National Aeronautics and Space Administration
PAX	Number of Passenger
SAR	Specific Air Range
SCAT	Supersonic Commercial Air Transport
SSBJ	Supersonic Business Jet
SST	Supersonic Transport
vs.	Versus
et al.	And Others
lb	Pound
ft	Foot
nm	Nautical Mile per Hour
AR	Aspect Ratio

b	Wing Span (ft)
b_f	Flap Span (ft)
$\frac{b_f}{b}$	Flap Span to Wing Span Ratio
c	Wing Chord (ft)
c'	Extended Flapped Wing Chord (ft)
$\frac{c'}{c}$	Extended Flapped Chord to Original Airfoil Chord Ratio
c_f	Flap Chord
$\frac{c_f}{c}$	Flap Chord to Wing Chord Ratio
C_D	Coefficient of Drag
$\left(C_{D_0}\right)_{SS\ wing}$	Supersonic Zero-Life Drag Coefficient
C_{D_f}	Supersonic Skin Friction Coefficient
$C_{D_{LE}}$	Supersonic Round Leading Edge Bluntness Coefficient
C_{D_W}	Supersonic Wave Drag Coefficient
C_f	Turbulent Flat Plate Skin Friction Coefficient
C_{f_i}	Skin Friction Coefficient over a Flat Plate
$\frac{C_{f_c}}{C_{f_i}}$	Compressibility Effects on Turbulent Skin Friction
C_{L_α}	Lift Curve Slope, $\frac{d_{C_L}}{d_\alpha}$ (per degree)
$C_{L_{\alpha_{wing}}}$	Wing Lift Curve Slope, (per degree)
C_{l_δ}	Leading Edge Flap Effectiveness Parameter
$\left(C_{l_\delta}\right)_{theory}$	Plain Flap Size and Thickness Ratio Factor

$\frac{C_{l_\delta}}{\left(C_{l_\delta}\right)_{theory}}$	Plain Flap Correction Factor
C_{L_α}	Lift Curve Slope, $\frac{dC_L}{d_\alpha}$ (per degree)
$C_{l_{MAX}}$	Maximum Coefficient of Lift (2D) (per degree)
$C_{L_{MAX}}$	Maximum Coefficient of Lift (3D) (per degree)
k'	Plain Flap Nonlinearities Correction Factor
k_1	Flap Factor to Account for Flap-Chord to Airfoil Chord Ratios Different from 25%
k_2	Flap Factor to Account for Angles Different from Reference Flap Angle
k_3	Flap Factor to Account for Flap Motions as a Function of Flap Deflection Angle
k_b	Flap-Span Factor
k_f	Final Flap Design Factor
k_{f_1}	Flap Configuration Factor 1
k_{f_2}	Flap Configuration Factor 2
K_{PIV}	Wing Variable-Sweep Factor
L	Airfoil Thickness Location Parameter
$\frac{L}{D}$	Lift to Drag Ratio
N	Ultimate Load Factor
S	Wing Area (ft^2)
S_e	Exposed Wing Area (ft^2)
S_{wet}	Wetted Wing Area (ft^2)

$\frac{S_{w_f}}{S}$	Flapped Wing Area
$\frac{t}{c}$	Thickness to Chord Ratio
$\left(\frac{t}{c}\right)_f$	Thickness to Chord Ratio of Flap
V_{lf}	Design Speed of Flaps in Landing Configuration
W_{tef}	Trailing Edge Flap Weight per Unit Area (lb/ft^2)
W_{wing}	Weight of the Wings with High Lift Devices (lb)
W_x	Statistical Empty Weight of the Aircraft without the Wings (lb)
α	Angle of attack (°)
α_δ	Airfoil Lift Effectiveness Parameter
$\frac{(\alpha_\delta)_{C_L}}{(\alpha_\delta)_{C_l}}$	Ratio of Three-Dimensional Flap Effectiveness Parameter to the Two-Dimensional Flap-Effectiveness Parameter
ΔC_l	Increment of Coefficient of Lift (2D) (per degree)
ΔC_L	Increment of Coefficient of Lift (3D) (per degree)
$\Delta C_{l_{MAX}}$	Maximum Increment of Coefficient of Lift (2D) (per degree)
$\left(\Delta C_{l_{MAX}}\right)_{base}$	Basic Airfoil Maximum Lift Coefficient Increment due to Flaps
$\Delta C_{L_{MAX}}$	Maximum Increment of Coefficient of Lift (3D) (per degree)
δ	High Lift Device Deflection Angle (°)
δ_f	Fowler Flap Deflection Angle (when used with other devices) (°)
δ_s	Slat Deflection Angle (when used with other devices) (°)
$\Lambda_{c/2}$	Mid Chord Sweep Angle (°)
$\Lambda_{c/4}$	Quarter Chord Sweep Angle (°)

Λ_{LE}	Leading Edge Sweep Angle (°)
Λ_f	Average Sweep Angle of Flap Structure (°)
λ	Taper Ratio

Abstract

Researcher: Aaron C. Smelsky

Title: A Comparative Study of the Low Speed Performance of Two Fixed Planforms versus a Variable Geometry Planform for a Supersonic Business Jet

Institution: Embry-Riddle Aeronautical University

Degree: Master of Science in Aerospace Engineering

Year: 2014

A numerical investigation of the effects of high lift devices on the low-speed performance of a generic swept wing and a delta wing was conducted. The two fixed planforms were initially sized to achieve the same high speed performance as the baseline variable geometry wing. Following a review of high lift devices a detailed analysis of their use was conducted with the aid of vortex lattice method and empirical formulations. The slat and Fowler flap combination proved to be the best mechanical solution. In comparison with the initially sized delta planform, the final delta planform required a 26% increase in wing area with high lift devices to achieve the required low speed performance. This increase in area resulted in a 14% reduction of the maximum lift-to-drag ratio at cruise. The fixed swept wing had an increase in area of 8% over the initially sized fixed swept planform. This resulted in a decrease of the maximum lift-to-drag ratio by 1.1% at cruise. The calculated specific air range ratio for the delta planform versus the variable geometry planform was 0.95. The calculated specific air range ratio for the fixed swept planform versus the variable geometry planform was 0.94. The resulting weight penalty for the variable geometry planform did not appear to be as detrimental as initially thought when comparing against larger fixed wing planforms with high lift devices. Leading edge extensions and vortex lift could provide an even further increase in $C_{L_{MAX}}$.

Chapter I

Introduction

1.1 Scope

Two fixed wing models, a fixed swept and a delta planform, were initially sized to have similar cruise performance to the baseline, variable geometry wing. Their clean high speed cruise and clean low speed approach performance were analyzed with VLAERO+©, a Vortex-Lattice Method (VLM) program. These fixed planforms were augmented by high lift devices, where the deltas in lift were empirically calculated. The deltas in lift were added to the clean, fixed planforms and compared to the unswept variable geometry model at the approach conditions. Vortex lift and any type of blown flaps will not be included in the study. The planforms were suggested as good candidates for a Supersonic Business Jet (SSBJ) while remaining generic for the high lift device application.

1.2 Statement of the Problem

The SSBJ must be efficient during supersonic cruise and as a result its low speed performance is compromised, especially when compared to subsonic business jets. Sweep angle and lift are inversely proportional; as sweep angle increases C_{L_α} and $C_{L_{MAX}}$ decrease. This results in a faster approach speed and consequently longer runways limiting the usefulness unless a solution is found. To have an acceptable and safe landing distance an increase in $C_{L_{MAX}}$ is needed. This has been achieved by variable geometry wings (Kubota, 2008). However, there are a number of concerns with variable geometry wings including their complexity, additional weight, and difficulties in certification (Warwick, 2012; HISAC 2008). Consequently, an alternative is sought with similar cruise and low-speed

performance without the complicated and heavy mechanisms needed for a variable sweep wing.

1.3 Purpose Statement

The purpose of this study is twofold: (1) propose an alternate solution to variable geometry by attempting to design a swept and delta planform with various high lift devices that are capable of achieving similar approach and cruise performance to that of a variable geometry wing planform; and (2) create a preliminary list of the effectiveness of various leading edge and trailing edge high lift devices on a swept and delta planform wing which are recommended for further detailed studies.

1.4 Significance of the Study

Low speed performance is important for all aircraft. However, for an SSBJ the slow speed performance is essential if a successful jet is to be produced. Although the SSBJ could save significant amounts of travel time between major intercontinental cities, if the aircraft were to be restricted to a limited number of large airports and runways then it could drastically hinder the commercial success of the concept. Landing distance is directly related to the approach speed which is inversely proportional to $C_{L_{MAX}}$, which is reduced by wing sweep. This can be achieved through wings with variable sweep. The first variable geometry concept started in the early 1930s with Westland-Hill Pterodactyl MK. IV – only used for longitudinal trim (Revel, 2001). It was not until the Bell X-5 that variable sweep was studied which helped develop the first production variable geometry aircraft, the F-111, in the 1960s (Pappalardo, 2006).

The advantages of variable sweep wings are offset by their large inherent weight penalty in addition to volume needed for the supplemental structure and mechanical devices. Furthermore, the complexity in terms of electrical and mechanical systems, not to mention the redundancies needed for operational safety, increase the difficulties with the design. Civil certification is another critical concern with variable geometry wings; to this day, a commercial aircraft with variable geometry wings has never been certified (HISAC, 2008). Safety concerns are closely associated with potential certification issues, especially when dealing with uneven wing sweep situations or in the event that one wing is stuck forward or aft. Not only will the stability requirements demand a large and powerful empennage to overcome such situations but the structural considerations in such a case could be complex with large and uneven aerodynamic loads. This case could worsen if the uneven wing sweep or a stuck wing malfunction occurred at higher speeds. Operating costs, specifically the cost of maintenance, was part of reason the F-14 Tomcat was retired and replaced by the fixed-winged F-18 Hornet, besides the large technical and operational improvements on the F-18 (Stickley, 2006). If a fixed-wing could create similar low speed performance to that of the variable geometry wing while maintaining similar cruise performance, it would produce the ideal candidate for an SSBJ. The development, production, and operating costs could be significantly lower and therefore drastically increase the feasibility of the concept.

1.5 Background

The combination of comfort, speed, reliability, safety, and cost has been the basis of business jets since they were introduced in the late 1950s. Business jets have come a

long way from the Morane-Saulnier MS 760 Paris and Lockheed JetStar to the Gulfstream G650 and the Bombardier Global 8000 (Padfield, 2008). Today, business jets have some of the longest ranges, fastest cruise speeds, and quietest engines to ever go into service (HISAC, 2008; Kubota, 2008). All of the current jet designs are limited by the compressibility drag rise and an unstable, high-frequency flow separation or shock wave oscillation known as the buffeting phenomenon (Bertin & Cummings, 2014). Although the current business jet designs are efficient at transonic speeds, business jets have yet to exceed a cruise speed of M0.935 (Cessna Aircraft Company, 2013). In addition, the current FAA regulations prohibit civil supersonic flight over land (14 CFR Part 91.821). There will always be a need to reduce travel time and Supersonic Transport (SST) will be a vital component in the future of air travel, not only for business but eventually commercial and cargo (Kubota, 2008).

There are three main areas of concern with regards to an SSBJ: market viability, environmental concerns, and aircraft technologies (Kubota, 2008). The questions concerning market viability are related to more of the unknown factors such as the developmental costs, true production costs, and maintenance costs. However, it is known that an SSBJ would be far more expensive to own and operate than a subsonic business jet. The concerns regarding environmental acceptability range from the exhaust emissions in the higher altitudes to the sonic boom production. Minimizing the sonic boom overpressure and aircraft technologies are closely related. Designing an aircraft to fly efficiently at supersonic speeds while emitting a very small sonic boom is an extraordinary engineering challenge. This requires small and smooth area transitions while tailoring the airframe to

create sinusoidal pressure signatures on the ground rather than the sharp N-wave which is associated with the large sonic boom (Warwick, 2012).

1.6 Limitations and Assumptions

While providing quick results, the Vortex Lattice Method (VLM) has some limitations as it cannot predict or simulate flow separation of any kind. Therefore the results cannot capture separation, stall, or any addition of vortex lift. In most modern supersonic aircraft, vortex lift can account for a large portion of low speed lift produced (Bertin & Cummings, 2014). Since the VLM cannot predict separation, vortex lift is not taken into account.

The empirical calculations were primarily sourced from Roskam's Airplane Design (1990) and Nicolai and Carichner's Fundamentals of Aircraft Design (2010) books. Their methods are primarily based on the methods presented in Finck, and Hoak USAF Stability and Control Datcom (1975). The following list summarizes the assumption behind the empirical calculations.

- Linear-lift range
  - No separated flow on wings and flaps
- $M<0.8$, $t/c<0.1$
- Mechanical flaps
- Plain trailing edge flaps had sealed gaps
- No beveled trailing edges
- No compressibility effects

- Single-slotted and Fowler flaps
  - Near fully extended position
  - Slot properly developed
- Slats
  - First order approximation

Chapter II

Review of the Relevant Literature

2.1 Brief History and Developments of the SSBJ

In the 1870s Ernst Mach was the first to explain the phenomenon of sonic booms (Benson, 2013). The first major milestone in aviation was in 1947 when Capt. Chuck Yeager in the Bell XS-1 (later X-1) flew M1.07 in level flight (Benson, 2013). Later, in the 1950s the Air Force started work on a new generation of interceptors and fighters known as the Century Series, F-100 through F-106. It was not until the Convair B-58 Hustler that sustained supersonic flight was capable (1,000+ miles) (Benson, 2013). With the sustained flights above Mach 1 the delta winged B-58 helped demonstrate the feasibility of Supersonic Transport (SST). These sustained flights also made the B-58 a symbol for sonic boom complaints; leaving a sonic boom wake approximately 20 to 40 miles wide, frightening residents, breaking windows, and making their dogs bark (Benson, 2013).

2.1.1 SSBJ Studies

The idea of an SSBJ first started with the Supersonic Commercial Air Transport (SCAT) programs started by NACA then inherited by NASA in 1958 (Chambers, 2005). The first test bed for the SCAT program was the XB-70A in 1959 and it was not until the early 1960s that three main concepts (of about 40) were used for industry studies and proposals (Benson, 2013). The Russian Tu-144 SST had a short lifespan as a passenger transport followed by the Concorde which was a technical success but not economically viable (Chambers, 2005).

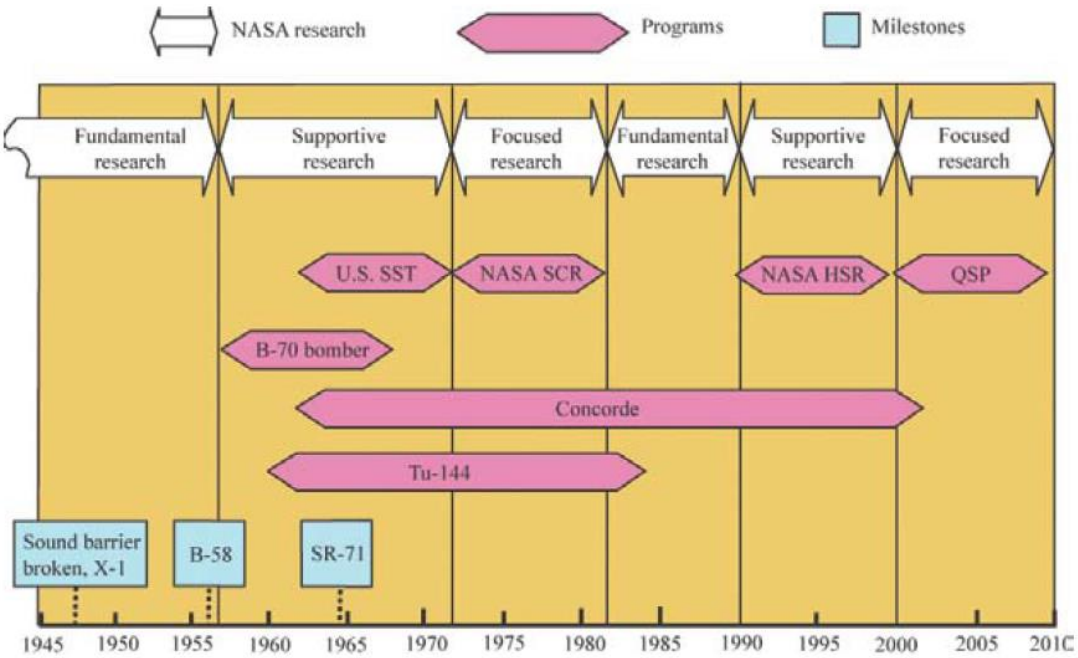

Figure 2.1 Chronology of supersonic research at NASA Langley Research Center (Chambers, 2005). This illustrates the various SST programs leading up to recent times.

Figure 2.1 shows the timeline of various NASA SST research projects culminating with the Quiet Supersonic Platform (QSP) (Chambers, 2005). Research showed the sonic boom depended on a number of factors including; aircraft maneuvering speed, flight path, atmospheric conditions, aircraft configuration, and the lift produced as well as the total volume of the aircraft (Chambers, 2005). The latter two factors, lift produced and the aircraft's volume, could be diminished if the design went from a 100-300 passenger SST configuration to an 8-12 passenger SSBJ configuration. Due to the many difficulties in developing a big, supersonic commercial aircraft in one step, an SSBJ seems a simpler and definite path to solve some of the issues with SST. The SSBJ alternative was suggested "to validate the critical supersonic technologies in a small research vehicle…" (Chambers,

2005). From 1963 to 1995 at least 22 studies and projects were done on various SSBJ concepts but the sonic boom overpressure was still too large. In 2001, the start of the QSP was directed towards technical development and validation of critical technologies including substantially reducing the sonic boom (Chambers, 2005).

High-Speed Aircraft (HISAC) is a European research project funded by the European Union between 37 organizations including Dassault, Sukhoi and Rolls-Royce (HISAC, 2008). The project studied the feasibility of a small SST. Some of the design requirements were: a) a cruise speed between M0.95 and M1.8 with some aircraft having the capability for short sprints at M1.2, b) minimum range between 3000 Nm and 5000 Nm with 8 PAX, c) maximum landing weight between 70% and 95% MTOW, d) an approach speed between 120 kt and 140 kt, and d) a Balanced Field Length (BLF) between 5,500 ft and 6,500 ft. The project studied various planforms of which the variable geometry will be

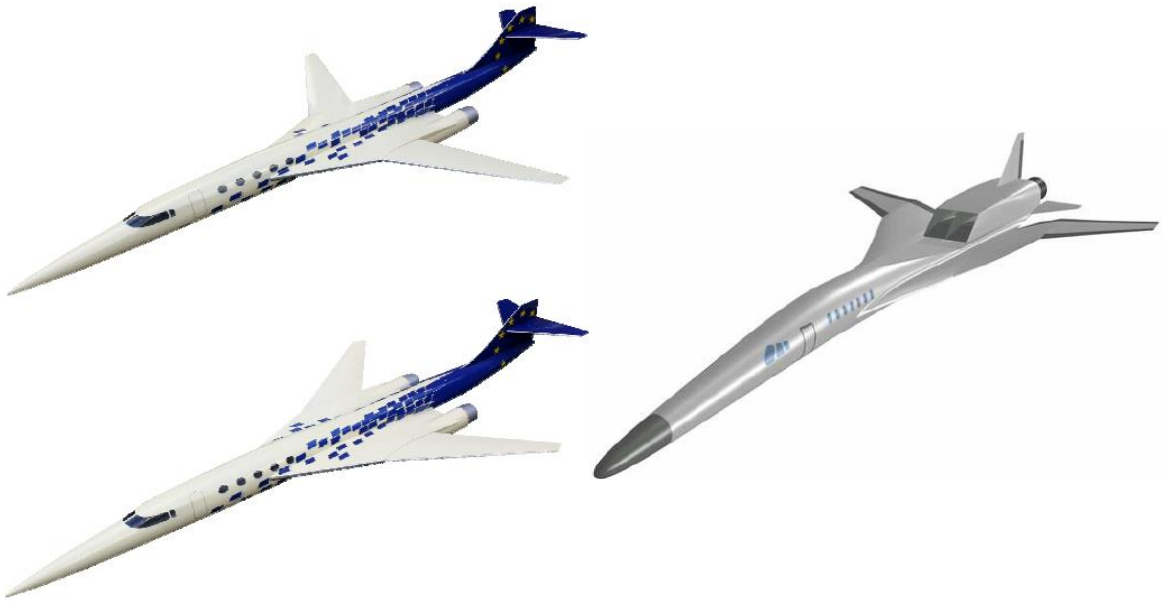

Figure 2.2 HISAC External Shapes of the Variable Geometry and Low Sonic Boom Configurations (HISAC, 2008). For the low sonic boom configuration, notice how there appears to be relatively bare below the wings.

discussed in the next section. Figure 2.2 and Figure 2.3 show some of the later stages of design results.

Figure 2.2 shows the variable geometry configuration on the left and the low sonic boom configuration on the right. The variable geometry configuration appears on par with past variable sweep SST configurations. The low sonic boom configuration is a little different having the engines on top which relieves some of the sonic boom transmitted below in addition to the cranked wing planform (HISAC, 2008). Figure 2.3 shows the low noise aircraft and the long range configuration which is primarily based on laminar flow.

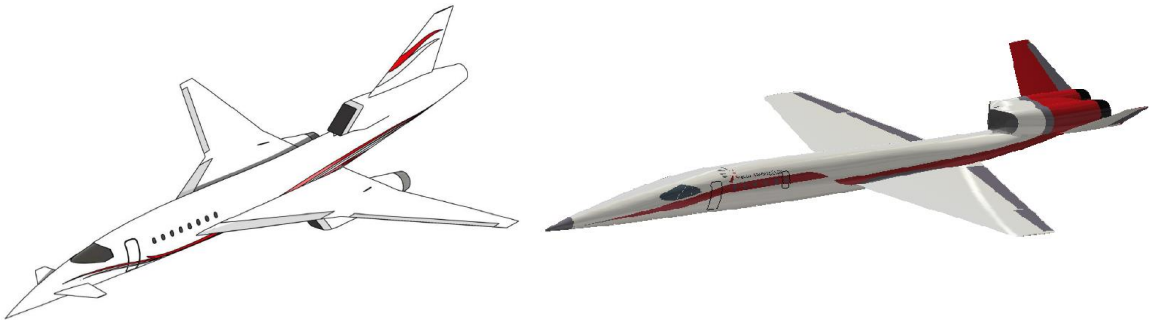

Figure 2.3 HISAC External Shapes of the Low Noise and Long Range Configurations (HISAC, 2008). The long rang configuration would use a supersonic leading edge with a very thin wing.

The study did some assessments of CFD prediction on capability for high-lift systems. While installed vortex generators reduced the areas of separation on the flap surface, they had adverse effects on the overall flow of the wing leading to earlier vortex bursting and a reduction in lift (HISAC, 2008).

After various low boom and shaped sonic boom projects including Gulfstream's Quiet Spike there is still the technical issue of having an efficient cruise with low sonic boom and sufficient low speed performance (Benson, 2013).

2.1.2 Variable Geometry

The HISAC research project demonstrated that variable geometry model showed good aerodynamic characteristics, with no need for leading edge vortices to obtain a high maximum lift requiring 30%-40% less thrust, resulting in much lower airport noise. The exact figures were not disclosed in the HISAC Public Report (2008). In addition, the variable geometry wing could be significantly smaller than a fixed wing counterpart. This could have a large impact on aircraft size, lift, fuel consumption and noise. However the study also indicated to the risks of increased weight, and drag of the hinge system, integration of the structures, systems in the hinge area and relatively sophisticated high lift system in a thin wing. Another question was feasibility of storing fuel in a moving wing box and options to control the aircraft due to shifts in aerodynamic center. In addition, there were difficulties with fatigue in the wing around the hinges. The first analysis showed difficulties to substantiate a single load path hinge, leading to a multiple load path design for the single pivot point (HISAC, 2008).

With the wings unswept, they can produce adequate lift at low speed conditions and with the wings swept aft, allowing for relative efficient cruise; aerodynamically, variable geometry is a great solution. As HISAC previously showed, mechanical complications, are the weak point. Boeing's first proposal to use the variable sweep wing had an estimated pivot weight of 40,000 lb for a 250 passenger aircraft and their weight concerns became real; having to make multiple design changes to still fall short of the original design goals. Figure 2.4 shows Boeing's multiple designs, ending with the 2707-300 after Boeing gave up on the variable sweep concept in 1966 (Chambers, 2005). Later

in 1964 the fixed wing SCAT-15F was conceived from the variable sweep concept SCAT-15 (Chambers, 2005).

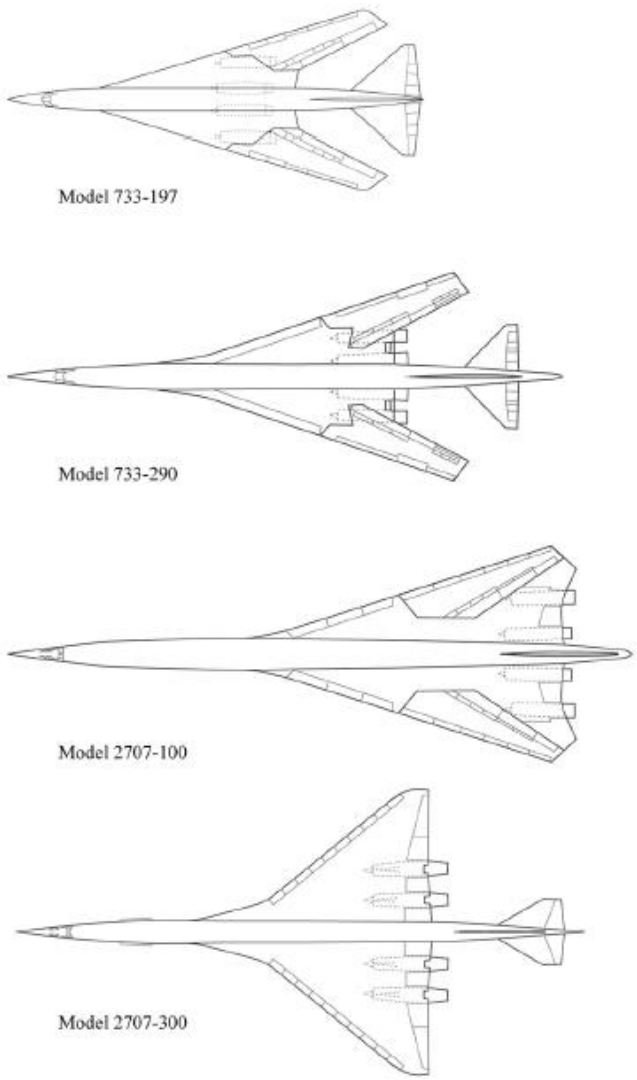

Figure 2.4 Evolution of the Final Boeing Supersonic Transport Configuration (Chambers, 2005). The various concepts of Boeing over the years show attempts to use the variable sweep wings but ultimately it would prove too difficult.

To this day, there has not been a civil certification of variable geometry wings. This could lead to additional work and higher technical risks, if civil certification were to take place (HISAC, 2008). One way around this challenge is to have a fixed wing. A large concern with a fixed wing is the planform, as it is optimized for efficient cruise, typically with a large sweep angle and or a very thin wing. The large sweep and thin wing is inherently inefficient at low speeds. Ideally a straight elliptical wing is preferred but of course would not be practical at supersonic speeds. In order to create this additional lift from the wing, a series of lift augmentation devices is required.

2.1.3 Lift Augmentation

The $C_{L_{MAX}}$ is typically driven by landing requirements to which the aircraft is typically designed to. The landing requirements are a design point chosen but the results are driven by the laws of physics, the airfoil and planform characteristics. High lift devices allow a change in geometric and aerodynamic characteristics of the wing section (Abbott & Von Doenhoff, 1959). High lift devices work by increasing the suction on the upper surface relative to the lower surface and by delaying or preventing separation, which increases the overall wing circulation (Nicolai & Carichner, 2010). The suction may be increased by the physical wing angle of attack or by making the wing appear as if it has (any one or combination of) more positive camber, chord, and area.

These high lift devices fall into two categories, unpowered mechanical (passive) devices or powered-lift (active) devices (Nicolai & Carichner; 2010, Gudmundsson, 2013). The mechanical devices are of two types: (1) Trailing Edge (TE) flaps which increase the camber of the airfoil and (2) Leading Edge (LE) devices which aid in flow separation delay

(Abbott & Von Doenhoff, 1959; Nicolai & Carichner, 2010). The high lift devices that will be discussed in this paper are displayed in Figure 2.5 for the trailing edge devices and Figure 2.6 for the leading edge devices. Note the inherent design differences from the simplicity of the plain flap to how complicated the mechanisms must be for the Fowler.

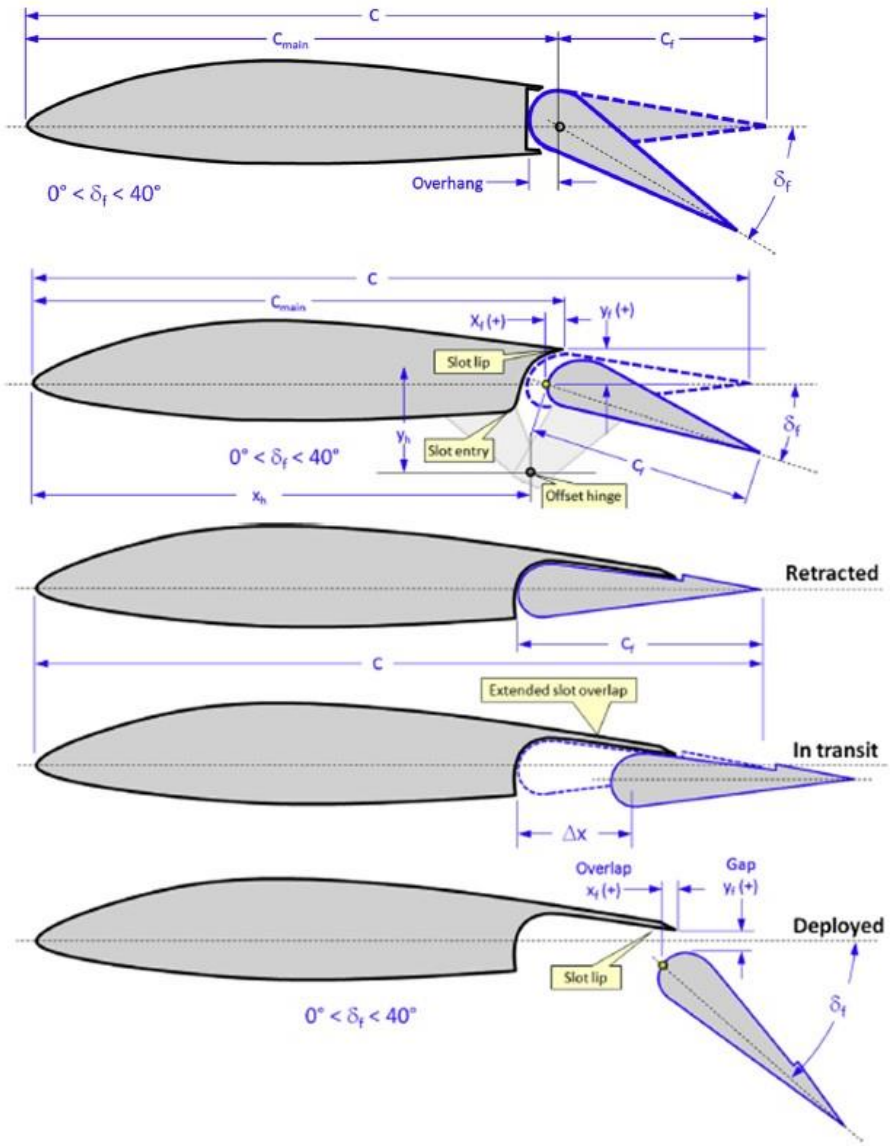

Figure 2.5 Trailing Edge Flap Devices Analyzed (Gudmundsson, 2014). These simple drawings illustrate the devices which will be compared. Top to bottom: plain flap, single slotted flap, and single Fowler flap.

Plain flaps are inherently simple to operate and maintain but are penalized in general effectiveness compared to other flap devices. In addition, plain flaps are sensitive to the condition of the boundary layer. As a result, plain flaps are severely affected by nonlinearity at higher deflection angles and large sweep angles (Bertin & Cummings, 2014; Roskam, 1990; Torenbeek 1982). Even though the flap may be sealed the break at the hinge line can have adverse effects on the separation point (Bertin & Cummings, 2014).

Slotted flaps can have significant increase in $C_{L_{MAX}}$ over plain in addition to a decrease in drag for the slotted configuration (Bertin & Cummings, 2014). Unlike the plain flaps, slotted flaps are typically not very affected by the wing's boundary layer as a new boundary layer forms over the flaps surface (Bertin & Cummings, 2014; Torenbeek 1982). The effectiveness is very sensitive to the flap geometry and hinge location (Torenbeek, 1982). The heavier, complex and more costly hinge systems, actuation systems and maintenance are the main downfall of slotted flaps.

Aerodynamically, the Fowler flap acts identically to that of the slotted flap however the effect of the chord extension is much larger (Bertin & Cummings, 2014; Torenbeek, 1982). Similar to the slat, the slotted flap allows for additional air to reenergize the upper boundary layer. The multi-elements not only aid in this feature but also help turn the air around the larger deflection angles (Abbott & Von Doenhoff, 1959; Hoerner & Borst, 1992). The Fowler flap employs a similar track and hinge system mentioned above for the slotted flap but is more complex with the addition of the lengthened wing chord. This could pose an issue for thin wings especially for supersonic aircraft if the mechanisms cannot be completely concealed inside the wing. Past approximately 40° of deflection the single

slotted flaps (slotted and Fowler) lose their effectiveness and typically require a second element or a type of turning vane to help recover the flow turning effectiveness (Torenbeek, 1982).

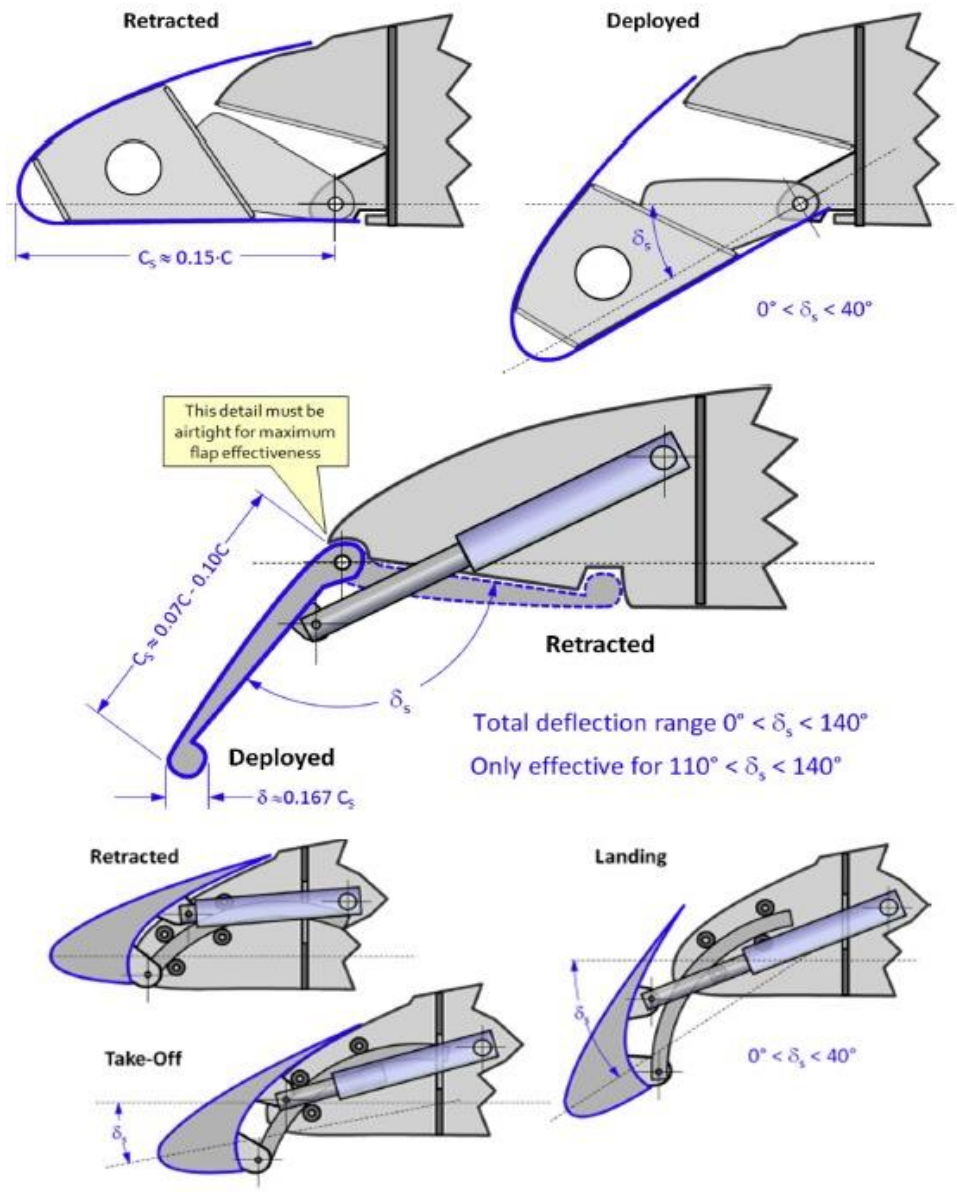

Figure 2.6 Leading Edge Flap Devices Analyzed (Gudmundsson, 2014). These simple drawings illustrate the devices which will be compared. Top to bottom: nose flap, Krueger flap and leading edge slat.

The nose flap has never been a popular choice among commercial aircraft because with highly cambered and rounded airfoils, the nose flap typically induces early separation (Rudolph, 1996). The $C_{L_{MAX}}$ is limited due to the radius of curvature on the upper surface. This may induce flow separation due to the lack of a slot and discontinuity in the curvature on the upper surface (Gudmundsson, 2013). That being said, it has been used on some fighter aircraft and is still being considered for future use in SST with benefits for vortex lift (Rudolph, 1996). This flow separation on thicker and more rounded airfoils with low to medium sweep would adversely affect performance. However, for a thin, highly swept wing, the nose flap helps trigger a stable vortex in the upper surface which helps promote vortex lift (Rudolph, 1996). This is a promising aspect of the mechanically simple nose flap or hinged leading edge.

Krueger flaps are often used on inboard section of wings in combination with outboard slats such as the Boeing 747. Krueger flaps improve the lift capability of the under-cambered airfoil near the root (Gudmundsson, 2014). There are various kinds of Kruger flap such as the simple Krueger, bull-nose Krueger and variable-camber Krueger (Gudmundsson, 2014). Although effectiveness with changes in angle of attack is generally considered poor, it does increase lift without changing the α_{stall} significantly and can be very effective at controlling stall progression along the wing (Gudmundsson, 2014).

The leading edge slat works by assisting in turning the air around the leading edge at high angles of attack. The slat ducts air from the lower surface to the upper surface in such a manner that helps delay the upper surface separation over the wing and flap by providing a form of Boundary-Layer Control (BLC) (Abbott & Von Doenhoff, 1959;

Hoerner & Borst, 1992). This results in the wing continuing to create lift well past the angle of attack where the original wing would have stalled (Hoerner & Borst, 1992).

Flaps have two effects on the lift curve slope of the wing. The use of flaps create a ΔC_L and $\Delta C_{L_{max}}$. The difference in these two are illustrated in Figure 2.7. The use of flaps shift the lift curve slope to the left which raises the C_L at α = 0° (ΔC_L). In addition, an increase in the maximum lift coefficient occurs ($\Delta C_{L_{max}}$). The new maximum lift coefficient now occurs at a lower angle of attack. The use of a slotted leading edge extends the lift curve slope to a higher angle of attack, allowing for a marked increase in lift as seen in Figure 2.7.

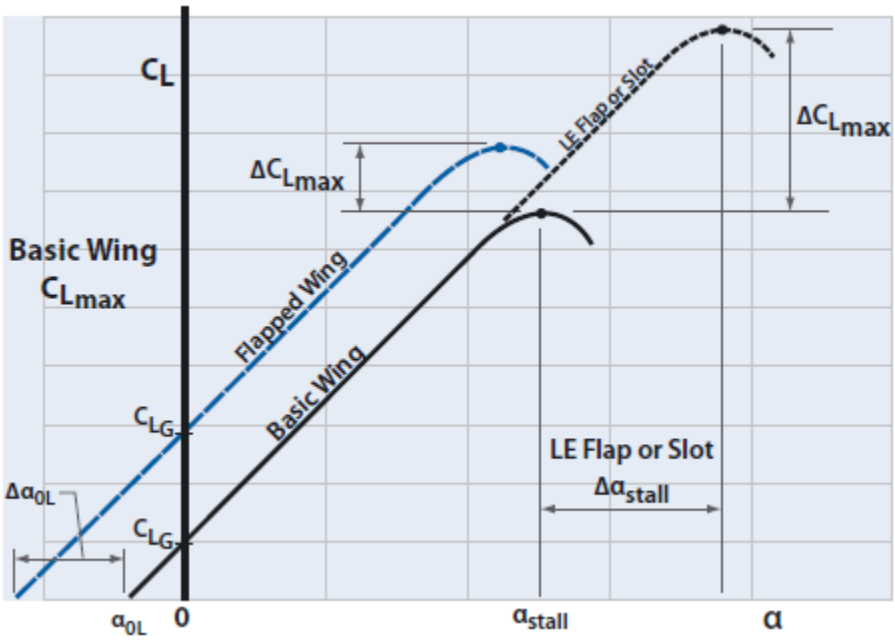

Figure 2.7 Construction of Wing Lift Curves for Mechanical High-Lit Devices (Nicolai & Carichner, 2010).

Leading edge devices can help with separation near the leading edge at high angles of attack but due to their wake, it may cause undesirable flow interference around the

trailing edge flaps (Torenbeek, 1982). This may lead to a decrease of some 15% in ΔC_L compared to the increment on unflapped airfoil (Torenbeek, 1982). This may be aided by the use of a slot but not completely avoided and only minimized, which is why slotted flaps are more frequently used today (Bertin & Cummings, 2014). In addition, with the advances in accuracies in CFD, the use of multielement airfoils has also decreased; only a single slotted flap is used on the Boeing 787 and the Airbus A380 (Bertin & Cummings, 2014). The effectiveness of a flap can vary greatly depending on a number of factors. First, the two-dimensional effectiveness depends on the specific airfoil; whether the airfoil is thick or thin, or has a large amount of camber can greatly influence a flaps effectiveness (Hoerner & Borst, 1992; Roskam, 1990). Secondly, and probably most importantly (two-dimension wise), the physical flap type has a very large influence; a split flap is simply operated but cannot come close to matching the increase in lift from a single or double slotted Fowler flap (Hoerner & Borst, 1992; Roskam, 1990). All of this produces a maximum two-dimensional C_l which is much higher than attainable by the wing. This is because of a series of three-dimensional factors that affects the two-dimensional lift which takes into account the three dimensional flow at the edges of the surface. These three-dimensional effects are based on features of the physical wing and planform. This depends primarily on the span of the flap (flapped wing area), the sweep of the wing, the aspect ratio and the taper ratio (Hoerner & Borst, 1992; Roskam, 1990). The effects in varying sweep angle, aspect ratio, and taper ratio can be seen in Figure 2.8. Increasing sweep angle, while decreasing the aspect ratio and taper ratio typically yield a decrease in $C_{L_{MAX}}$.

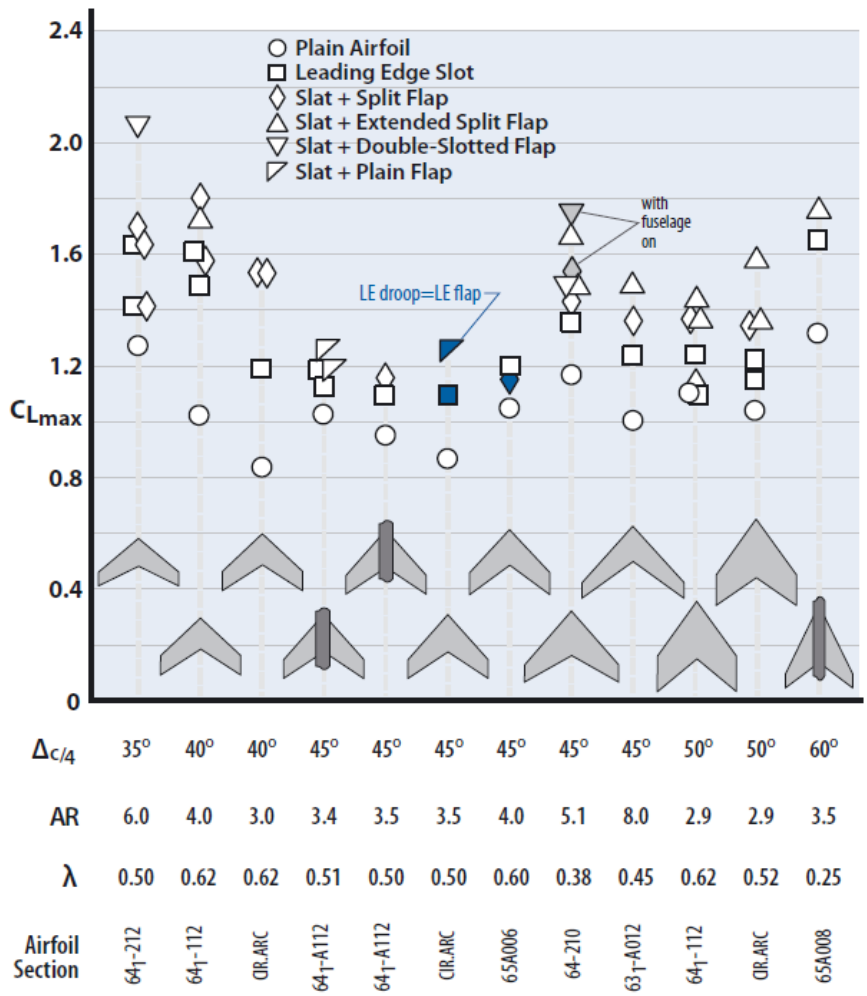

Figure 2.8 Trend of $\mathbf{C_{L_{MAX}}}$ for various three-dimensional planforms (Nicolai & Carichner, 2010). This shows trend of increasing $\mathbf{C_{L_{MAX}}}$ with increasing AR, lower Λ angle and flap sophistication system.

Besides the flap design, the sweep angle of the wings is one of the largest factors when it comes to flap effectiveness. Trailing edge flaps are very effective on wings swept up to about 35° (Nicolai & Carichner, 2010; Roskam, 1990). A correction factor called sweep correction factor, is a number which takes into account wing sweep in determining the flap effectiveness. For a straight wing, the sweep correction factor is 1 but for typical

wing sweeps up to $\Lambda_{c/4}$ = 35° the sweep correction factor ≈ 0.9 – 0.8, defined in section 3.1.4, Figure 3.17). Beyond that, the flap effectiveness drops rapidly somewhere between $\cos^2\Lambda°$ and $\cos^3\Lambda°$, resulting in a sweep correction factor ≈ 0.6 – 0.25 (Hoerner & Borst, 1992; Nicolai & Carichner, 2010; Roskam, 1990). This becomes a key problem for most fixed wing designs of an SSBJ. However, slots and slats still prove to be effective for sweep angles greater than 45° as they reduce separation near the tip and therefore reduce tip stall (Hoerner & Borst, 1992; Nicolai & Carichner 2010).

Most trailing edge flaps are susceptible to a nonlinear decrease in incremental effectiveness with an increase in flap deflection angle beyond approximately δ=20° (Bertin & Cummings, 2014). For example, one method described in Roskam's Airplane Design Part VI, 1990, in Figure 3.4, illustrates the use of a correction factor for nonlinear lift behavior of plain flaps at higher deflection angles. For a flap chord to wing chord ratio (c_f/c), c_f/c = 0.25 at a deflection angle of δ=15° the resulting factor is 0.97 and with a δ=30° the resulting factor is 0.65 which only decreases as c_f/c increases. Certain types of flaps are more susceptible to sweep angle effects, such as plain and split flaps. Unlike, the slotted types of flaps, there is no mechanical way to reduce the upper surface separation before the flow reaches the trailing edge (Bertin & Cummings, 2014).

Some flaps are inherently more efficient at producing lift but typically it is at a compromise of the complexity of the mechanisms and flap design. Flap design is an entirely different optimization problem depending on the size of the flap, internal or external linkages, what size gap or is the gap open or sealed.

Conventional (passive) high lift devices can typically produce a $\Delta C_{l_{MAX}}$ in the neighborhood of 0.5 for plain flaps or as much as 2.2 for a double/triple slotted Fowler with slats (Roskam. 1990; Gudmundsson, 2013). This translates to $C_{L_{MAX}}$ in the order of 1.5 for plain trailing edge flaps with leading edge flaps to 3.2 with double slotted Fowler, full span leading edge slats with dropped ailerons (Roskam. 1990; Gudmundsson, 2013; Nicolai & Carichner, 2010). The Airbus A321-200 with a $C_{L_{MAX}}$ of 3.2 represents the current practical limit of conventional mechanical high lift devices (Nicolai & Carichner, 2010). The most effective mechanical devices have proven to be the leading edge slat in combination with a single or double slotted Fowler flap. Most of the major commercial airliners and more of the recent business jets have begun to use these types of slotted flap systems, as their benefit and effectiveness have been demonstrated over other high lift systems for many years.

When conventional mechanical high lift devices are not capable of producing the required lift, active or powered systems have been employed rather than a large wing or engine which would penalize the overall performance of the aircraft. Some of these systems are displayed in Figure 2.9. The inherent complex nature of these systems usually need a long development time unless a previous design can be used (Nicolai & Carichner, 2010). Boundary Layer Control (BLC) is one example. BLC works by controlling the behavior of the flow by means of reducing adverse pressure gradients and separation over the wing. This may be done by suction or ingestion of the slower boundary layer closest to the surface

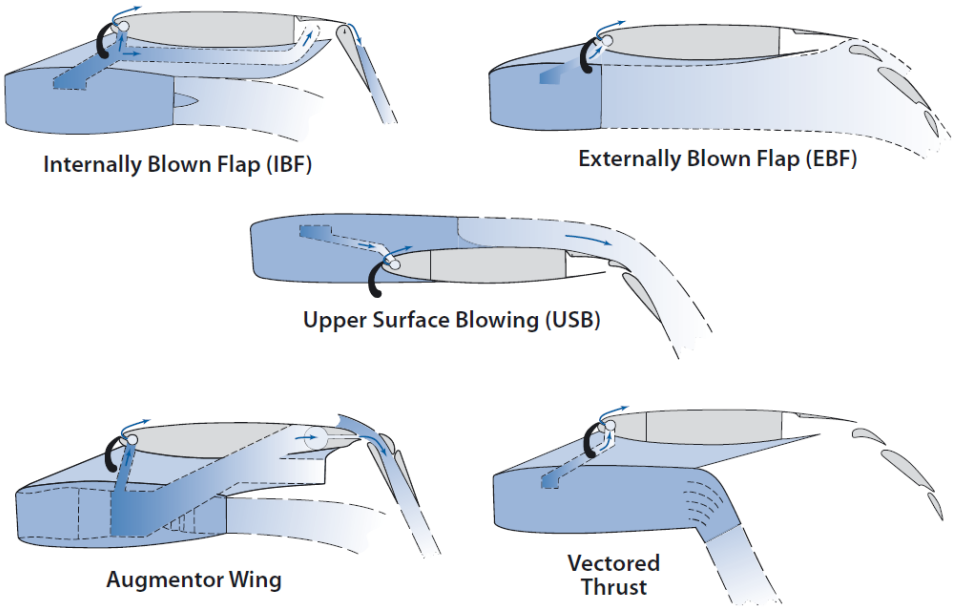

Figure 2.9 Powered-lift STOL Concepts (Nicolai & Carichner, 2010). This shows various ways to employ active flaps systems using a deflected slipstream system.

or, by injecting air tangentially to the surface (Bertin & Commings, 2014). The latter adds energy to the air particles in the boundary layer either at one point or various points over the wing or flap (Bertin & Commings, 2014). This increases energy in the flow over the wing helping the flow to remain attached due to the Coandă effect ("the tendency of a fluid to remain attached to a curved surface") (Bertin & Commings, 2014). The system has numerous operational issues such as the large power required for the pumps, a large increase in maintenance to keep all of the holes/slots free which can cause a rough surface at higher speeds when the system is not operational (Nicolai & Carichner, 2010). When operating correctly, a properly designed BLC control can prove to be very successful. The F-104 Starfighter, A-5 Vigilante and the F-4 Phantom II were the first few aircraft to successfully employ BLC. Table 2.1 summarizes some successful examples of BLC.

Table 2.1
Experimental Trimmed Maximum Lift Coefficients for Several Airplanes with Active Flap Systems (Roskam, 1990).

Model	AR	$\Lambda(°)$	b_f/b	HLD Type	${C_{L_{Clean}}}^*$	${C_{L_{MAX}}}^*$
McDonnell F4	2.78	45	0.65	Plain Blown Flaps + Inbd. LE Flaps + Outbd. Blown LE Flaps	1.05	1.40
Hawker Siddeley Buccaneer	3.58	24	1.0	Blown Plain Flaps + Blown LE	0.96	2.2
Gen. Dynamics F-111	6.0	13	0.665	Blown Plain Flaps + Blown Center & Outer LE Flaps	1.55	2.45
North Am. F-100A (Exp.)	3.72	45	0.8	Blown Plain Flaps + Blown LE Flaps	1.2	1.5
Boeing 707-120 (Exp.)	7.0	35	0.665	Blown Plain Flaps + LE Flaps		2.34
Lockheed C5A	8	25	0.74	Double Slotted Flaps + LE Kruger Flaps + External Jet Blowing	1.45	3.8[a]
Douglas A3D	6.75	36	.575	Blown, Single Slotted Flaps + LE Slats	1.37	1.9

Note. Adapted from "Airplane Design, Part VI," by J. Roskam, 1990, p.361. Copyright by Roskam Aviation and Engineering Corporation. HLD = High Lift Device(s) Down, *Trimmed, Gear-up, Inbd = Inboard, Outbd = Outboard.
[a]From NASA TN D-4928. Wind-tunnel investigation of a large jet transport model equipped with an external-flow jet flap.

Besides BLC are deflected slipstream systems as shown in Figure 2.9 through Figure 2.11. This can be thought of as a kind of thrust vectoring in addition to BLC. Either the propeller's slipstream or jet exhaust is deflected (partial or full) by the flap arrangement over part or the entire span. In order for these systems to be used safely, there is typically a cross-over duct that allows for the deflected slip stream system to still function under engine failure(s) (Nicolai & Carichner, 2010). Figure 2.10 show the potential performance of various powered-lift systems.

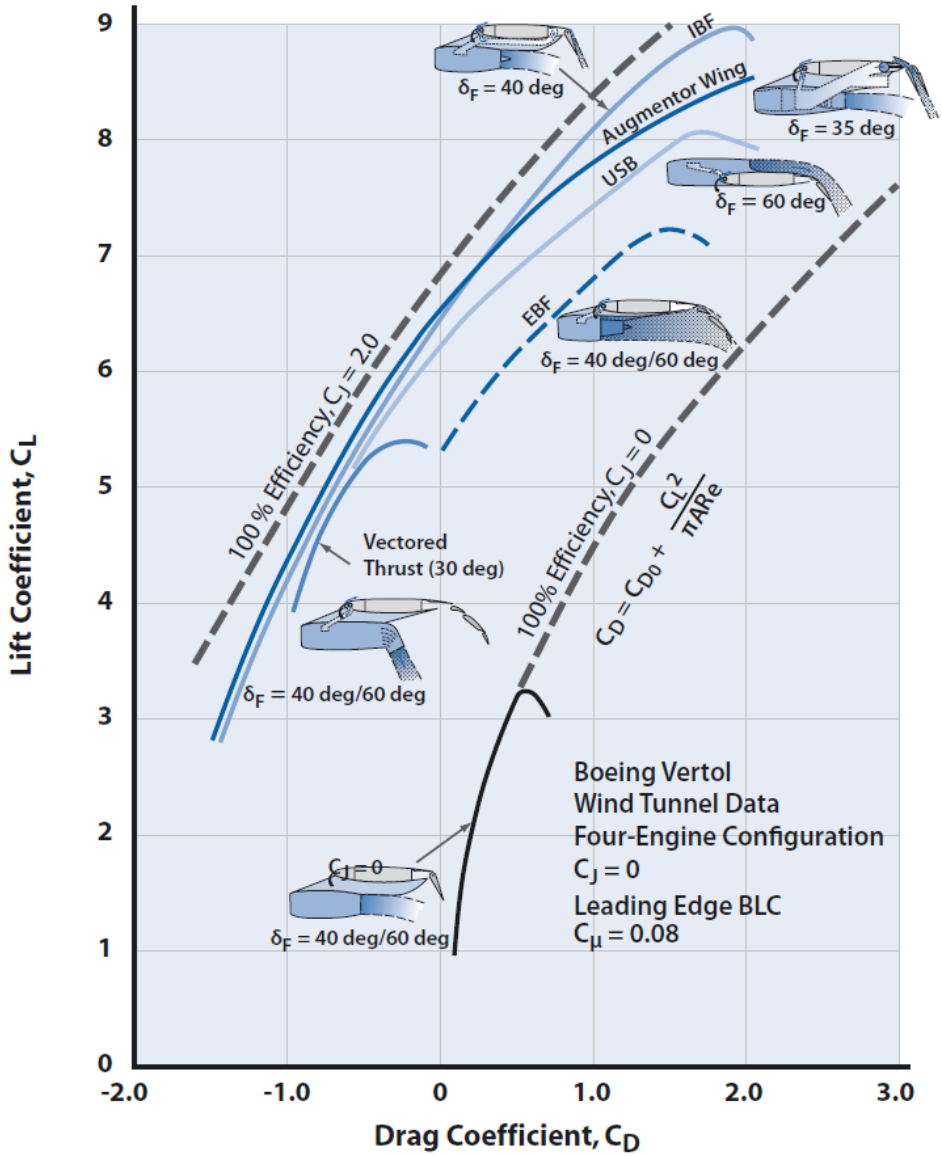

Figure 2.10 Low-Speed Drag Polars for Various Powered-Lift Concepts (Nicolai & Carichner, 2010).

Deflected slipstream systems are very effective in augmenting lift but are very harsh on the flap section exposed to the hot jet exhaust. Not only are the temperatures beyond ambient, the forces exerted by the jet blast are many times stronger than a typical

flap would experience (Nicolai & Carichner, 2010). These effects can be seen on the C-17 in Figure 2.11 with a reinforced surface behind each engine on the flaps.

Figure 2.11 C-17 with Externally Blown Flaps (Jones, M. Jr. 2010). It is evident the externally blown flaps on the C-17 have some additional structural features where the jet blast comes in contact with the flaps

2.1.4 Vortex Lift

Flap effectiveness reduces with sweep angles. Highly swept wings with low aspect ratio experience a nonlinear lifting phenomenon called vortex lift at high angles of attack. Vortex lift is generated by sheets that are shed off the leading edge and eventually roll up into pairs of stable vortices over the upper surface of the wing. Figure 2.12 illustrates these

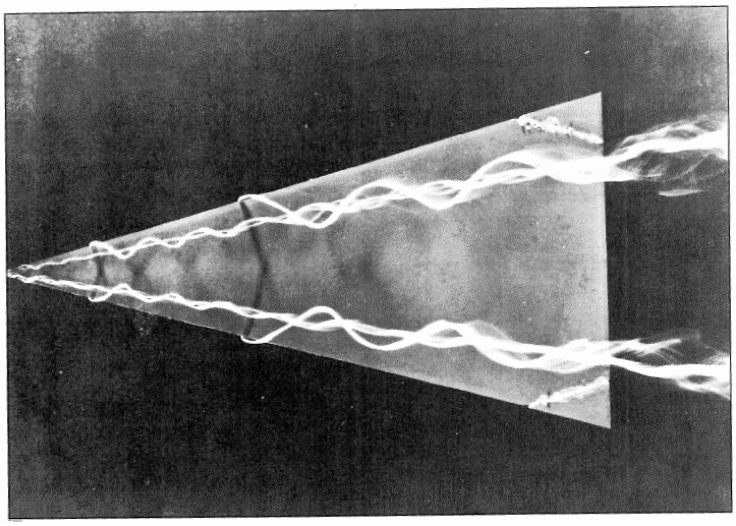

Figure 2.12 Leading Edge Vortices Over the Top Surface of a Delta Wing at an Angle of Attack (Anderson, 2007). The vortices are made visible by dye streaks in the water flow.

vortices. These vortices appear because the pressure on the bottom surface of the wing at high angles of attack is higher than the pressure on the top of the wing. The flow on the bottom surface in the vicinity of the leading edge flows up and around the leading edge. If the leading edge is sharp, the flow will separate along its entire length. After separating at the leading edge, flow curls into a primary vortex. This vortex exists just inboard and above the leading edge, and then reattaches along the primary attachment line, see Figure 2.13.

Vortex lift primarily occurs on delta type planforms but has also been known to appear on other highly swept planforms (Anderson, 2007).

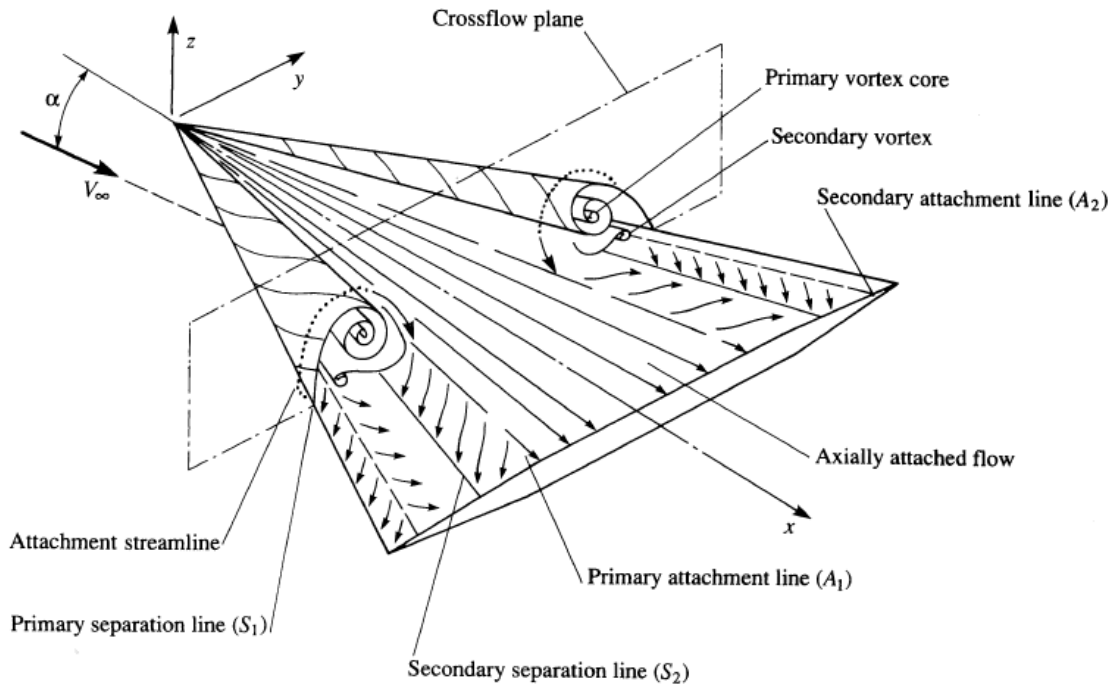

Figure 2.13 Schematic of Flow Field Over Top of Delta Wing at an Angle of Attack (Anderson, 2007). This illustrates the concept of how the flow over delta wings uses vortex lift at high angles of attack

These vortices appear on the top of the wing and increase in strength downstream of the wing apex, as each segment downstream adds to this circulating vortex. These leading-edge vortices are fully developed by the time they reach the trailing edge (Hoerner & Borst, 1992; Clark & Yeh, 2007). A secondary vortex is formed underneath the primary vortex with its own separation shown in Figure 2.13 (Hoerner & Borst, 1992; Anderson, 2007). The developed vortices can be seen Figure 2.14 with the Concorde taking off. These vortices can be very stable and defined until vortex breakdown initiates as seen in Figure 2.15.

With an increase in angle of attack, the strength of the vortex also increases up to a point of vortex breakdown or vortex bursting illustrated in Figure 2.15. Vortex breakdown

Décollage d'un Concorde d'Air France
An Air France Concorde taking off

Photographe/Photographer : Ph DELAFOSSE Ref : 014053
Tout usage sauf publicitaire / Not for advertising purposes

Figure 2.14 Leading Edge Vortices Forming on Takeoff (Delafosse, P. (Photographer). (2003). An Air France Concorde Taking off [Print Photo]. Retrieved from http://arcus.centerblog.net/rub-avions--2.html). The relatively high angle of attack for the Concorde on takeoff shows these leading edge vortices following the leading edge where they expand and lead to vortex breakdown.

is very irregular and greatly influences the flow patterns especially through higher angles of attack (Hoerner & Borst, 1992). Once the vortex starts to break down it does not lead to a complete absence of vortex lift but it can be expected that the vortex lift increment will decrease with further increases of angle of attack (Hoerner & Borst; 1992; Anderson, 2007). There are two forms of vortex breakdown, the first called spiral-type of breakdown where the vortex progressively twists along the core in various directions. The other form

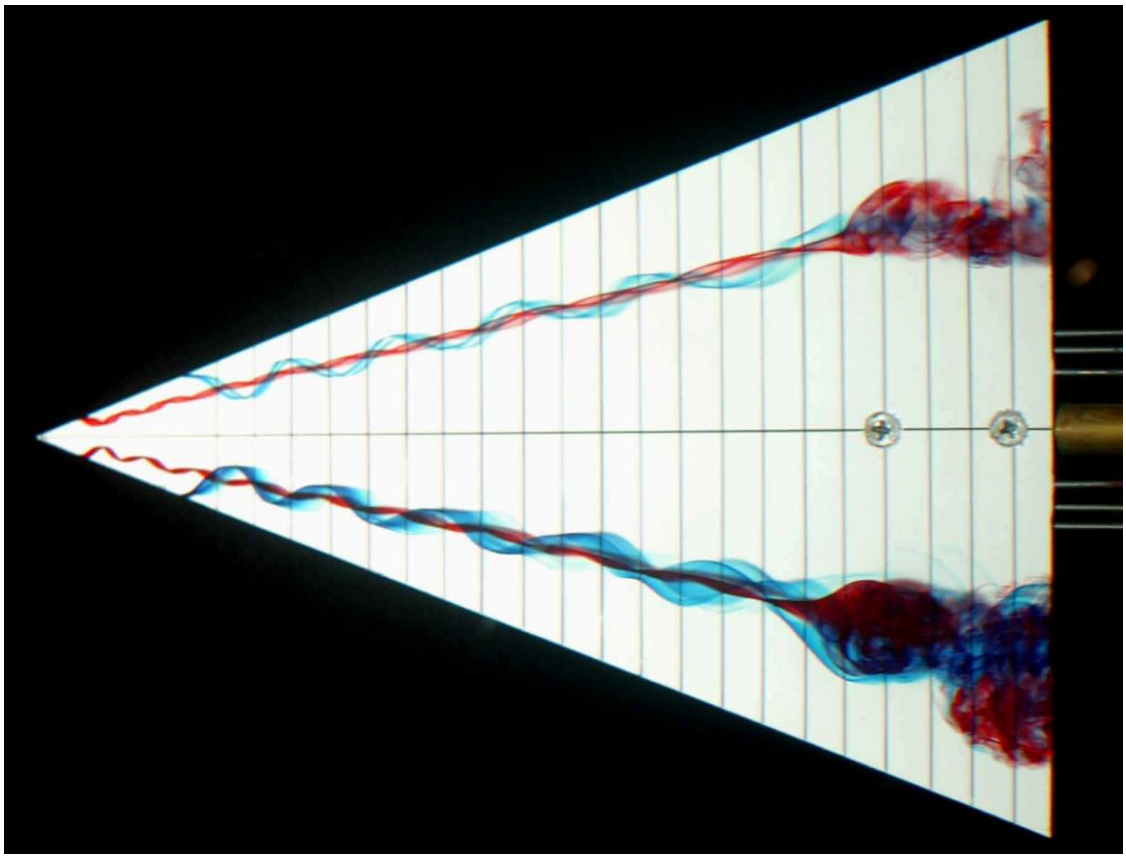

Figure 2.15 Vortex Breakdown Over a Delta (Lim, T. T. (Photographer). (2005). Vortex Breakdown over a Delta Wing (using dye) [Print Photo]. Retrieved from http://serve.me.nus.edu.sg/limtt/). This was performed using dye to visually show the vortices.

is bursting as shown in Figure 2.15 where large bubbles form and burst in a chaotic and abrupt manner; spiral breakdown is more common (Anderson, 2007). An interesting note, CFD solutions of the Euler equations (inviscid flow) have successfully captured this vortex, resulting in the conclusion that friction appears to not play a critical role in vortex formation and breakdown (Anderson, 2007). There are ways to augment vortex strength and thus vortex lift over highly swept wings beyond that of regular mechanical flaps.

A Leading-Edge Vortex Flap (LEVF), apex fence (apex flap), and a Leading Edge Extension (LEX) contribute to higher lift at subsonic speeds due to the ‘nonlinear’ vortex

lift and can have a reduction in net drag (Anderson, 2007; Clark & Yeh, 2007; Rinoie, 2003). Typical mechanical flap systems as previously discussed work to promote attached flow or suppress leading edge vortices therefore conventional flap systems typically do not aid much in vortex lift. There, however are various devices that aid in increasing the vortices strength, and help increase the force components in the thrust and lift directions.

An LEVF is a full span deflectable surface attached to the leading edge of a delta wing, similar to a nose flap (Rinoie, 2003). By deflecting the LEVF, the vortex can be formed over the forward-facing surface resulting in a force which generates a thrust component forward (Anderson, 2007; Rinoie, 2003). An LEVF can be seen in Figure 2.16 with a sharp and rounded noise on the left and the spanwise pressure distribution on the right. These show the forward facing thrust vectors. Figure 2.17 shows that the flow reattachment line is very near the flap/wing junction (Brandon, Hallissy, Brown & Lamar, 2001).

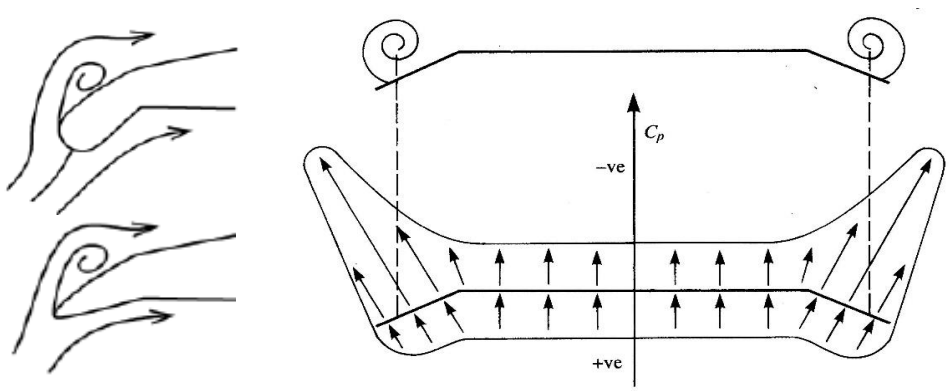

Figure 2.16 (Left) Rounded and Sharp Edged Examples of LEVF (Rinoie, Kwak, Miyata & Noguchi, 2002). (Right) Schematic of Spanwise Pressure Coefficient Distribution over the Top of a Delta Wing Modified by a LEVF (Anderson, 2007).

Figure 2.17 Detail of Forward Sections of the Vortex Flap with Oil Flow Pattern, on an F-106B α=13°, 40° Vortex Flap (Brandon, Hallissy, Brown & Lamar, 2001). The solid oil line on the LEVF shows the edge of the vortex on the flap.

The apex fence works very simply by deflecting a surface vertically into the airflow at the apex of the wing increasing the vortex strength (Moskovitz, Vess & Wahls, 1986). This is an upper surface, hinged panel originally planned for use as vortex control device on delta, cranked or arrow wings (Moskovitz et al., 1986). Apex fences appear to work well at lower angles of attack by effectively augmenting the suction level over the apex, whereas at higher angles of attack the apex suction was reduced. As a result of higher suction, a nose-up pitching moment is created. This aids in longitudinal trim to counteract the nose-down pitching moment from the deflecting of the trailing edge flaps (Moskovitz et al., 1986). Apex fences have been found to noticeably increase trimmed lift capabilities (Hoffler, Dhanvafa & Frassinelli, 1986).

Vortex lift is used by most highly swept, thin wing, modern aircraft such as the F-18 and F-22. Instead of an apex fence, these aircraft use variations on LEXs or strakes

as seen in Figure 2.18 through Figure 2.21. A LEX is a highly swept leading edge, and may be viewed as a very thin and slender delta wing which is installed in front of the main wing. With this low profile, the LEX adds very little drag at cruise conditions. A top view of a LEX can be seen in Figure 2.18 on an F-18 model.

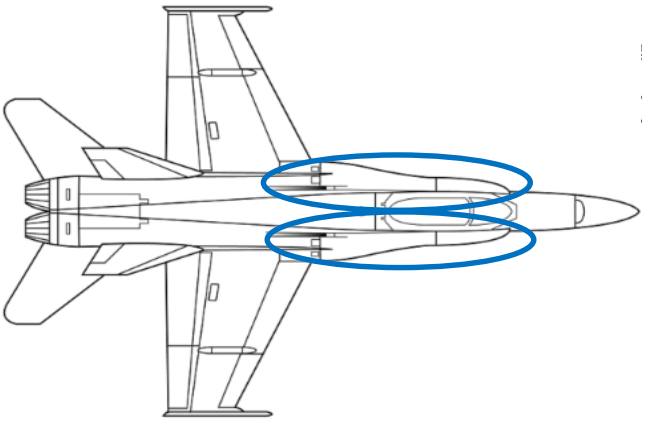

Figure 2.18 Leading Edge Extensions on an F-18 Model (Curry, M. 2003). Circled in blue are the leading edge extensions on the F-18 model, image may not be to scale.

The formation of the larger vortices due to the LEX on the F-18 is clearly illustrated in Figure 2.19. The leading vortices help the flow to remain attached over the upper surface of the wing at higher angles of attack.

Figure 2.19 An F-A-18E Takeoff (Mass Communication Specialist 2nd Class, Evans, James R. (Photographer, 2011). Use of released U.S. Navy imagery does not constitute product or organizational endorsement of any kind by the U.S. Navy. The LEX on the F-18 produces a very evident vortex going over top of the wings.

Figure 2.20 shows the various formations of the leading edge vortices from the LEX on an F-18 model at different angles of attack. The upper and lower right images are at a higher angle of attack (≈25°) while the lower left image is at a lower angle of attack. Figure 2.20 shows how a LEX can function at the two different angles. Without a LEX, at a high angle of attack, a large percentage of the F-18 wing will operate stalled and not be able to produce the lift required. The LEX helps to create a new vortex lift segment which is generated near the root. By producing this high speed vortex on the upper surface of the wing, smooth air flow is maintained well past normal stall conditions and stall is delayed (Gülçat, 2010). The effect is achieved by creation of a strong suction on the upper surface, which adds to the tip vortex of the wing and increases the total lift (Gülçat, 2010).

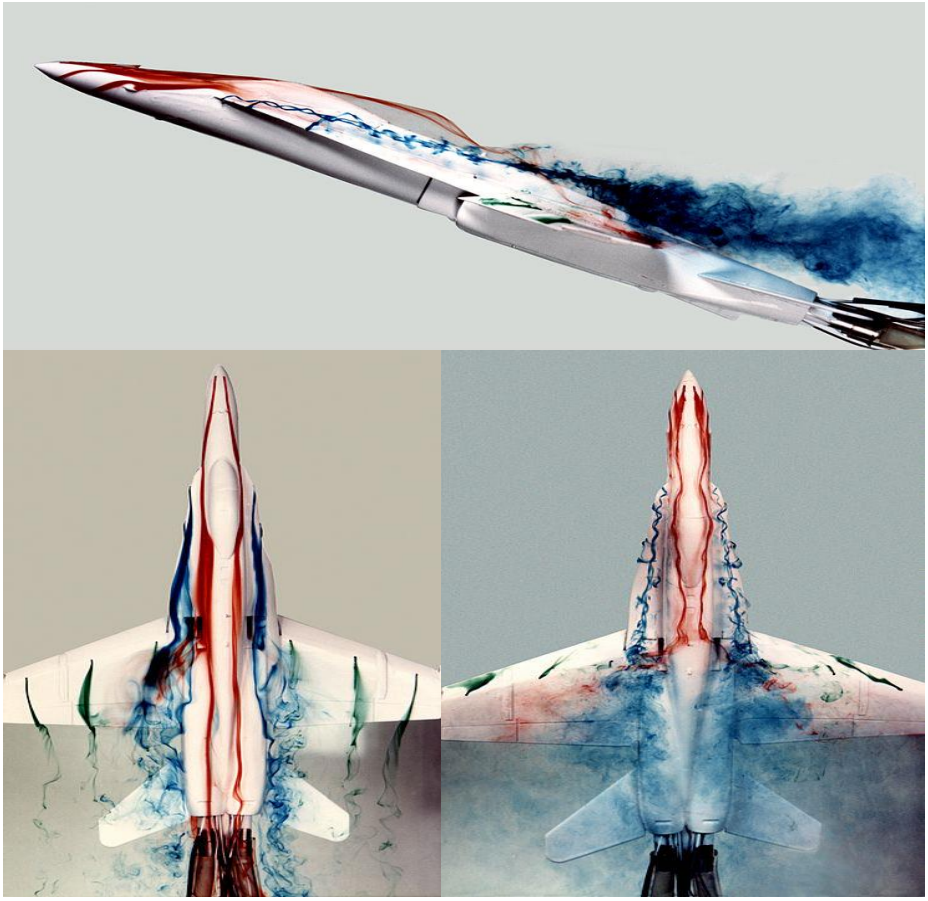

Figure 2.20 1/48-scale model of an F-18 during water tunnel test in the Dryden Flow Visualization Facility (NASA, 1985). The top and bottom right image are at high angle of attack while the lower left is at a lower angle of attack. The dyes allow for easy visualization of the vortices produced by the LEX.

Figure 2.21 shows different flow patterns over the upper portion of the wing. Without the LEX at an $\alpha = 12°$, there is a reverse flow field near the tip which transitions to a stagnant flow at $\alpha = 18°$. With the addition of the LEX, Figure 2.21 shows an improvement in flow with the leading edge vortex over the wing. Even at an angle of attack $\alpha = 18°$, the vortex is still strong enough to significantly suppress the stagnant zone on the

outer portion of the wing. This creates a noticeable increase in lift. Vortex lift results in $\Delta C_{L_{MAX}}$ increases of around 0.6 at 28°, and 0.4 at 18° (Huenecke, 1987).

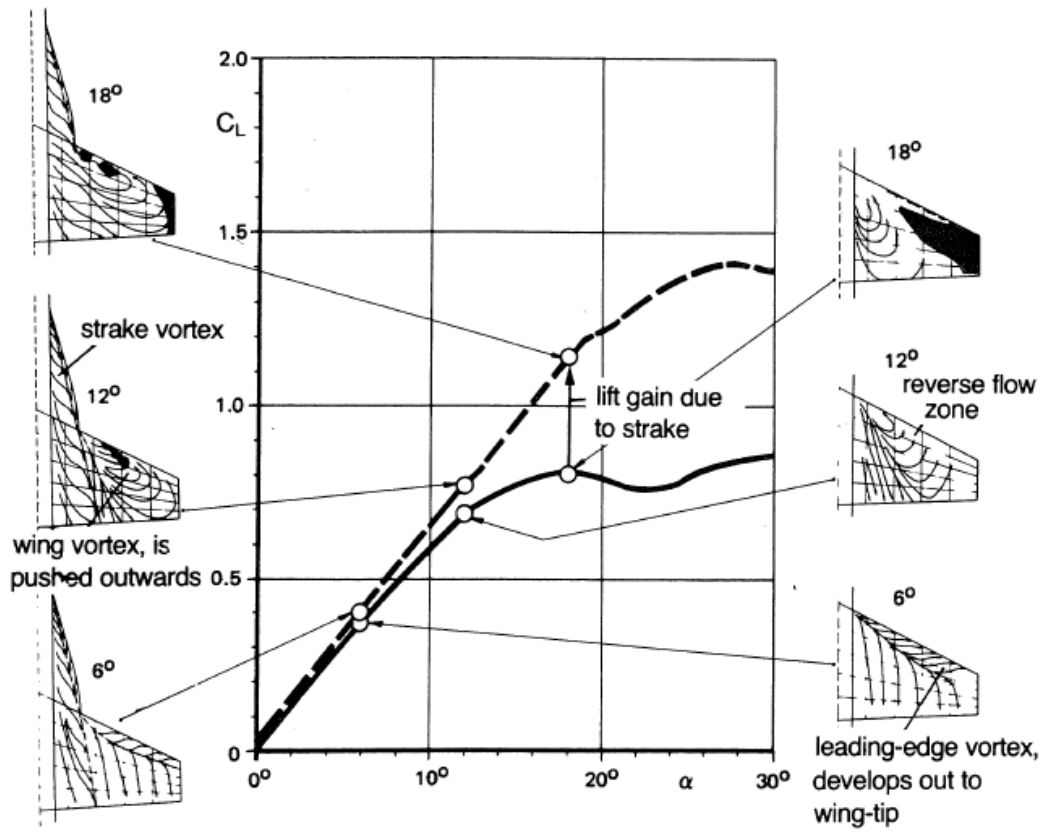

Figure 2.21 Comparison of Flow Field and Lift Development over a Wing with and Without LEX (Huenecke, 1987).

Although this study cannot calculate the vortex lift directly, it is recommended for further detailed study. Low-speed, high-lift conditions around most fixed wing, supersonic aircraft are dominated by flow separation and vortex flows (Anderson, 2007; Bertin & Commings, 2014; Clark & Yeh, 2007). However the lift increment from vortex lift may be estimated by a method developed by Polhamus, for sharp leading edge delta type wings

base upon the leading-edge suction analogy (Polhamus, 1966, 1968, 1971; Hoerner & Borst, 1992). The Leading-Edge Analogy depends on the assumption

> …That the total lift is comprised of two parts: (1) a lift associated with the reattached flow which can be estimated by an appropriate application of potential-flow lifting-surface theory, and (2) a vortex lift which is equal to the force required to maintain the equilibrium of the potential theory-type flow around the sprial vortex. (Polhamus, 1968).

Full description, assumptions and limitations can be found in the various papers published by Polhamus in 1966, 1968, 1971.

A much less mature technology emerging now is the use of smart materials and adaptive or morphing structures. A joint NASA and Wright Laboratory demonstration program in 1990 on an F-111A aircraft investigated the active control of chordwise camber, spanwise camber, and wing sweep while maintaining a smooth continuous airfoil (Sater, Crowe, Antcliff & Das, 2000). At the time of the study, the linkages and devices required to obtain the shape alterations were too complex and the system was deemed impractical for implementation (Sater et al., 2000). However, recently, smaller scale studies have shown more positive results. Studies have shown successful application on micro aerial vehicles, small scale and or low speed tests (Wickramasinghe, Chen, Martinez, Wong, & Kernaghan, 2011). The small scale studies have shown positive results because of the relatively low forces required to maneuver the small scale aerial vehicles. These test have used active trailing edges driven by piezoelectric and electroactive polymers (Wickramasinghe, et al., 2011). Piezoeletrically driven synthetic jets have shown positive

results on flow control and low speed maneuvering when small forces are required (Koklu, 2007).

More recently, an ongoing research group called Smart High Lift Devices for Next Generation Wings (SADE) which comprises of 13 European aerospace partners is heavily invested in smart high lift devices. Its proof-of-concept, full-scale wind tunnel test was successful in showing that on a morphing droop nose and morphing trailing edge, that large deformations are possible even for load carrying structures (Smart High Lift Devices for Next Generation Wings, 2012). The next step is to carry out tests related to operational requirements such as bird strikes. There is however, a large primary technical challenge dealing with the elasticity required for the smart material operations versus the stiffness required for a typical wing:

> However, the high elasticity required for efficient adaptability of the morphing structure is diametrically opposed to the structural targets of conventional wing design like stiffness and strength. To find the optimum compromise, precise knowledge on target shapes for maximum high lift performance and sizing loads is mandatory. (European Commission, 2008).

Technology from plasma actuators for benefit in boundary layer transition to altering variable camber morphing airfoils shows good small scale or low speed conceptual ideas. So far however, the use of smart materials in large scale, everyday commercial applications, is still in the preliminary phase (Duchmann, Simon, Tropea & Grundmann, 2014; Yokozeki & Sugiura, 2014).

Chapter III

Methodology

3.1 Research Approach

VLAERO+© commercial code was used to explore and estimate the changes in lift between a variable geometry and fixed geometry planforms with addition of empirical calculations to estimate the lift increment due to high lift devices. VLAERO+© was used to capture the C_L and C_{Di} of a variable geometry, fixed swept, and delta planform at cruise and approach conditions. All of the planforms were initially sized to have identical cruise performance. After the initial sizing for cruise, the planforms were analyzed at approach condition. The $C_{L_{max}}$ was assumed from the stall conditions using the lift equation and was the goal for the planforms. The variable geometry wing was the baseline model without use of high lift devices. The ΔC_L and $\Delta C_{L_{max}}$ of various high lift devices were estimated from empirical methods and were applied to the initially sized fixed swept and delta planforms. After the increments in lift were added to the initially sized fixed swept and delta planforms, the wing areas were increased until the planforms are able to meet to required C_L. For not employing variable geometry, the fixed swept and delta planform were penalized by an increase in wing area. An increase in wing area would result in a higher wing weight and drag at cruise which decreases the L/D ratio. With a decrease in L/D ratio, the aircraft burns more fuel making the aircraft less efficient and more costly to operate. The increases in wing area for the fixed swept and delta planforms were minimized by the use of flaps. With the use of flaps and an increase in wing area, weight of the planforms would increase over the initial size. The increase in weight would further penalize the

planforms requiring more lift which results in higher drag and an increase in fuel consumption. This is all a consequence of the wing needing to supplement the low-speed lift that the sweep diminished. The weight penalty for the variable geometry planform was taken in account in the wing weight calculations. The overall impact of the increase in area and weight was taken into consideration with use of a Specific Air Range (SAR) ratio between the planforms.

3.1.1 Mission Requirements and Parameters

The flight conditions and basic aircraft parameters were designed to mimic a typical SSBJ in terms of profile and general requirements. They were as follows: (1) Business Jet class vehicle, (2) cruise speed twice as fast as current production vehicles, (3) day trip (4-5 hour flight) operational range, and (4) general aviation airport operational restrictions. Table 3.1 summarizes the design parameters.

Table 3.1
Aircraft Design Parameters.

Design Condition	Units	Target
Range	nm	4,000 – 4,800
Cruise Mach	---	1.7 – 1.9
Ceiling	FL	510
Balanced Field Length	feet	5,000 – 6,000
MTOW	lb	90,000 – 100,000
OEW	lb	40,000 – 50,000
PAX	---	8 - 12

A design condition imposed was to ensure a subsonic leading edge which results in a minimum leading edge sweep of 56° plus a 2° margin resulting in a Λ_{LE} of 58° for all planforms. Having a subsonic leading edge would have beneficial results to mitigate the sonic boom over pressure. An iterative process was performed to create the cruise and

approach planform size; the planforms went through this iterative process to arrive at their final shape and dimensions, based on the lift requirements. Flaps were added to the delta and fixed swept planforms but not the variable geometry planform. No fuselage or tail plane was used in the analysis in order to judge the results solely on the wings to capture the principal effects. The empennage and fuselage could have different effects at various angles of attack and could unevenly influence the results. These effects could be more realistic but the empennage would need to be sized according to the stability needs adding further variables and complexity to the problem. The shape of the fuselage would need to be optimized for supersonic flight which in itself a large problem. The center line of the model is where the wings would normally meet the fairing. An upper limit of $\alpha = 15°$ was imposed on this study for pilot visibility consideration. The planforms were designed to satisfy the approach conditions with the calculations at cruise taking into account any penalties or benefits from the change in area needed to satisfy the approach conditions. Table 3.2 summarizes these conditions.

Table 3.2
Flight Condition.

Condition	Units	Value
CRUISE		
Altitude	FL	500
Cruise Mach	---	1.8
Cruise True Airspeed	kt	1032.42
Weight	lb	80,000 (80%MTOW)
APPROACH		
Altitude	---	Sea Level
Approach Mach	---	0.2419
Approach True Airspeed	kt	160
Weight	lb	80,000 (80%MTOW)

3.1.2 Planform Geometry

For simplicity the NACA 63 – 66 series airfoils were used. A subsonic airfoil study over a range of angles of attack on the fixed swept planform revealed identical performance for the NACA series airfoils but also revealed their superior performance over similar geometric airfoils such as RAF26, AH21 MA409, AG17 and NACA M13. The NACA 63-206 was selected as the airfoil of choice. The thickness of this airfoil is the same as supersonic wings of past designs 3% - 6% (HISAC, 2008).

The general process is discussed here as it applies to all planforms with specific limitations and results in each of the respective planform sections. The sweep angle was calculated from the Mach angle for cruise at 1.8 with a margin of 2°, yielding the leading edge sweep angle for all planforms of $\Lambda_{LE} = 58°$. The preliminary trend of the planform and flaps configurations was the main concern; a full optimization of the planform was not considered. An $\alpha_{max} = 15°$ was chosen taking pilot visibility into consideration. The delta and fixed swept planforms used high lift devices whereas the baseline variable geometry did not.

The approach design point was assumed to be 160 kt (M0.249, 270.0 ft/sec) at sea level based on suggested data and an estimated stall speed of 123 kts (M0.1859, 207.6 ft/sec) per, 14 CFR Part 25, **§**25.103: Stall speed. Briefly, this states the stall speed need to be equal to or less than $\frac{V_{Approach}}{1.3}$

3.1.2.1 Variable Geometry – The Baseline Planform

The initial variable geometry planform was inspired by the HISAC variable geometry model. The following process was used to create the variable geometry

(baseline) planform. The required $\boldsymbol{C_L}$ was found from the lift equation with a fixed α_{max} = 15°, V_{Stall} = 123 kts and the one variable, the wing area. Therefore the required amount of lift needed to occur by α = 15°. Once the planform was capable of creating the lift at low speed, the wings were swept aft for the high speed analysis.

The wing pivot point was located at mid-chord of the unswept wing and the centerline of the model. The wing fairing was determined by the point at which the leading edge of the unswept wing intersected the leading edge of the swept aft wing. The pivot point was based on previous designs, simplicity, and in order to minimize the change in wing area between the different configurations. With the wing unswept, the fairing is evident but with the wing swept aft, the fairing blends into the wing which is typical on most variable geometry planforms. The fairing is located in order to cover the hinge and mechanisms. This provides a type of leading edge extension of the unswept configuration and in actuality would most likely be thicker than the rest of the wing. However, the actual thickness is unknown and therefore not modeled.

The wing is unswept about the pivot to 20° with a trailing edge sweep angle of 0° which is the resulting value from typical values of similar aircraft. The wing span of the unswept planform used the Aspen Colorado airport limited value of 95 ft. This was done as the Aspen airport is an important airport for business jets to be capable to takeoff and land at. The swept aft span is the resultant of the leading edge sweep angle. The taper ratio was assumed from typical values. No flaps added

to the planform in order to see whether the aircraft could fly at the approach conditions.

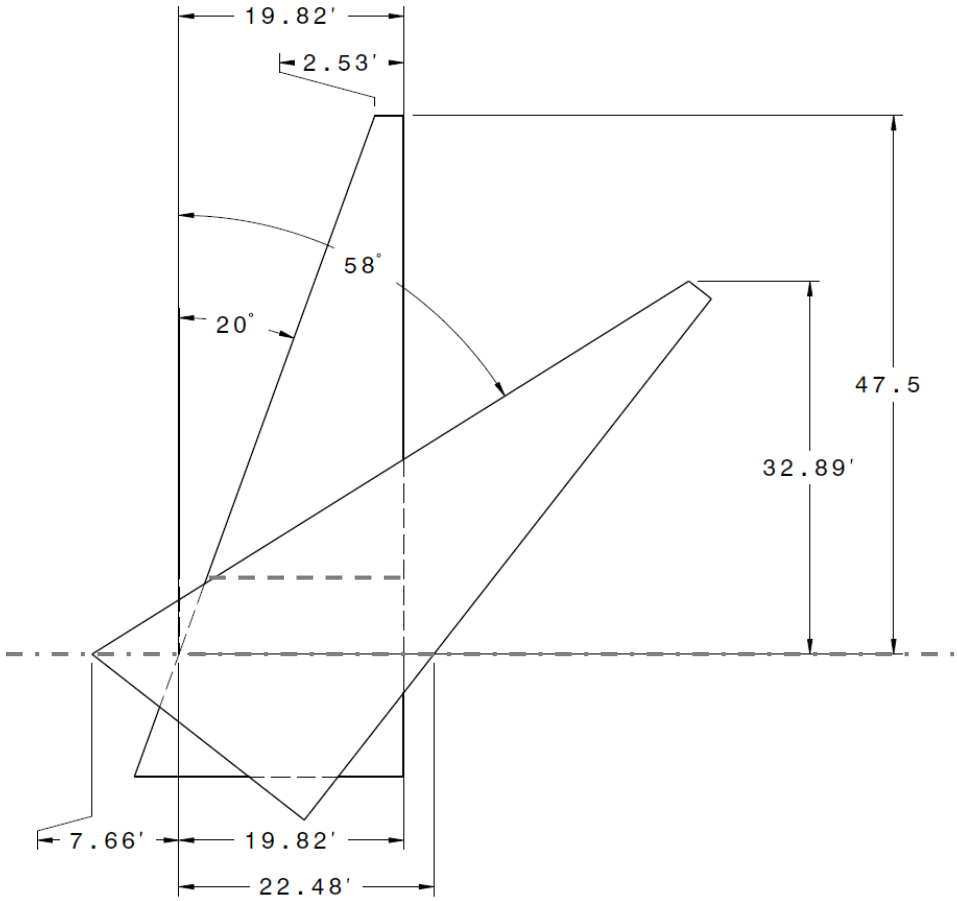

Figure 3.1 Variable Geometry Wing Dimensions.

Figure 3.1 shows a dimensioned top view of the variable geometry planform with further wing dimensions in Table 3.3 and Table 3.4.

Table 3.3
Unswept Variable Geometry Wing Dimensions.

Unswept							
Root to Fairing		Fairing to Tip					
Chord at Root (ft)	Taper Ratio	Chord at Fairing (ft)	Taper Ratio	Half Span (ft)	Aspect Ratio	Total Span (ft)	Total Area (ft^2)
27.48	0.645	17.72	0.143	41.4	8.1	95	1,114

Table 3.4
Swept Aft Variable Geometry Wing Dimensions.

Swept Aft				
Root Chord (ft)	Taper Ratio	Aspect Ratio	Total Span (ft)	Total Area (ft^2)
30.15	0.149	3.9	65.78	1,092

Table 3.3 and Table 3.4 show the dimensions for the unswept and swept wings. The swept aft model lost an area of 22 ft^2 which translates to a difference of 2% in comparison to the unswept model. Lastly in Figure 3.2 the two VLAERO+© models are shown. The unswept model clearly shows the wing fairing.

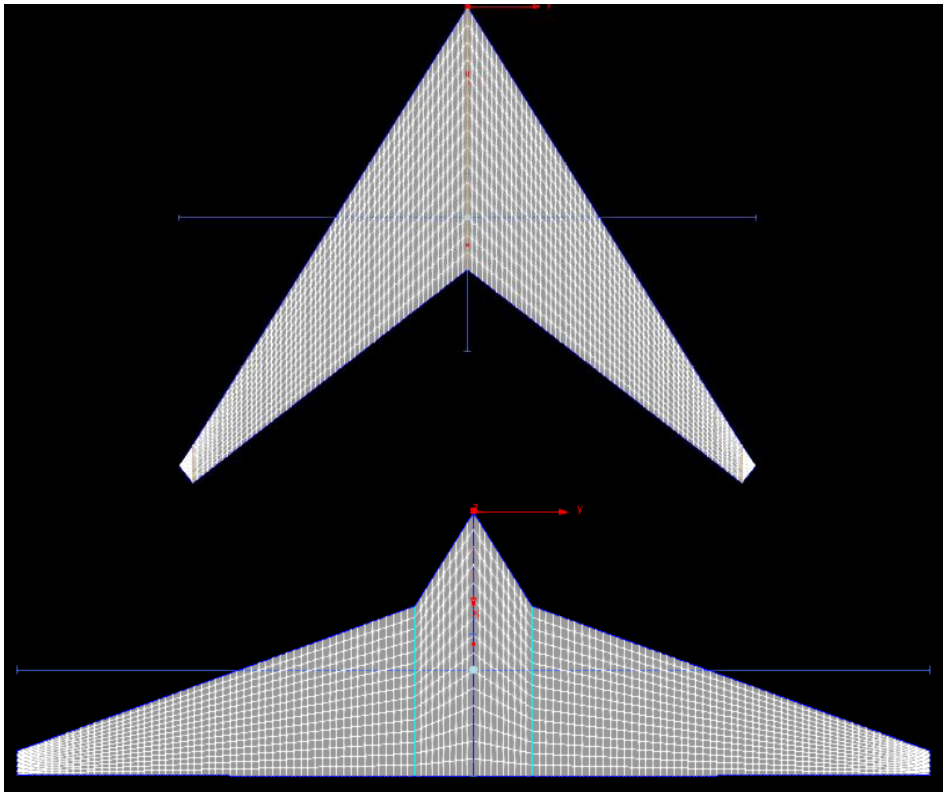

Figure 3.2 VLERO+ Swept Aft and Unswept Models. The swept aft model on top and the swept forward model on the bottom. The fairing is evident in the bottom image.

3.1.2.2 Fixed Sweep Planform

The planform started with the swept aft model for the variable geometry wing. From there, an identical iterative process that was used in finalizing the variable geometry planform was applied to finalize the fixed sweep planform. The only difference in the iterative process was the use of high lift devices during the low speed calculations.

3.1.2.3 Delta Planform

At an initial cruise C_L= 0.161 the delta planform started with the same area as the variable geometry. These dimensions are shown in Table 3.5.

Table 3.5
Initial Delta Planform Geometry Wing Dimensions

Initial Delta Planform				
Root Chord (ft)	Taper Ratio	Aspect Ratio	Total Span (ft)	Total Area (ft^2)
44.2	0.15	0.863	43.9	1,114

A typically low value for taper ratio was chosen of 0.15. The wing span was a result of a non-zero trailing edge to mitigate adverse sonic boom properties. No angle was selected. The aspect ratio should be between 1.5 and 3. The root chord had a fixed maximum value to no exceed 50 ft. The largest constraint on the delta planform was the subsonic leading edge. This resulted in a planform that would have a relatively long root chord and short wing span, yielding a low aspect ratio. To minimize the increase in area high lift devices were used.

3.1.3 High Lift Device Geometry

Wing flap geometry was obtained from recommendations in Roskam's Airplane Design (1990), Gudmundsson's General Aviation Applied Methods and Procedures

(2014), and Rudolph's High-Lift Systems on Commercial Subsonic Airliners (1996). All of the flap dimensions and values were chosen based on reasonable figures from past successful designs. The general flap types and nomenclature were discussed in section 2.1.3. The specific dimensions will be presented here.

As previously discussed there are many methods to augment the lift of any planform. The following flap systems were selected as they represent the best mechanical systems and an empirical method that could be used in estimating the incremental lift coefficient was available. Because of its nature, VLAERO+© does not deal with devices that delay stall such as slotted or Fowler flaps, Krueger and slats. In this study, the general impact of these devices on the lift characteristics of the aircraft is estimated by empirically derived methods.

The basic leading and trailing edge flap dimensions are shown in Table 3.6 with the assumptions listed just below.

Table 3.6
Basic Trailing Edge Flap Dimensions.

Flap	$\frac{c_f}{c}$	δ (°)	$\frac{b_f}{b}$	$\frac{c'}{c}$
Trailing Edge Devices				
Plain	0.25	10,20, 30	0.6	0
Single Slotted	0.25	20, 30, 40	0.6	0
Single Slotted Fowler	0.25	20, 30, 40	0.6	1.05 - 1.1
Leading Edge Devices				
Nose Flap	0.2	5, 15, 25	0.75	0
Krueger Flap	0.1	20, 30, 40	0.75	1.1 - 1.05
Slat	0.2	5, 15, 25	0.75	1.04 - 1.08

Note: Per dimension definitions in section 3.2.1

Below in Figure 3.3 the results of the high lift device configuration are displayed for the swept and delta planforms.

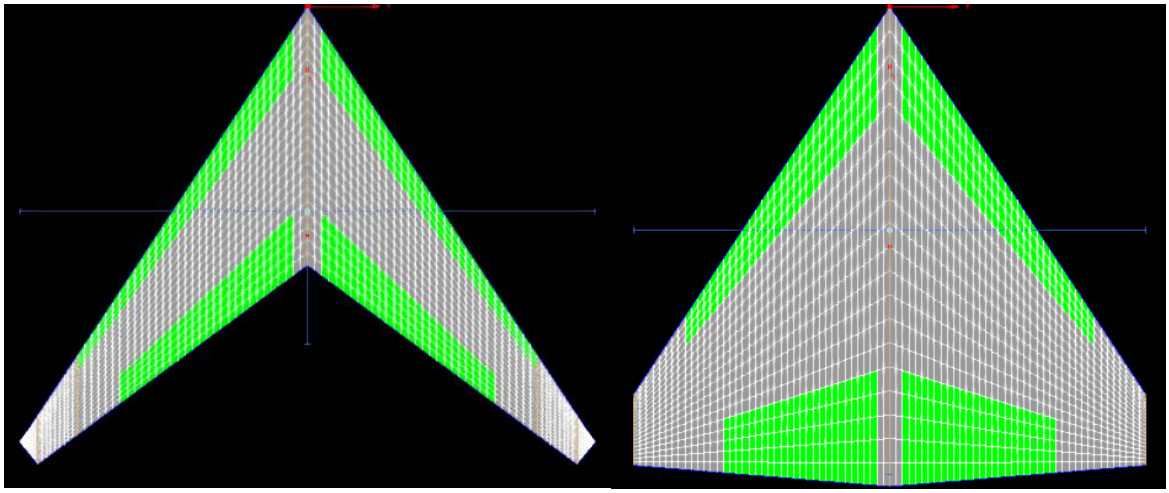

Figure 3.3 Swept Planform Displaying High Lift Device Configuration

The trailing edge flap assume all flaps start at 0.05b to account for the wing fairing and end at 0.65b to allow room for ailerons. No dropped ailerons were taken into account. All flaps are assumed to be well designed including the gaps for slotted and Fowler flaps.

The leading edge flaps assume all flaps start at 0.05b to account for the wing fairing and end at 0.75b. All flaps are well designed including the radius for the Krueger flap in addition to the gap for the slat.

In order to size the fixed swept and delta planforms for the approach conditions appropriately, the increment in lift, both ΔC_L and $\Delta C_{L_{MAX}}$ need to be calculated. Since VLAERO+© can only calculate plain flaps and nose flaps a consistent calculation method needed to be used for all high lift devices. As a result empirical formulations were used to calculate increment in lift from the high lift devices.

3.1.4 Incremental Lift Calculations

The results from VLAERO+© for the clean planforms were not altered. The increment in lift curve slope (ΔC_L) and the increment in maximum lift coefficient ($\Delta C_{L_{MAX}}$) were based on methods presented in Roskam's Airplane Design Part VI, (1990), which quoted frequently Hoak, D.E., et al USAF Stability and Control Datcom, (1978).

In order to estimate the lift increment due to flaps, ΔC_L and $\Delta C_{L_{MAX}}$ of the flaps needed to be calculated. First the airfoil section lift increment due to flaps ΔC_l was calculated then corrected for three-dimensional characteristics of the wing planform resulting in ΔC_L. Similarly the airfoil section $\Delta C_{l_{MAX}}$ was calculated and then corrected for three-dimensional characteristics of the wing planforms yielding $\Delta C_{L_{MAX}}$.

Plain Flap ΔC_l:

$$\Delta C_l = \delta_f \left(\frac{C_{l_\delta}}{\left(C_{l_\delta}\right)_{theory}} \right) \left(C_{l_\delta}\right)_{theory} \cdot k' \tag{1}$$

Where:

k' = Is a correction factors which accounts for nonlinearities at high flap deflections in Figure 3.4.

$\left(C_{l_\delta}\right)_{theory}$= Is found from Figure 3.5. It accounts for flap size and for thickness ratio.

$\frac{C_{l_\delta}}{\left(C_{l_\delta}\right)_{theory}}$ = Is a correction factor for plain flaps found from Figure 3.6.

δ_f = Is the flap deflection in radians.

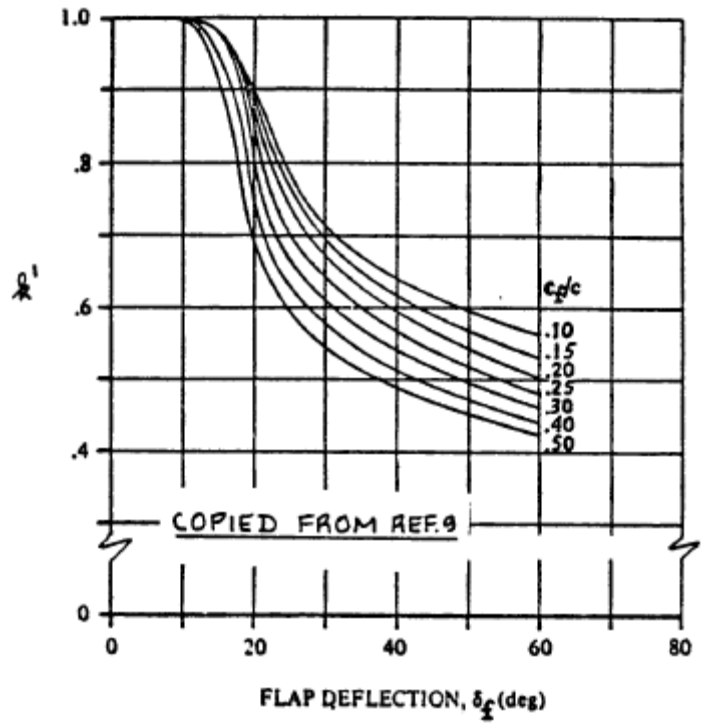

Figure 3.4 Correction Factor for Nonlinear Lift Behavior of Plain Flaps (Roskam, 1990).

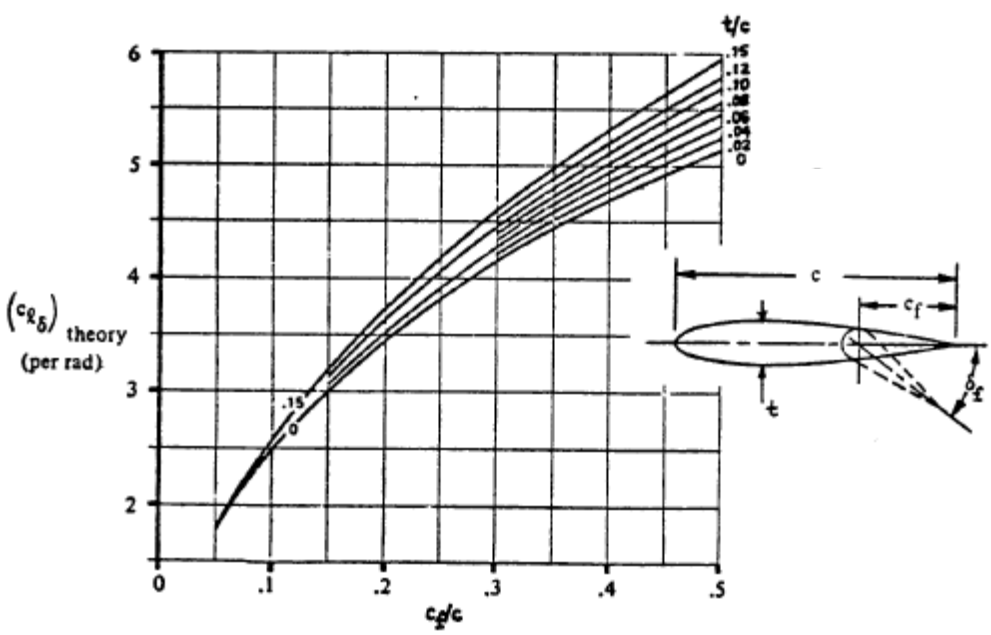

Figure 3.5 Lift Effectiveness of a Plain Flap (Roskam, 1990).

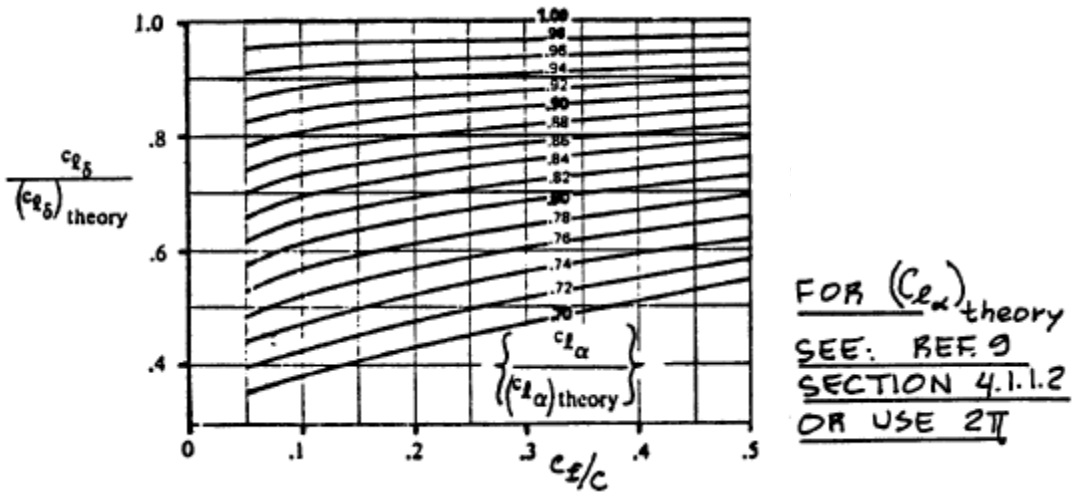

Figure 3.6 Lift Effectiveness of a Plain Flap (Roskam, 1990).

Slotted Flap ΔC_l:

$$\Delta C_l = C_{l_\alpha} \cdot \alpha_\delta \cdot \delta_f \tag{2}$$

Where:

C_{l_α} = Is the airfoil lift-curve slope with flaps up.

α_δ = Is the airfoil lift effectiveness parameter found from Figure 3.7.

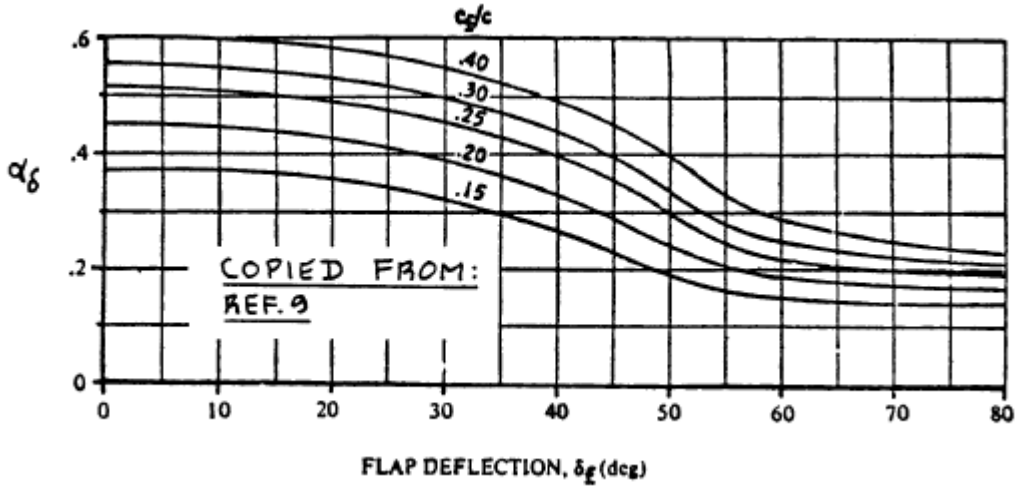

Figure 3.7 Lift Effectiveness of a Single Slotted Flap (Roskam, 1990).

Single Fowler Flap ΔC_l:

$$\Delta C_l = C_{l_\alpha} \cdot \alpha_\delta \cdot \left(\frac{c'}{c}\right) \delta_f \tag{3}$$

Where:

$\frac{c'}{c}$ = Is defined in Figure 3.8.

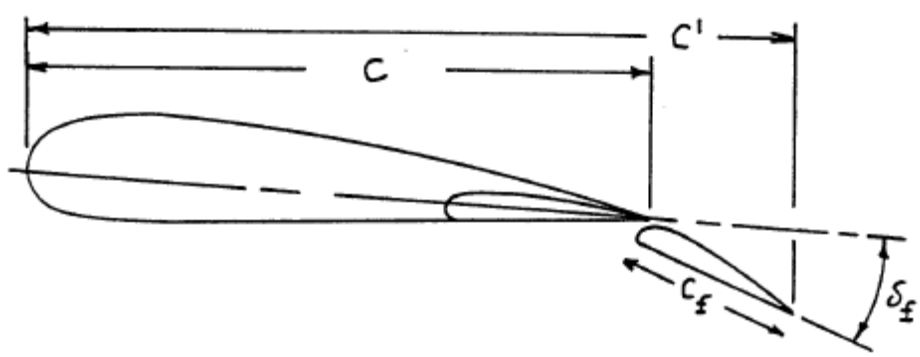

Figure 3.8 Fowler Flap Geometry (Roskam, 1990).

Trailing Edge Devices $\Delta C_{l_{MAX}}$:

$$\Delta C_{l_{MAX}} = k_1 k_2 k_3 \left(\Delta C_{l_{MAX}}\right)_{base} \tag{4}$$

Where:

k_1 = Factor which accounts for flap-chord to airfoil chord ratios different from 25 percent in Figure 3.9.

k_2 = Factor which accounts for flap angles different form the reference flap angle in Figure 3.9.

k_3 = Factor which accounts for flap motion as a function of flap deflection in Figure 3.10.

$\left(\Delta C_{l_{MAX}}\right)_{base}$ = Airfoil increment, maximum lift coefficient due to flaps as determined in Figure 3.11. Note that the data in Figure 3.11 are based on a 25 percent referenced flap-chord to airfoil chord ratio and on a reference flap deflection angled defined in Figure 3.9.

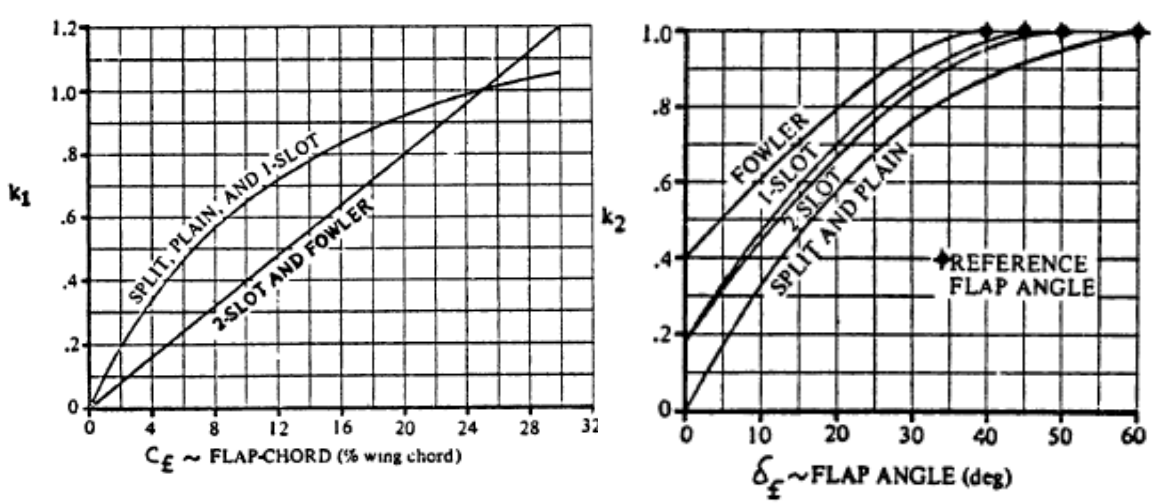

Figure 3.9 Flap Chord Correction Factor (k_1) and Flap Angle Correction Factor (k_2) (Roskam, 1990).

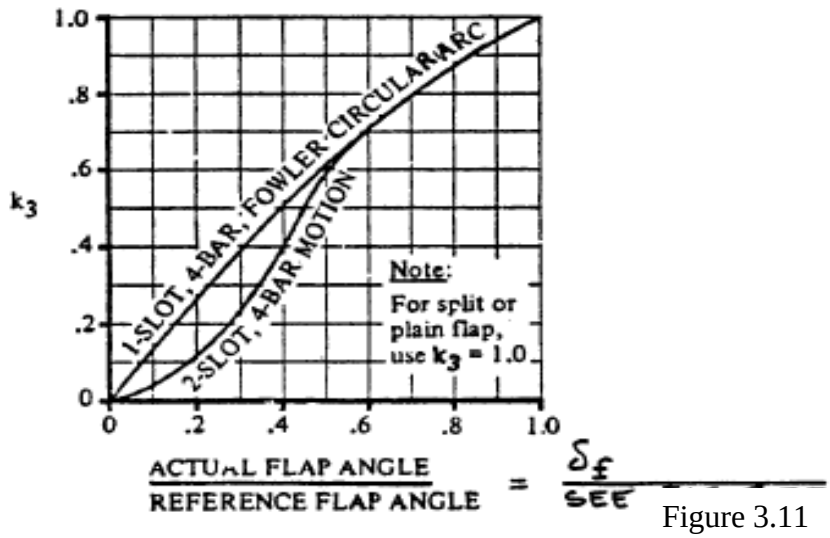

Figure 3.10 Flap Motion Correction Factor (Roskam, 1990).

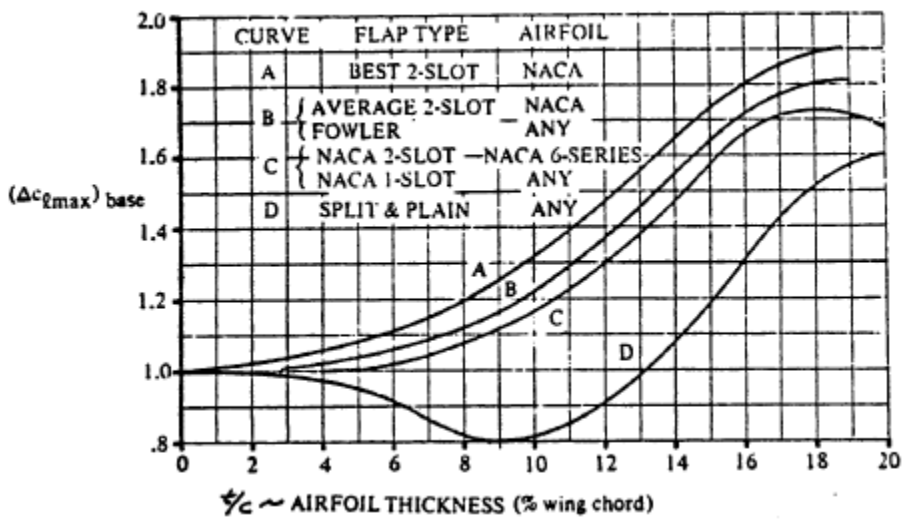

Figure 3.11 Basic Airfoil Maximum Lift Increment due to Trailing Edge Flaps (Roskam, 1990).

Even though empirical estimations for leading edge devices are not as reliable or developed as those for trailing edge devices a similar process was used to calculate ΔC_L for the various leading edge devices.

Nose Flap

$$\Delta C_l = C_{l_\delta} \cdot \delta_f \tag{5}$$

Where:

C_{l_δ} = Leading edge flap effectiveness parameter for a nose flap from Figure 3.12.

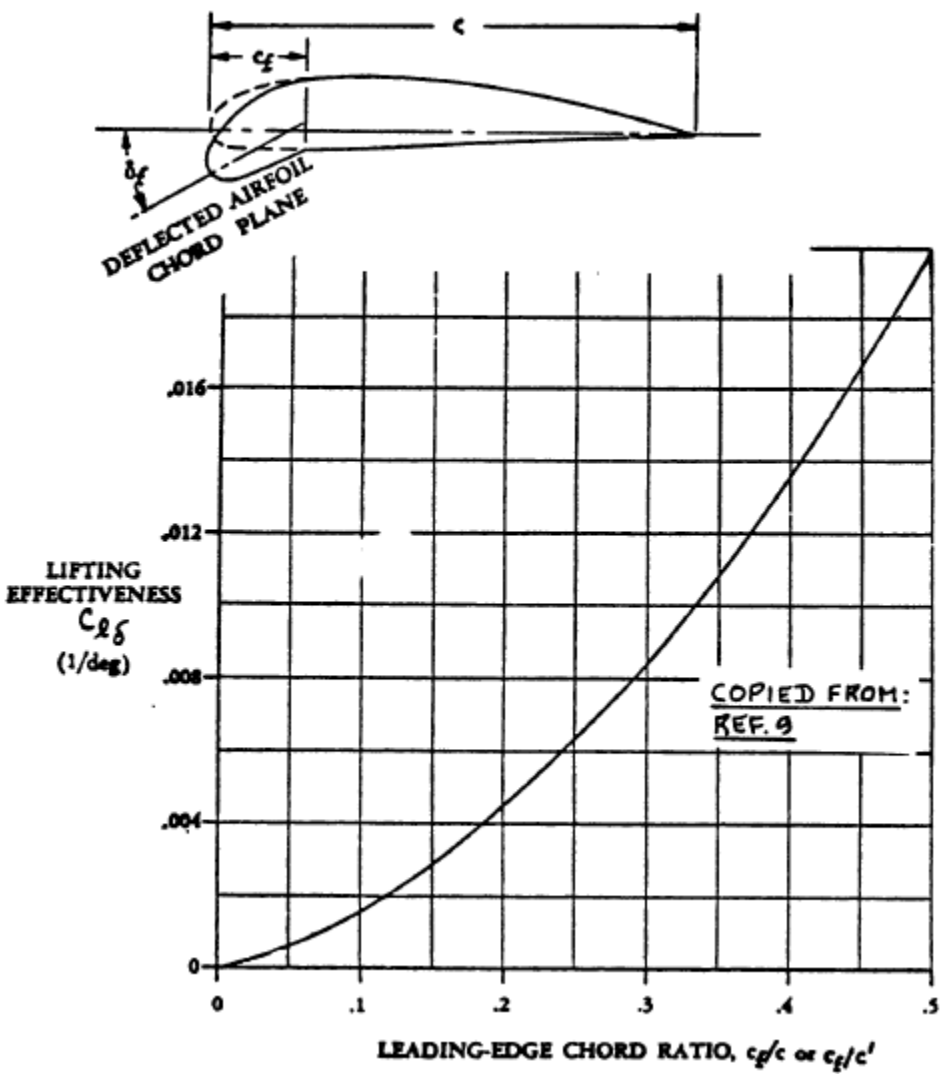

Figure 3.12 Lift Effectiveness of a Leading Edge Flap (Roskam, 1990).

δ_f = Nose flap deflection angle in (°) referenced in Figure 3.12.

Krueger Flap

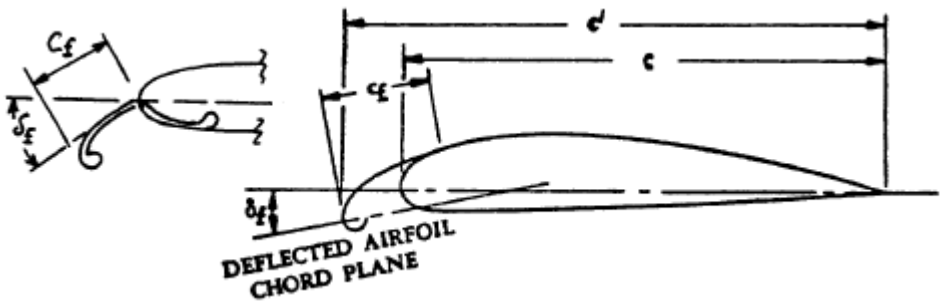

Figure 3.13 Krueger Flap Geometry (Roskam, 1990).

$$\Delta C_l = C_{l_\delta} \cdot \delta_f \left(\frac{c'}{c}\right) \tag{6}$$

C_{l_δ} = Leading edge flap effectiveness parameter for a Krueger flap from Figure 3.13. Use $\frac{c_f}{c'}$ as the flap-chord to wing-chord ratio.

δ_f = Krueger flap deflection angle in (°) referenced in Figure 3.13.

$\frac{c'}{c}$ = Krueger flap chord ratio defined in Figure 3.13.

Leading Edge Slat

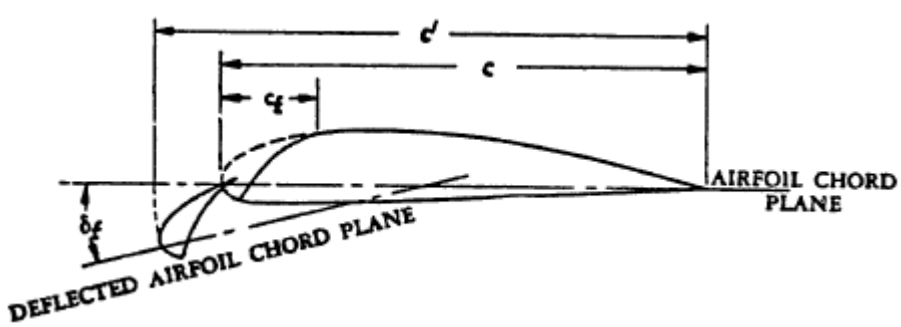

Figure 3.14 Leading Edge Slat Geometry (Roskam, 1990)

$$\Delta C_l = C_{l_\delta} \cdot \delta_f \left(\frac{c'}{c}\right) \tag{7}$$

C_{l_δ} = Leading edge flap effectiveness parameter for a leading edge slat from Figure 3.14. Use $\frac{c_f}{c'}$ as the flap-chord to wing-chord ratio.

δ_f = Slat deflection angle in (°) referenced in Figure 3.14.

$\frac{c'}{c}$ = Leading edge slat chord ratio defined in Figure 3.14.

The maximum wing incremental lift coefficient due to trailing and leading edge high lift devices were found from

$$\Delta C_{L_W} = K_b(\Delta C_l)\left(\frac{C_{L_{\alpha_W}}}{C_{l_\alpha}}\right)\left(\frac{(\alpha_\delta)_{C_L}}{(\alpha_\delta)_{C_l}}\right) \tag{8}$$

Where:

K_b = Flap-span factor as obtained from the procedure suggested in the upper part of Figure 3.15 but with the data from the bottom section of Figure 3.15.

ΔC_l = Airfoil lift increment due to flaps.

$C_{L_{\alpha_W}}$ = Wing lift curve slope.

C_{l_α} = Wing airfoil lift curve slope.

$\left(\frac{(\alpha_\delta)_{C_L}}{(\alpha_\delta)_{C_l}}\right)$ = Ratio of the three-dimensional flap effectiveness parameter to the two-dimensional flap-effectiveness parameter found in Figure 3.16.

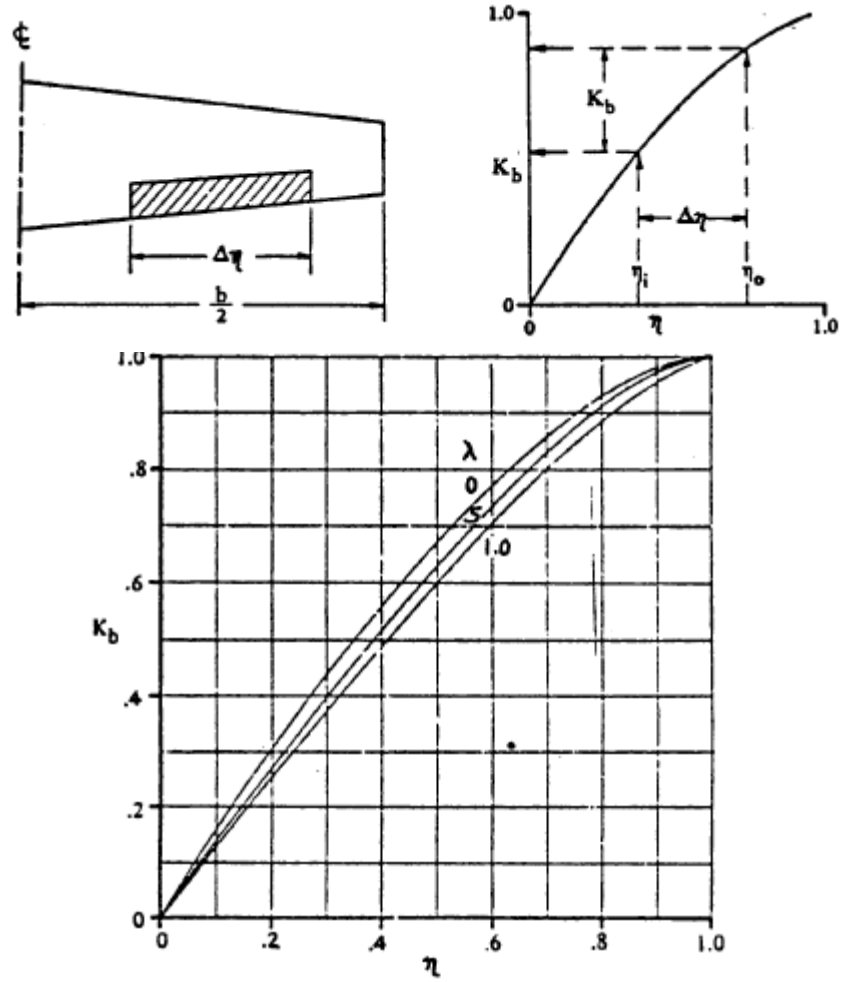

Figure 3.15 Effects of Taper Ratio and Flap Span on Kb (Roskam, 1990).

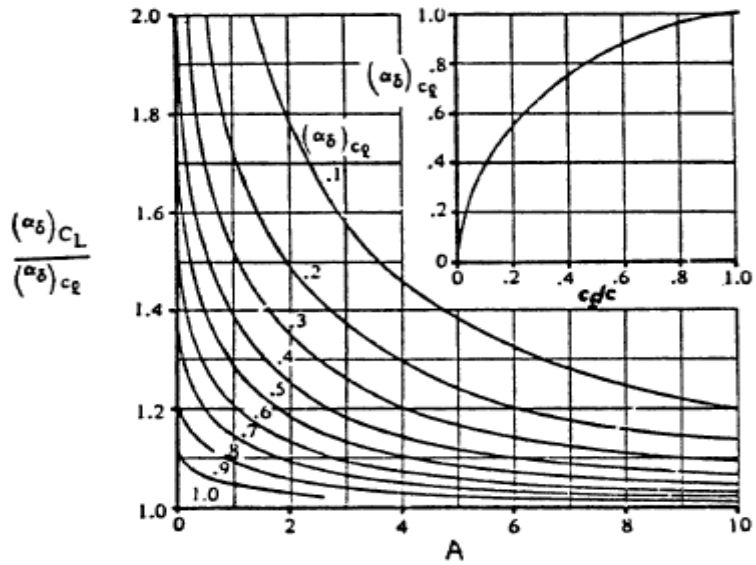

Figure 3.16 Effects of Aspect Ratio and Flap-Chord Ratio on Three-dimensional Flap Effectiveness (Roskam, 1990)

Roskam also adds a note: "If a mechanical high lift system consists of a combination of leading and trailing edge high lift devices, the method should be applied to each type of device separately. This resulting increments in lift coefficients can then be added."

The maximum wing incremental lift coefficient due to trailing edge flaps were found from

$$\Delta C_{L_{MAX}} = \left(\Delta C_{l_{MAX}}\right)\left(\frac{S_{w_f}}{S}\right)K_{\Lambda} \tag{9}$$

Where:

$\Delta C_{l_{MAX}}$ = Airfoil incremental lift coefficient due to trailing edge flaps in Eq. 4.

$\frac{S_{w_f}}{S}$ = Flapped wing area defined visually in Figure 3.18 and calculated with Eq.10

K_Λ = Planform correction factor found from Figure 3.17.

$$\frac{S_{w_f}}{S} = \frac{\eta_0 - \eta_i}{b}\left(1 + \frac{1-\lambda}{1+\lambda}\left(1 - \frac{\eta_0 - \eta_i}{b}\right)\right) \tag{10}$$

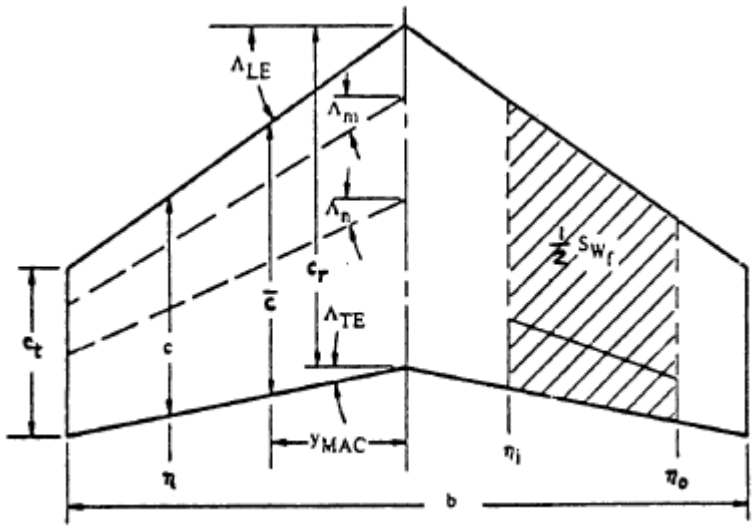

Figure 3.18 Definition of Flapped Wing Area (Roskam, 1990).

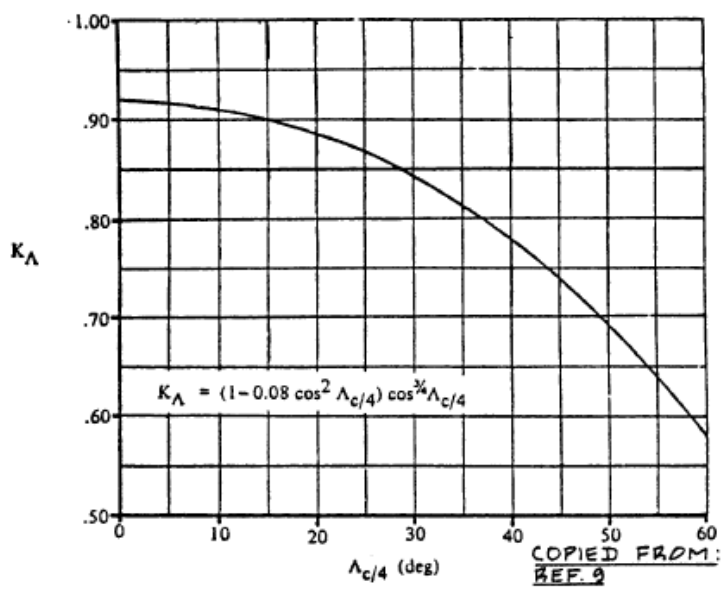

Figure 3.17 Effects of Sweep on Planform Correction Factor (Roskam, 1990).

3.1.5 Drag

VLAERO+© only calculates induced drag. Thus, alternate methods were needed to estimate the total drag of the wing. The drag of the models was calculated using the methods presented in Nicolai and Carichner, Fundamentals of Aircraft and Airship Design, (2010).

The following was used to estimate the subsonic drag during approach:

$$C_D = \left(C_{D_0}\right)_{wing} + C_{D_i} \tag{11}$$

Where:

$\left(C_{D_0}\right)_{wing}$ = Subsonic zero lift drag coefficient of the wing from Eq. 11.

C_{D_i} = Induced drag coefficient.

$$\left(C_{D_0}\right)_{wing} = C_f \left(1 + L\left(\frac{t}{c}\right) + 100\left(\frac{t}{c}\right)^4\right) R \frac{S_{wet}}{S_{ref}} \tag{12}$$

Where:

C_f = Turbulent flat plate skin friction coefficient from Figure 3.19.

L =Airfoil thickness location parameter.

L = 1.2 for maximum $\frac{t}{c}$ located at $x \geq 0.3c$.

L = 2.0 for maximum $\frac{t}{c}$ located at $x < 0.3c$.

$\left(\frac{t}{c}\right)$ = Maximum thickness ratio of the airfoil.

R = Lifting surface correlation factor obtained from Figure 3.20.

$\frac{S_{wet}}{S_{ref}}$ = Wetted area of the wing from Eq.13.

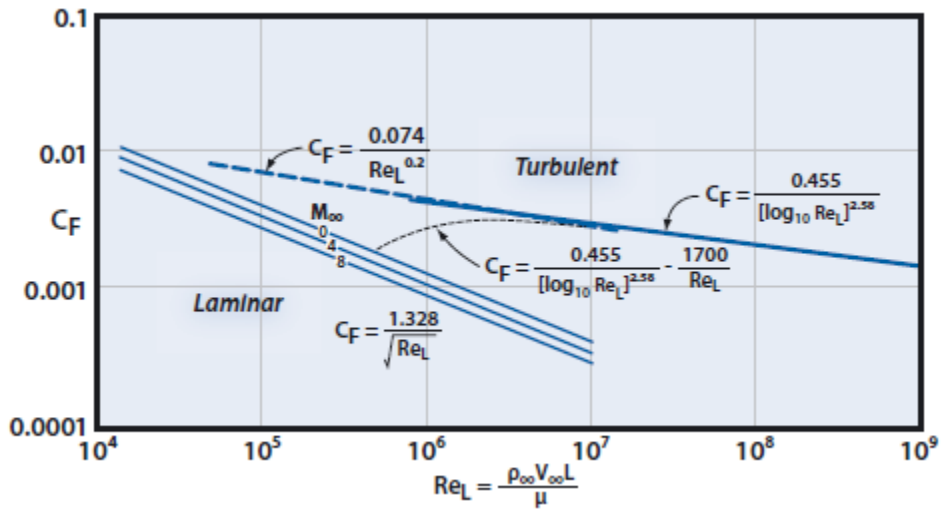

Figure 3.19 Skin Friction Coefficient over a Flat Plate (Nicolai & Carichner, 2010)

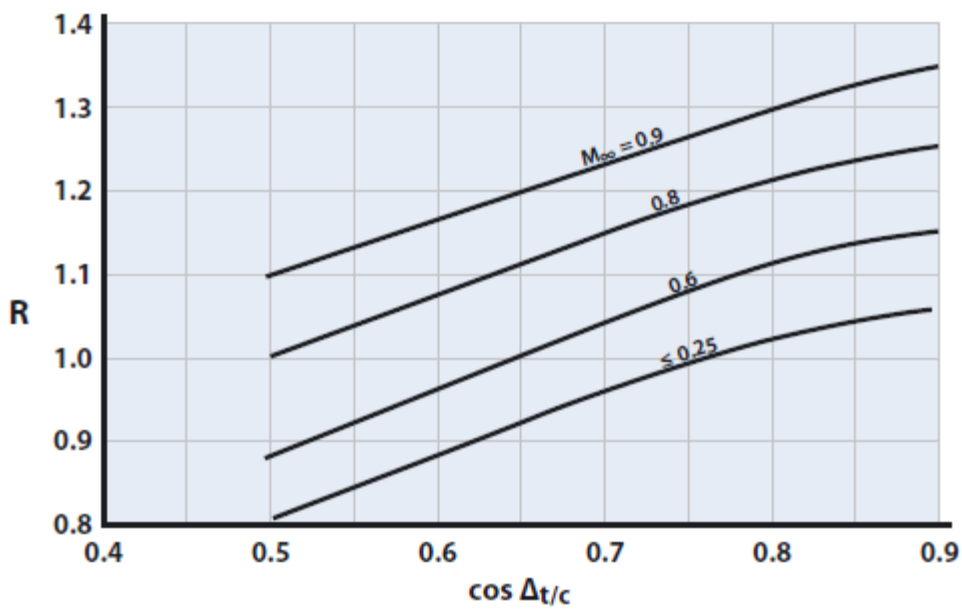

Figure 3.20 Lifting Surface Correlation Factor for Wing Subsonic Induced Drag Coefficient (Nicolai & Carichner, 2010).

$$\frac{S_{wet}}{S_{ref}} \approx 2\left(1 + 0.2\frac{t}{c}\right)S_e \tag{13}$$

Where:

S_e = Exposed area

The following was used to estimate the supersonic drag during cruise:

$$C_D = \left(C_{D_0}\right)_{SS\ wing} + C_{D_i} \tag{14}$$

Where:

$\left(C_{D_0}\right)_{SS\ wing}$ = Supersonic zero lift drag coefficient of the wing from Eq. 15.

$$\left(C_{D_0}\right)_{SS\ wing} = C_{D_f} + C_{D_W} \tag{15}$$

Where:

C_{D_f} = Supersonic skin friction expressed in Eq. 16.

C_{D_W} = Wing supersonic wave drag coefficient developed from supersonic linear theory expressed in Eq. 18 for a round-nose, subsonic leading edge.

$$C_{D_f} = C_f\frac{S_{wet}}{S_{ref}} \tag{16}$$

Where:

$$C_f = \left(\frac{C_{f_c}}{C_{f_i}}\right)C_{f_i} \tag{17}$$

Where:

$\frac{C_{f_c}}{C_{f_i}}$ = is obtained from Figure 3.21.

C_{f_i} = is determined the same way for subsonic using cutoff and flight Reynolds number comparisoin.

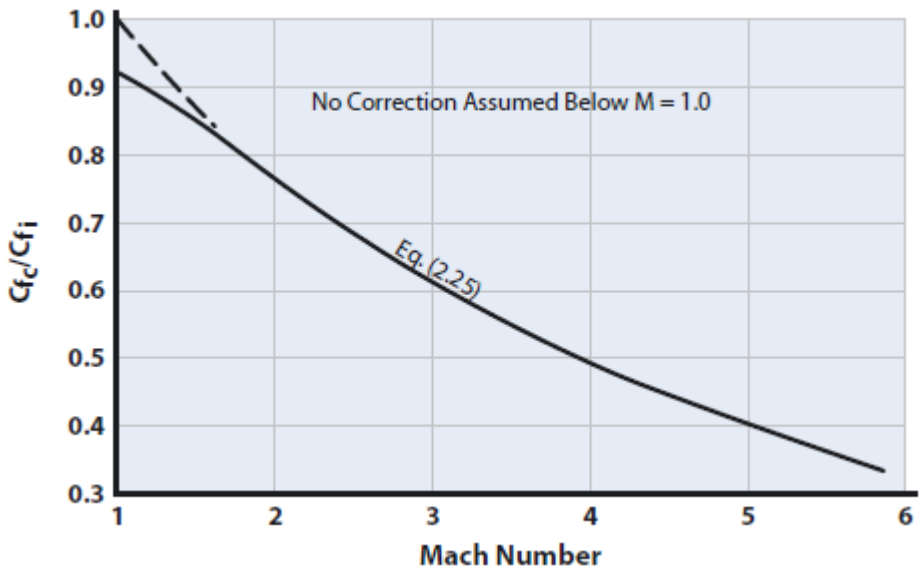

Figure 3.21 Compressibility Effect on Turbulent Skin Friction (Nicolai & Carichner, 2010).

$$C_{D_W} = C_{D_{LE}} + \frac{16}{3} cot\Lambda_{LE} \left(\frac{t}{c}\right)^2 \frac{S_e}{S_{ref}} \tag{18}$$

Where:

$C_{D_{LE}}$ = Supersonic round leading edge bluntness coefficient from Figure 3.22. Where b is the span (ft), r_{LE} is the radius of the leading edge at the mean aerodynamic chord (ft).

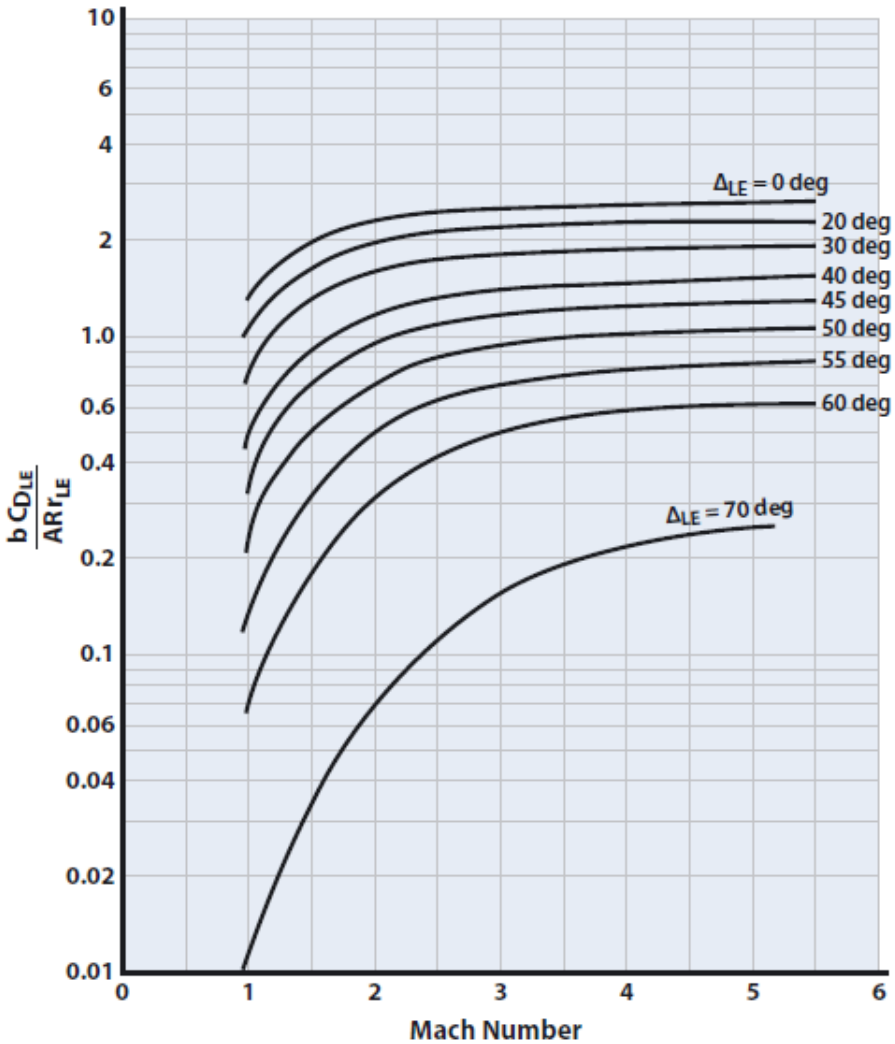

Figure 3.22 Supersonic Round Leading Edge Bluntness Drag Coefficient (Nicolai & Carichner, 2010).

3.1.7 High Lift Device Weight

The total weight of the high lift devices may be estimated by adding the individual weights of the leading edge device and the trailing edge device. This method is from Torenbeek (1982):

$$\frac{W_{tef}}{S_f} = Constant \cdot k_f \left(S_f b_{fs}\right)^{\frac{3}{16}} \cdot \left[\left(\frac{V_{lf}}{100}\right)^2 \frac{\sin\delta_f \cos\Lambda_f}{\left(\frac{t}{c}\right)_f}\right]^{3/4} \tag{19}$$

Where:

$\frac{W_{tef}}{S_f}$ = Trailing edge flap weight per flap area (lb/ft^2)

$Constant =$ 0.105 when W_{tef} is in lb, S_f in ft^2, b_{sf} in ft and V_{lf} in kts or 2.70 when W_{tef} is in kg, S_f in m^2, b_{sf} in m and V_{lf} in m/s

$k_f = k_{f1} + k_{f2}$

k_{f1}= 1.0 : Single slotted; double slotted, fixed hinge

1.15: Double slotted, 4-bar movements; single slotted Fowler

1.30: Double slotted Fowler

1.45: Triple slotted Fowler

k_{f1}= 1.0 : Slotted flaps with fixed vane

1.25: Double slotted flaps with “variable geometry”, i.e. extending flaps with separately moving vanes or auxiliary flaps

S_f= Flap area (ft^2)

V_{lf} = Design speed flaps in landing configuration

b_{sf} = Structural flap span along average sweep angle of flap structure

Λ_f= Average sweep angle of flap structure

$\left(\frac{t}{c}\right)_f$ = Thickness/chord ratio of flap

The specific weight of leading edge high lift devices can be read from Figure 5.1.

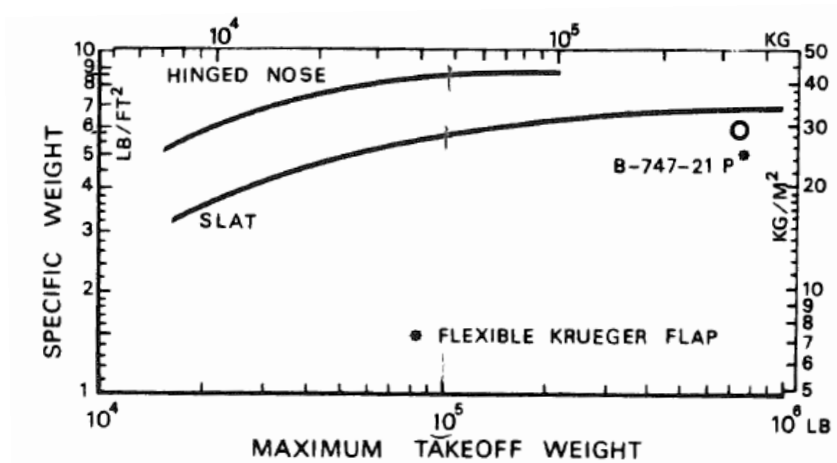

Figure 3. 23 Specific Weight of Leading Edge High Lift Devices (Torenbeek, 1982)

3.1.8 Wing Weight

The metal wing weight estimation method is from Nicolai and Carichner Fundamentals of Aircraft and Airship Design (2010). The wing weight is shown in Eq. 21 with the weight of trailing edge high lift devices in Eq.22 and leading in Figure 5.1.

U.S. Air Force (USAF) Fighter Aircraft:

$$W_t = 3.08\left(\frac{K_{PIV}\cdot N\cdot W_{To}}{\frac{t}{c}}\left\{\left[\tan\Lambda_{LE} - \frac{2(1-\lambda)}{AR(1+\lambda)}\right]^2 + 1.0\right\}\times 10^{-6}\right)^{0.593} \quad (20)$$

$$[(1+\lambda)AR]^{0.89}{S_w}^{0.741}$$

Where:

K_{PIV} = Wing variable-sweep factor

= 1.00 for fixed wings

= 1.175 for variable-sweep wings

N = Ultimate load factor

= 13.5 for fighter aircraft (based on a design limit load factor of +9.0 and a margin of safety of 1.5)

= 4.5 for bomber and transport aircraft (based on a design limit load factor of +3.0)

AR = Aspect ratio

λ = Taper ratio

S_w = Wing area (ft^2)

3.1.8 Statistical Aircraft Empty Weight

Although the planform weights cannot be precisely calculated, a weight estimation was used in an attempt to compare a first order approximation of their specific air range (SAR) ratios using Eq. 20. This comparison is under the assumption of the same cruise speed in addition to the same thrust specific fuel consumption. Even though the actual specific fuel consumption of the planforms would be different, the values are likely to be in the same order of magnitude. Typically the weight used is the weight of the entire aircraft, however in this case, the aircraft weight is not known. Instead, a series of weights were calculated and added together to estimate the aircraft's empty weight. This method

assumes the structure of the aircraft would be identical except the wings. The aircraft weight consists of a statistically estimated empty weight (W_X) and a wing weight (W_{wing}). The W_{wing} consists of the weight of the wing in addition to the weight of any high lift devices. W_X is the empty weight of the aircraft without the wings. W_X was found by creating an expression that relates wing weight to the empty weight minus wing weight from statistical data of other aircraft with similar MTOW. This result is expressed in Eq. 21. The data pool of aircraft consisted of only straight tapered wings. As a result, the wing area of the fixed swept wing was used to calculate W_X in order to keep a consistent basis with the historical data and to give all planforms an equal starting point.

Statistical W_X function:

$$W_X = 2.665\left(W_{wing}\right) \tag{21}$$

This equation produces an estimated W_X of 33,831 lb. This value will be used for all three planforms as the base weight of the structure minus the wing weight. To obtain the wing weight and flap weight Eq. 19 and Eq. 20 were used.

3.1.9 Specific Air Range (SAR) Ratio

The low speed aerodynamic performances of the three planforms are comparable in the sense that they all satisfy their specific lift-goal requirements. In order to further understand how the results may affect the cruise performance of the swept and delta planform, an attempt to quantify the results was made.

The specific range ratios were determined from Eq. 22.

$$\frac{SAR_{Planform}}{SAR_{Baseline}} = \frac{\frac{V\cdot(L/D)_{Planform}}{c\cdot W}}{\frac{V\cdot(L/D)_{Baseline}}{c\cdot W}} = \frac{(L/D)_{Planform}}{(L/D)_{Baseline}} \frac{\left((W_X)+W_{wing}\right)_{Baseline}}{\left((W_X)+W_{wing}\right)_{Planform}} \tag{22}$$

Where:

$(L/D)_{Planform}$ = 94.3% $(L/D)_{Max}$

W_X= Weight of the empty aircraft without wings.

W_{wing}= Weight of wing and high lift devices.

3.2 VLAERO+©

VLAERO+© is a classical flat surface vortex-lattice method based aerodynamic program. The effects of Mach number are included through Prandtl-Glauert scaling. VLAERO+© can perform supersonic calculations by limiting the influence of each panel to the region inside the Mach cone with an apex at the section leading edge and an angle equal the Mach angle. Since shock formation is not modeled, wave drag is not computed (Analytical Methods, Inc., VLAERO+© User Manual, 2007).

3.2.1 Mesh Density for the Study

A panel density study was performed using the swept aft model with α = 0° at approach conditions in order to observe any changes in the results. VLAERO+© limits the number of chordwise panels to 20. Therefore 20 chordwise panels were used. The study therefore focused on the spanwise distribution and any noticeable variations with the overall C_L. The study is visually represented in Figure 3.24.

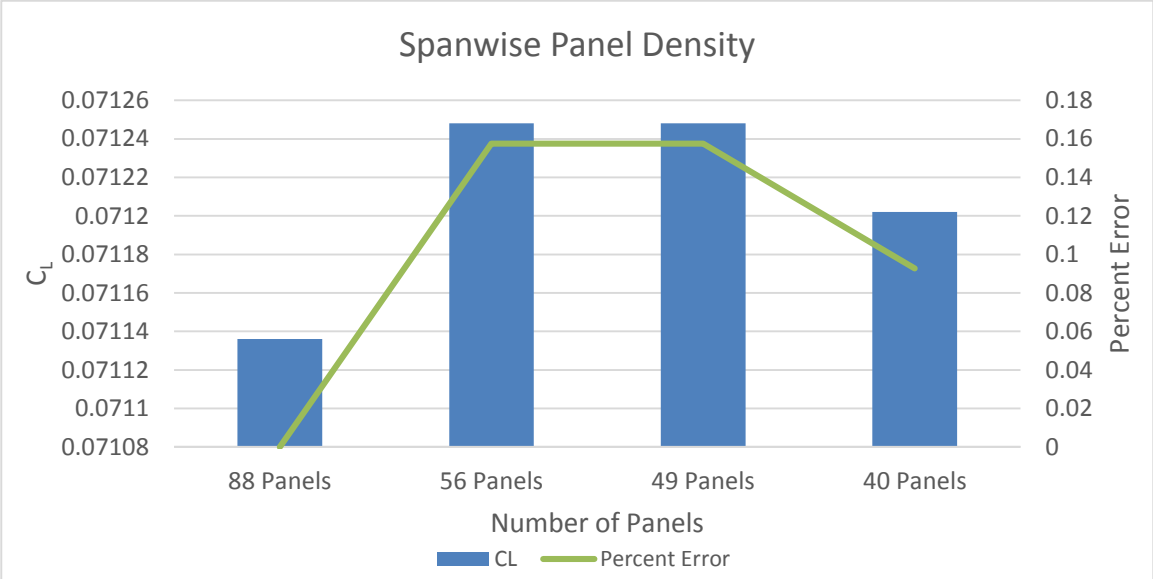

Figure 3.24 Spanwise Panel Density Study.

Figure 3.24 shows little variation between the panel densities with the percent difference in C_L at α = 0° is less than 0.2% when compared to the highest density of spanwise panels. The variation in lift coefficient did not happen until the 10^{-4} decimal place, which is well beyond the sensitivity of this study. Therefore, 88 spanwise panels were used.

Chapter IV

Results

4.1 Initial Fixed Swept and Delta Planform

4.1.1 Fixed Swept Wing

As the swept wing began as the swept aft position of the variable geometry wing, the final swept wing is similar to the variable geometry wing but slightly larger.

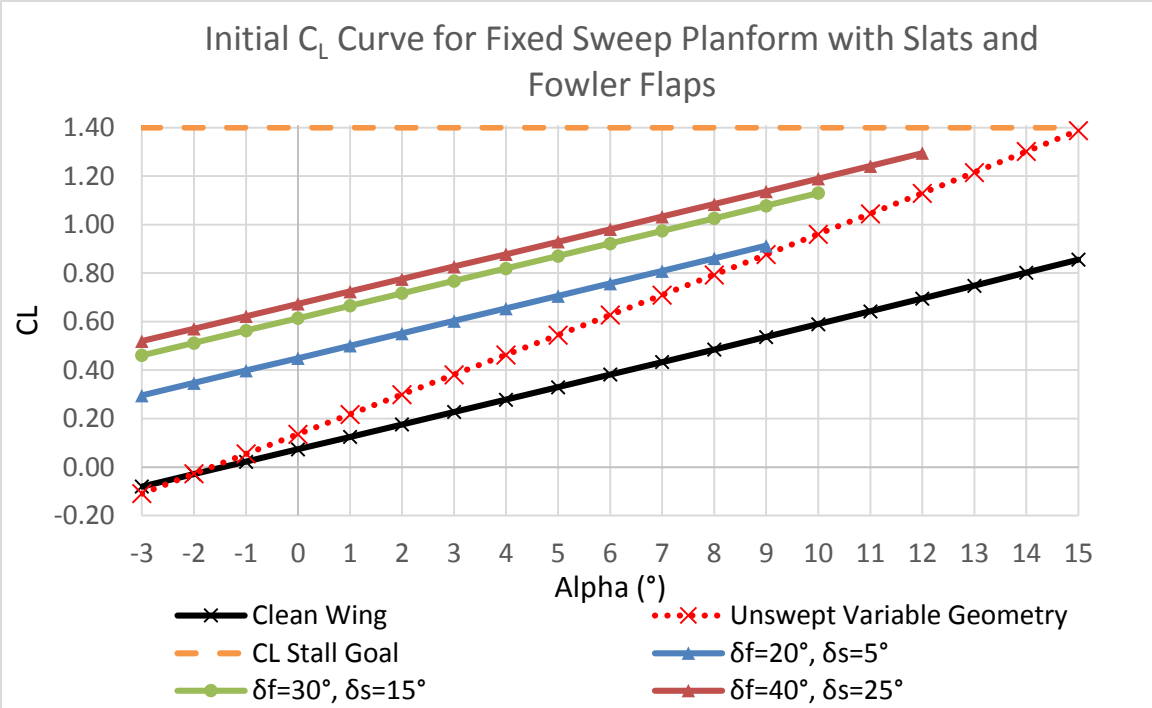

Figure 4.1 Initial Lift Curve Slope of Fixed Sweep Planform 1,114 ft^2

Figure 4.1 shows the initial fixed sweep planform not capable of producing the required lift below α = 15°, even with the addition of Fowler flaps and slats. An increase in planform area was required in order to achieve this goal. The root chord and span were increased until the planform produced the required lift at the stall condition.

4.1.2 Delta Wing

The area required to have similar cruise performance will be drastically less than that required for the low speed performance. Figure 4.2 shows the planform is not capable of producing the required at less than α = 15°. An increase in planform area is required in order to achieve this goal. Therefore the area of the delta planform will need a large increase in area from what is shown above.

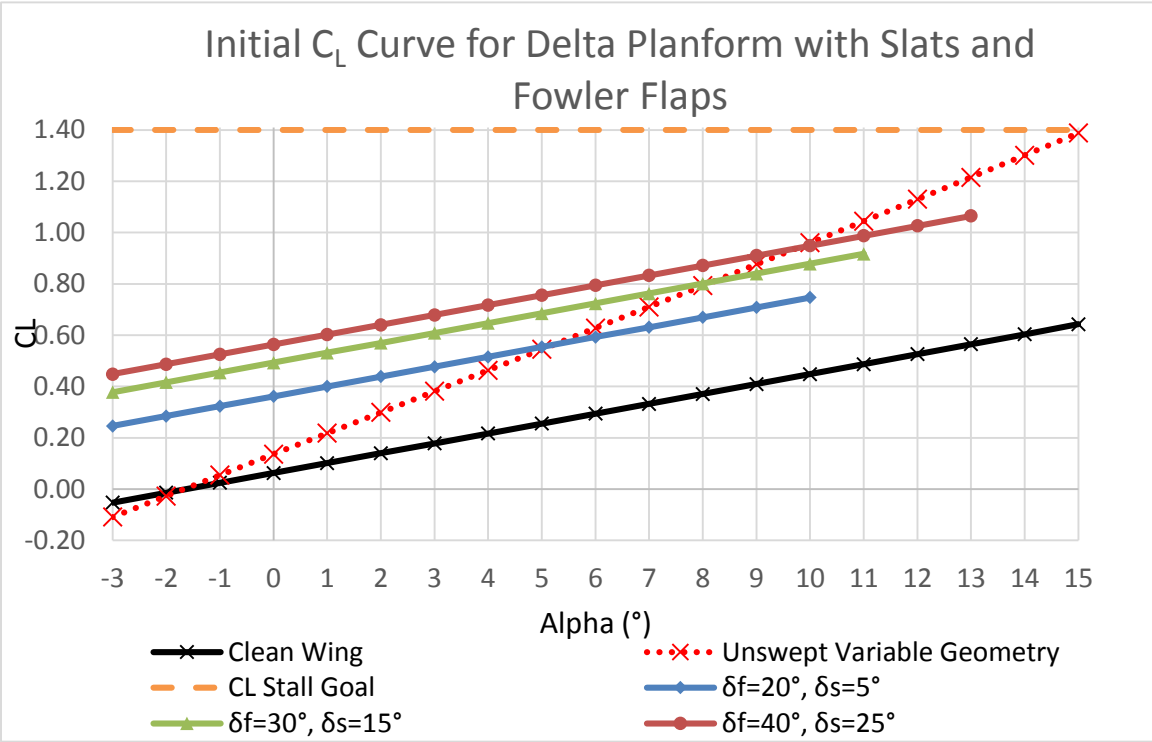

Figure 4.2 Initial Lift Curve Slope of Delta Planform1,114 ft^2

It is very apparent that both planforms need an increase in area. To minimize this, high lift devices were used and their maximum increment in lift were determined.

4.2 Lift Augmentation Devices

Shown are the results for the various high lift devices applied to the respective planforms. Figure 4.3 shows the results from the addition of trailing edge devices on the fixed sweep and delta planforms. With the method outlined in Roskam (1990), the nonlinearity of the flap effectiveness with increasing flap deflection angle was captured.

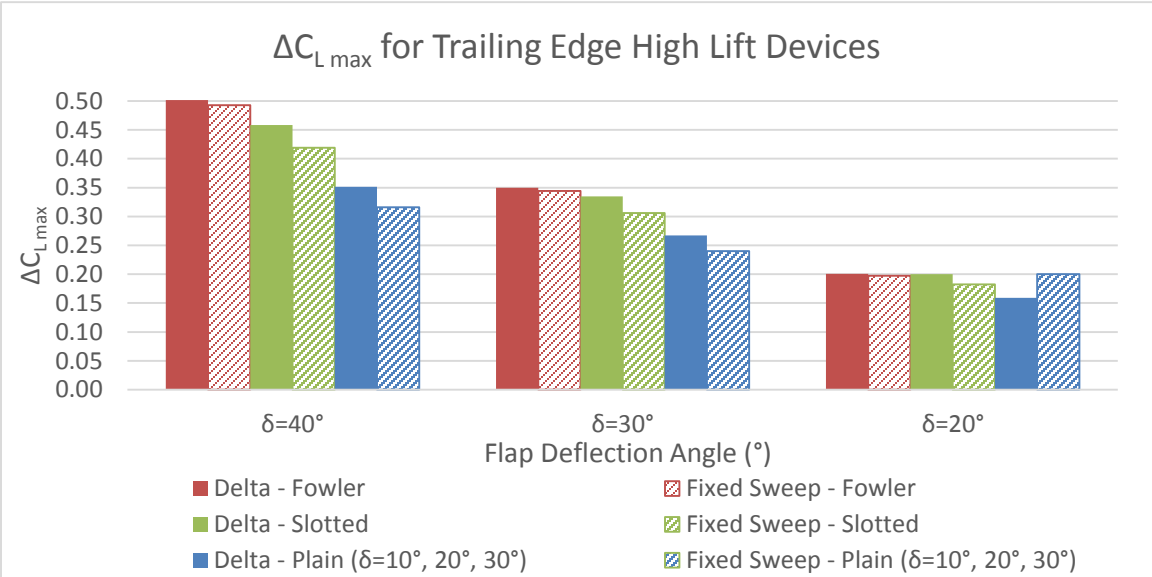

Figure 4.3 $\Delta C_{L_{max}}$ Results for Trailing Edge Devices Results on the Swept and Delta Planforms at Approach Conditions.

The plain flap is comparable to the single slotted and single Fowler flap at the lower deflection angles but when deflected past δ = 20° the slotted and Fowler flap significantly outperform the plain flap.

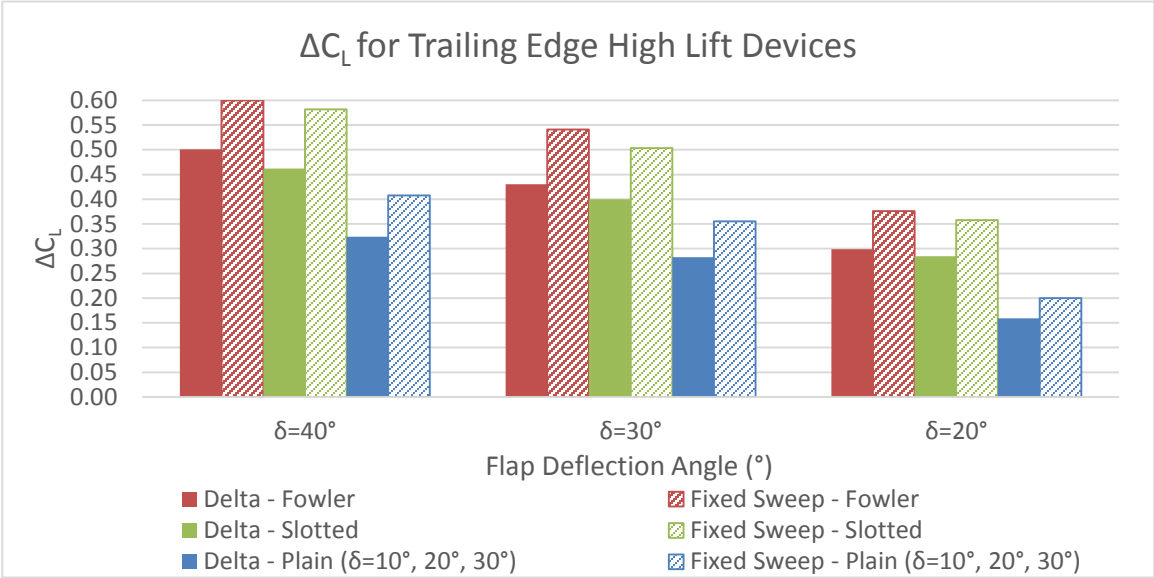

Figure 4.4 $\Delta \boldsymbol{C_L}$ Results for Trailing Edge Devices Results on the Swept and Delta Planforms at Approach Conditions.

Figure 4.4 shows the results of the ΔC_L due to trailing edge flaps. Unlike the $\Delta C_{L_{max}}$ the fixed sweep planform produces a larger lift increase than that of the delta wing. The fixed sweep planform increment is larger across all the deflection ranges.

Figure 4.5 shows the results from the addition of leading edge devices on the fixed sweep and delta planforms. The nose flap had a relatively consistent lift increment with deflection angle, whereas the slat, similar to the slotted and Fowler flaps, only seemed to be effective at the higher deflection angles where separation is likely to occur. The Kruger flap was effective at all of the deflection angles (δ = 40°, 30°, 20°).

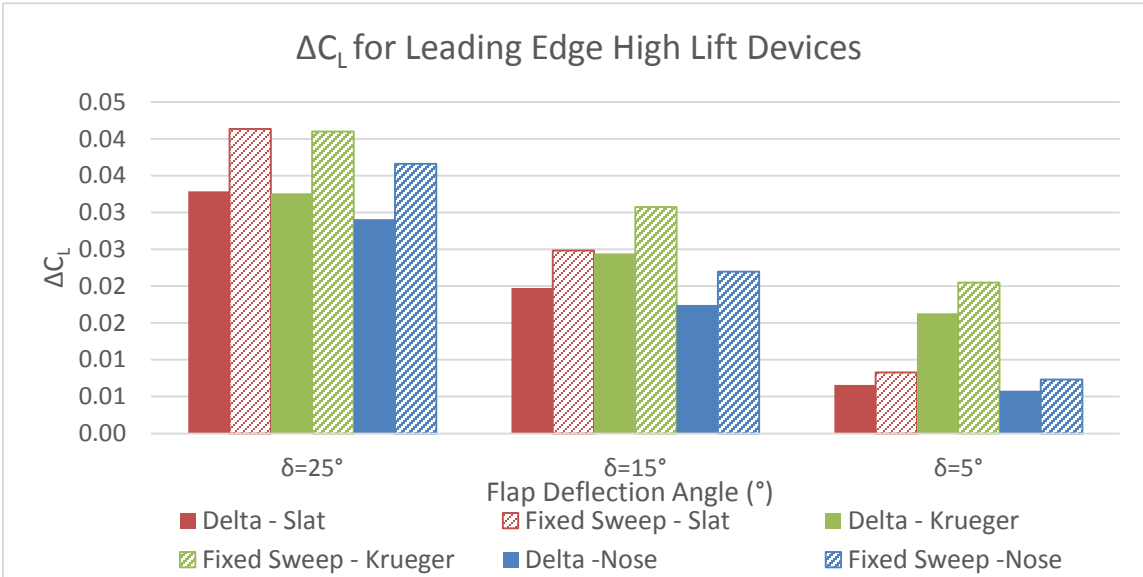

Figure *4.5* ΔC_L Results for Leading Edge Devices Results on the Swept Planform at Approach Conditions.
NOTE: Kruger deflection angles are (δ = 40°, 30°, 20°) left to right on the graph.

Figure 4.6 shows the C_L for the swept planform with use of slats and Fowler flaps. The planform was successfully able to produce the required amount of lift.

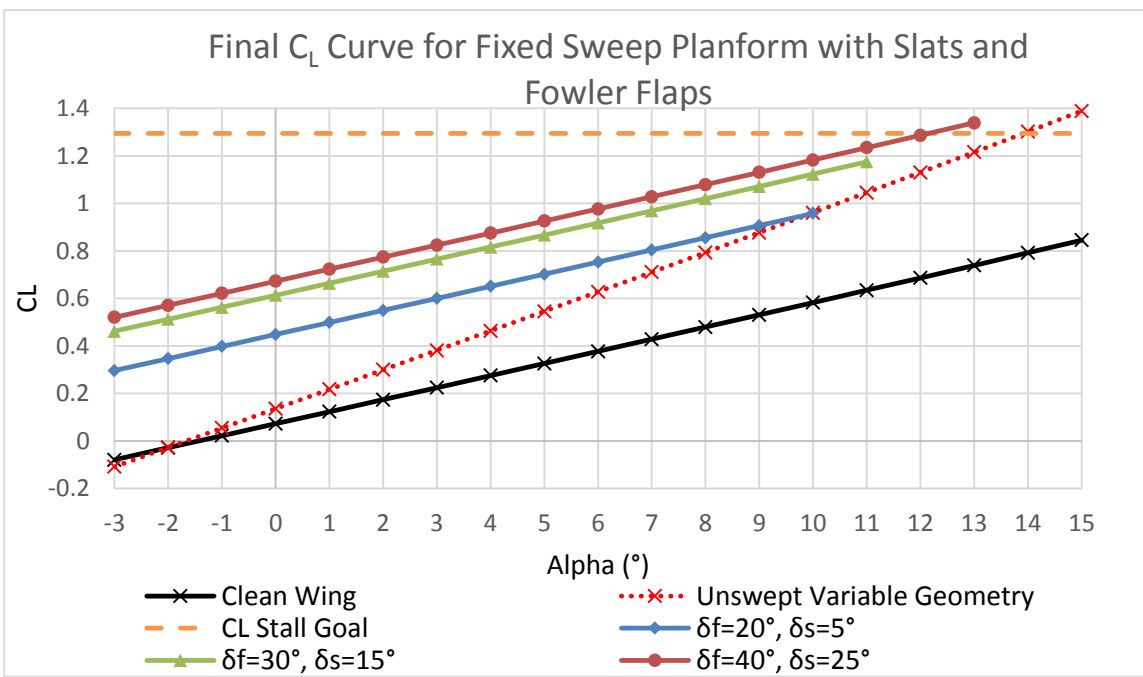

Figure 4.6 Final C_L Results for the Swept Planform with High Lift Devices. This is with slats and Fowler flaps.

The C_L goal is lowered from the initial graph shown Figure 4.1 because of the area increase. The $\Delta C_{L_{MAX}}$ of the Fowler flap at higher flap deflection angles is evident from Figure 4.6. $C_{L_{MAX}}$ occurs at α = 13° with a flap deflection angle δ_f = 40° and a slat deflection angle δ_s = 25°. As previously shown, the maximum incremental lift from the Fowler flaps is poor at low deflection angles but substantially increases in effectiveness at higher flap deflections angles, especially when compared against other non-slotted high lift devices.

Figure 4.7 shows the lift coefficient for the Delta planform with slats and Fowler flaps. Even though the $C_{L_{MAX}}$is less than that of the swept forward wing it has a large enough area to compensate and still reach the C_L goal as shown. The C_L goal is even lower than the goal for the swept planform because of the larger increase in wing area. Similar to

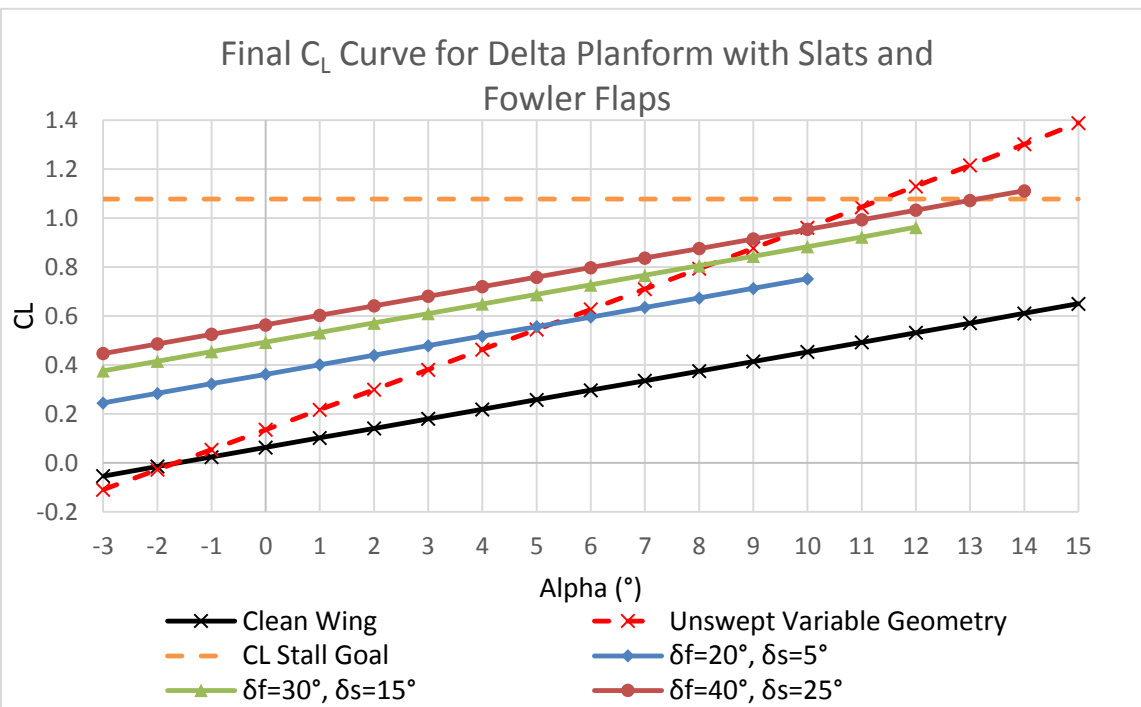

Figure 4.7 Final C_L Results for the Delta Planform with slats and Fowler flaps.

the fixed sweep wing, the $\Delta C_{L_{MAX}}$ at low deflection angles is small, but significantly

increases as flap deflection increases. $C_{L_{MAX}}$ occurs at α = 14° with a flap deflection angle δ_f = 40° and a slat deflection angle δ_s = 25°.

Using this Leading-Edge Suction Analogy by Polhamus mentioned in section 2.1.4, an estimate of the possible lift increase of vortex lift on the delta planform can be performed. Figure 4.8 has been reproduced from Polhamus (1966), to show the potential lift increment over the delta clean wing.

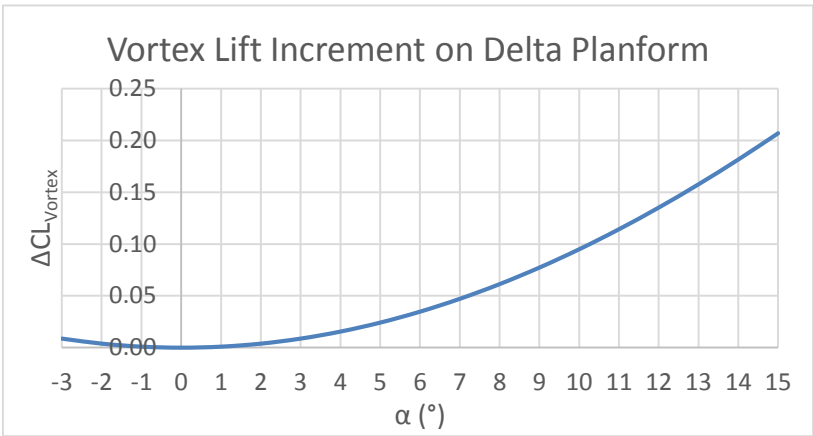

Figure 4.8 Polhamus Leading-Edge Suction Analogy Vortex Lift Increment for the Baseline Delta Planform (Polhamus, 1966, 1968, 1971).

Figure 4.9 illustrates the potential of vortex lift. This has been done without using nose flaps to increase the vortex strength. Figure 4.10 shows the percent difference between the vortex lift increment without leading edge devices and slats at δ_s = 25° on the final delta planform. From Figure 4.10, it can be seen that vortex lift does not have an improvement on C_L until after α = 8° with the largest increase in lift of 12% occurring at α = 14° resulting in a C_L of 1.39 versus 1.11 without the addition of vortex lift. The previous C_L at α = 15° without the vortex lift estimate is 1.2. That lift coefficient is achieved 2°earlier as shown in Figure 4.13 and is actually attainable with a flap deflection angle δ = 30°.

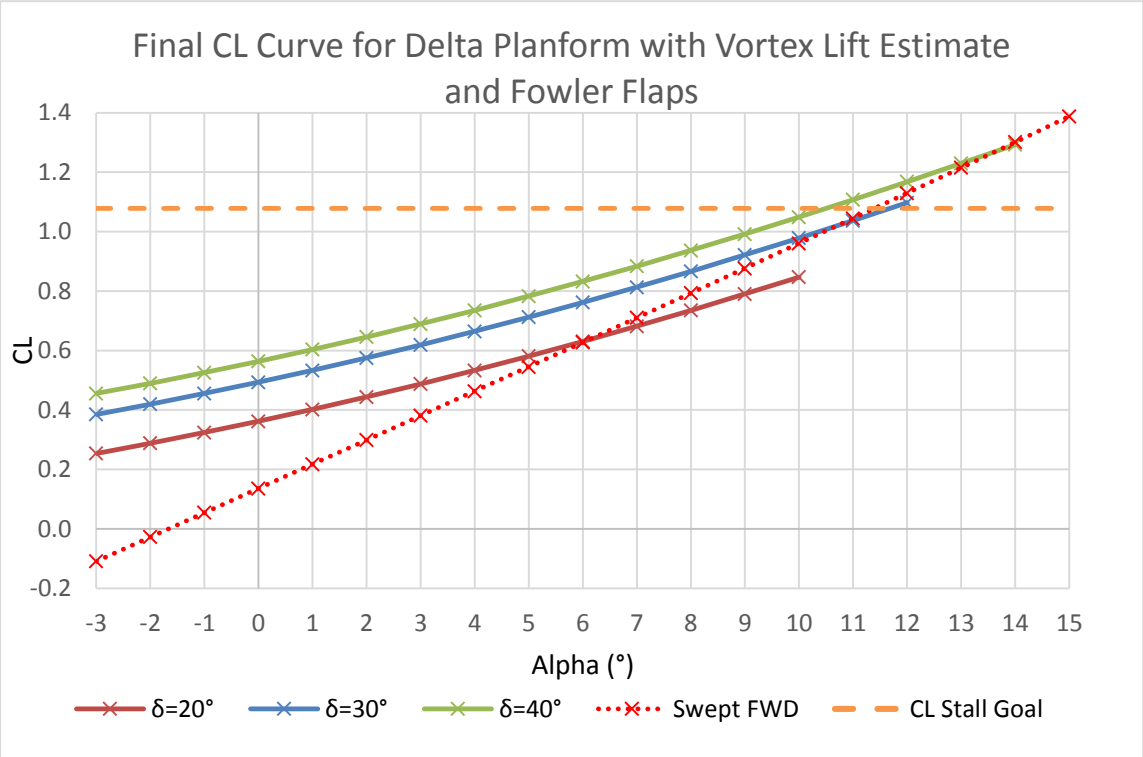

Figure 4.9 C_L Results for the Delta Planform with use of Polhamus Vortex Lift Increment and Fowler flaps.

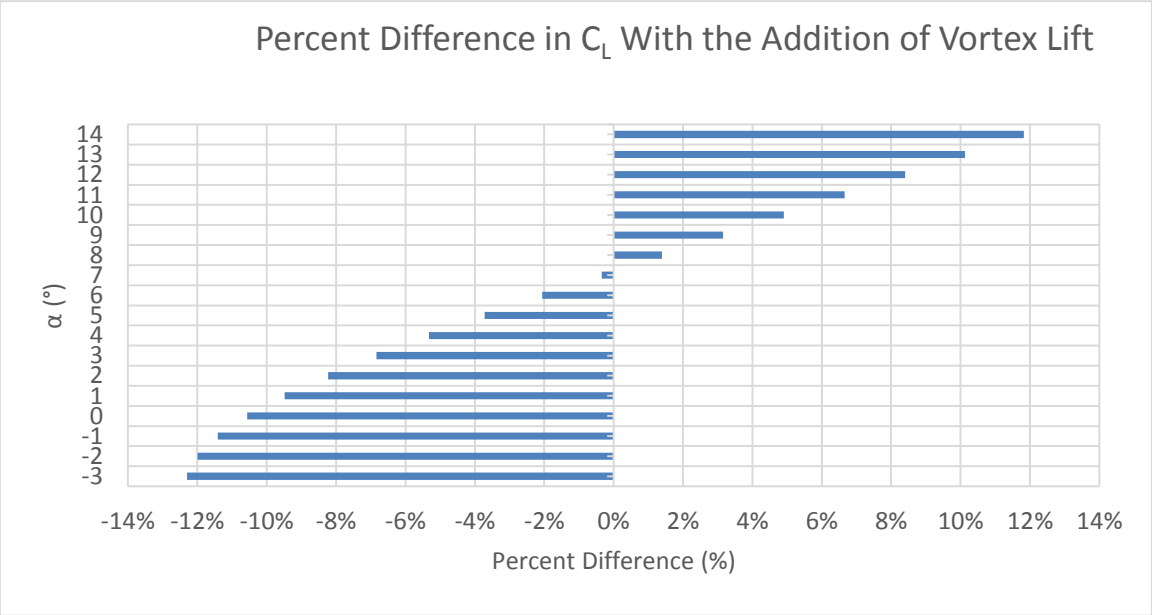

Figure 4.10 Potential Percent Difference With The Additon of Vortex Lift Without the use of a Leading Edge Device.

4.3 Final Fixed Swept and Delta Planform Geometries

The final results of the fixed swept planform geometry are shown in Table 4.1.

Table 4.1
Fixed Sweep Wing Dimensions

Fixed Sweep					
Root Chord (ft)	Taper Ratio	Half Span (ft)	Aspect Ratio	Total Span (ft)	Total Area (ft^2)
31.54	0.194	2.12	3.7	66.34	1,206

The final dimensions for the delta planform are listed below in Figure 4.11 with further dimensions in Table 4.2. The root chord did reach the maximum value of 50 ft resulting in a swept forward trailing edge angle of 7° as seen below.

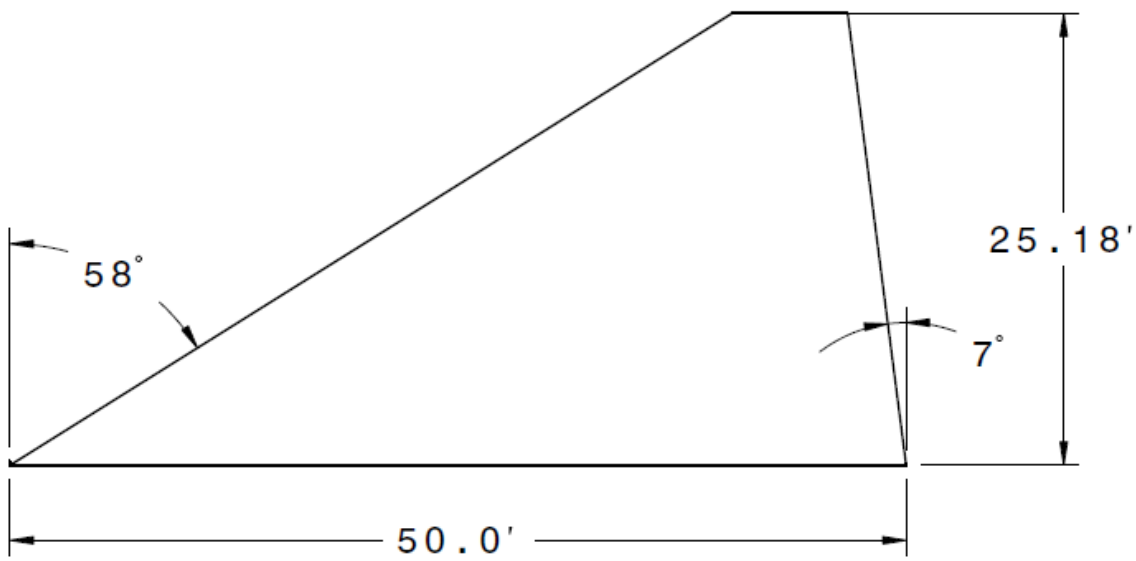

Figure 4.11 Final Delta Planform Dimensions.

Table 4.2
Delta Planform Final Dimensions.

Delta					
Outer					
Root Chord (ft)	Taper Ratio	Half Span (ft)	Aspect Ratio	Total Span (ft)	Total Area (ft^2)
50	0.15	25.18	1.75	50.4	1,448

Figure 4.12 shows an overlay over the 4 different planforms. Notice how the slight increase for the swept wing over the swept aft version of the variable sweep. The large increase in chord for the delta planform makes up for the lost area in span. The reason the swept aft and fixed sweep planforms do not start at (0, 0) is because of the way the variable geometry wing was created using the midchord as the pivot point. There would be wing

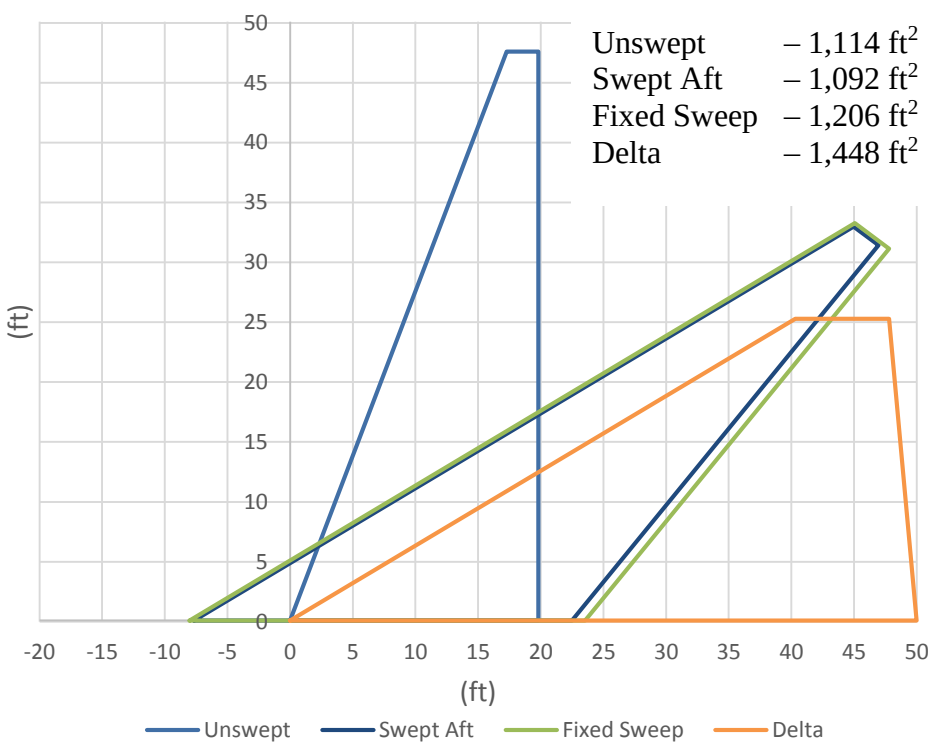

area that is hidden inside the wing fairing such that when the wing is swept aft, there is no gap in the leading edge. This method allowed the wing fairing to be easily defined for the variable geometry model seen below.

Typical values were found to obtain a range of expected results for different aspects of the model to ensure reasonable agreement with past studies or aircraft. Typical values were based on previous SSBJ designs in addition to other jets with similar MTOW. The complete set of values can be found in Appendix B under Typical Values. Table 4.3 summarizes the results in comparison to the VLM models. Most of the final VLM geometry agrees well with the typical findings with few outside the typical values such as wing span, for the variable geometry and the fixed sweep planform. Also the area of the delta planform was slightly larger than the typical values. In addition to the wing loading of the variable geometry and the delta planforms were on the lower end of the typical values. The wing span of the variable geometry planform was larger than the typical values because the limit span at Aspen was used. The swept wing span is only slightly larger than that of the study. The wing area of the delta planform is larger than expected most likely because of the subsonic leading edge restriction in place, in addition to the lack of vortex lift taken into account.

Table 4.3

Comparison Between Final VLM Model Geometry and Typical Values.

Dimension	VLM Models			Trade Study	
	Variable Geometry	Fixed Sweep	Delta	Fixed Wing	Variable Geometry
Wing Span (ft)	65.8 - 95	66.3	50.4	55 - 65	35 - 65
Wing Area (ft^2)	1,114	1,206	1,448	1,100 - 1,400	850 - 1100
Taper Ratio (λ)	0.14	0.19	0.15	0.1 - 0.3	0.1 - 0.3
Aspect Ratio (AR)	3.96 -8.1	3.7	1.75	1.5 - 3	1.5 - 3
LE Sweep ($\Lambda°$)	58-20	58	58	72 - 50	65 - 20
Dihedral ($\Gamma°$)	0	0	0	≈0	≈0
MTOW (lbs)	100,000	100,000	100,000	90,000 – 100,000	90,000 – 100,000
PAX	8 - 12	8 - 12	8 - 12	8 - 12	8 - 12
Vmax (KTS)	1.8	1.8.	1.8	M=1.7 - 1.9	M=1.7 - 1.9
Wing Loading at MTOW (lb/ft^2)	89.8	82.9	69.1	70 - 80	90 - 110

4.4 Clean Planforms

Below are the various results from the clean planforms with no high lift devices.

4.4.1 CL

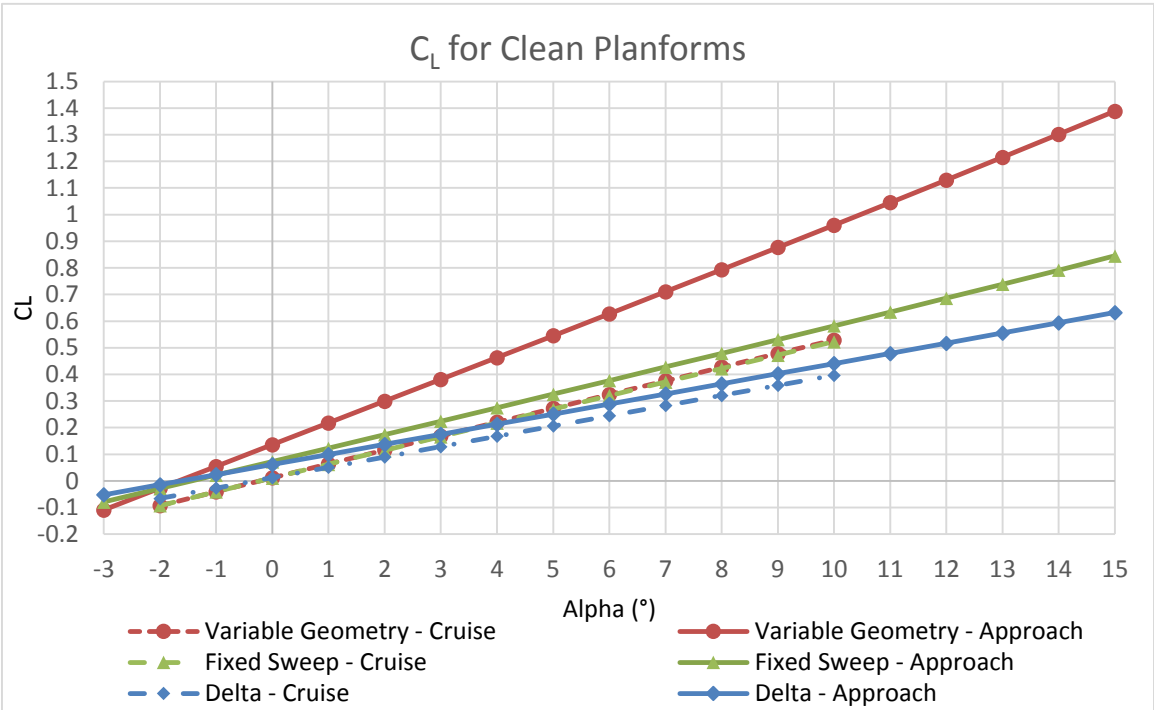

Figure 4.13 C_L for the Three Final Clean Planforms at Cruise and Approach Conditions

Figure 4.13 shows the C_{L_α} where, the curves from α = -3° to α = 15° were performed at approach conditions while the curves from α = -2° α = 10° were performed at the cruise conditions. The lift curve slope is noticeably steeper for the unswept variable geometry wing versus the reest of the planforms for a number of reasons. First, for the geometric variation is the decrease in wing sweep angle which increases the wing span effectively increasing the aspect ratio. This has a positive effect on the lift curve slope. Before the critical Mach number the lift curve slope increases and then decreases shortly after the critical Mach number is reached. In addition, the peak of the of the lift coefficient decreases

with increasing supersonic Mach numbers (Stevens, Lewis, 2003). In order to obtain the cruise L/D ratio, the drag needed to be calculated.

4.4.2 Drag

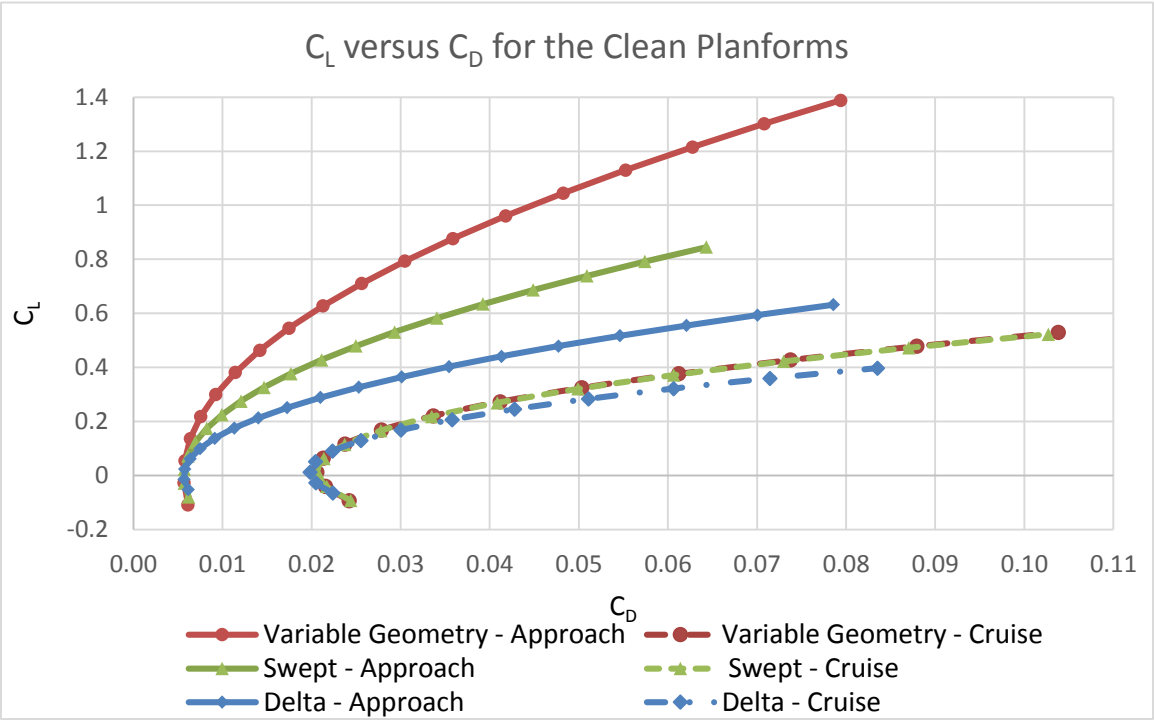

Figure 4.14 Drag Polar for the Three Final Base Planforms at Cruise and Approach Conditions.

Figure 4.14 shows the drag polar where the curves from α = -3° to α = 15° were performed at approach conditions while the curves from α = -2° α = 10° were performed at the cruise conditions. The large increase in drag between the approach and cruise condition is due to the effect of compressibility. Further, at higher lift coefficients, it can be seen that the increase in drag at cruise is significantly larger than that at approach. Again, this is due to the effect of wave drag created at cruise speeds.

4.4.3 L/D

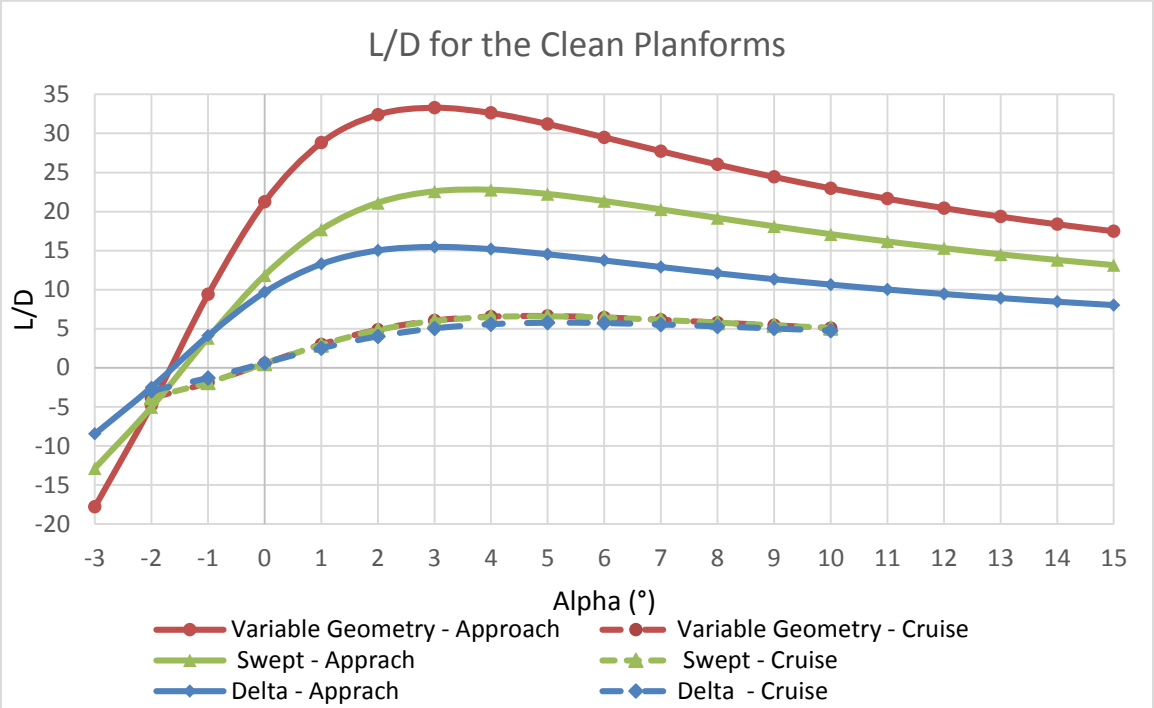

Figure 4.15 L/D for the Three Final Clean Planforms at Cruise and Approach Conditions.

Figure 4.15 shows the L/D where the curves from α = -3° to α = 15° shows performance at approach conditions while the curves from α = -2° α = 10° shows performance at cruise conditions. The effect of wave drag is evident in this figure as well. The addition of wave drag significantly scaled down the respective L/D curves of planforms. Notice the subtle variations in L/D for the planforms at cruise, where compressibility is the dominating factor. The differences in performance of the planforms are more apparent at the lower speeds.

4.5 Specific Air Range

Table 4.4
Comparison of Specific Range with Wing Weight and Flap Weight Estimates

Planform	Specific Air Range Ratio
$\frac{Variable\ Geometry}{\text{Variable Geometry}}$	1.000
$\frac{Fixed\ Sweep}{Variable\ Geometry}$	0.938
$\frac{Delta}{Variable\ Geometry}$	0.949
$\frac{Delta}{\text{Fixed Sweep}}$	1.011
	Wing Weight with Slats & Fowler Flaps (lb)
Variable Geometry	13,434
Fixed Sweep	12,696
Delta	5,448

Table 4.4 shows the final results of the SAR comparison with the variable geometry planform outperforming the fixed planforms by a small margin. The Delta planform was able to achieve the best results with 95% of the SAR when compared to the variable geometry planform. The fixed swept planform performed the poorest achieving 94% of the SAR of the variable geometry.

Chapter V

Discussion, Conclusion, and Recommendations

5.1 Discussion

The initial clean, fixed sweep and delta planforms could not produce the required lift which was clearly shown in Figure 4.1 and Figure 4.2. The clean planforms were well below the goal lift coefficients. This was caused by the high sweep angle and the thin wings required for supersonic flight. Without the addition of wing area or high lift devices, these planforms would not meet the required lift for approach conditions. Even after the addition of high lift devices, the initial planforms were not capable of producing the necessary lift. In order to make up the difference, the planforms would either need to fly at a much higher angle of attack or be increased in size. Since the increase in angle of attack was limited, an increase in wing area was required.

As shown in section 4.1.1 the resulting fixed swept planform required an increase in wing area of 8% with use of Fowler flaps and slats. Shown in section 4.1.2 the resulting delta planform required an increase in wing area of 26% with Fowler flaps and slats. The delta planform required a much larger increase in area because of its significantly lower lift curve slope. The much lower aspect ratio of the delta further penalized the lift curve slope.

5.1.1 Validation of Results

The lift curve slopes for the swept aft, fixed sweep and delta planforms were within 6% of those experimentally tested in USAF Datcom which were reproduced in Roskam's Aircraft Design (1990). In addition, all of the geometric values were within or very close

to the typical values, except for that of unswept span for the variable geometry wing. This is due to the constraint imposed on the unswept wing span which used the limit wing span at Aspen airport in Colorado, USA.

The ΔC_L trends from the various high lift devices in this study are similar to those found in the literature review, specifically those in Rudolph (1990). Similar to the findings in Rudolph (1990), the trailing edge devices outperformed the leading edge devices in $\Delta C_{L_{MAX}}$ and particularly at the higher deflection angles the Fowler flap outperformed the other devices. However, the specific ΔC_L found here from the more complex flap systems are not as large as found in Rudolph's study. One reason for this difference is due to the high sweep angles of the planforms. Although the planform properties are different, the trends are still identical to those found in Rudolph's (1990) study. The nonlinear dependence of ΔC_L on flap deflection angle was successfully captured.

The delta planform results were similar to those discussed in Corsiglia and Koenig (1966). Corsiglia and Koenig, studied the results of plain flaps and nose flaps on a delta wing of similar geometric properties. The aspect ratio of the delta wing was 1.3 with a leading edge sweep of 73°. This higher sweep angle would have increased vortex lift. The tests were done in a large-scale 40 x 80 foot wind tunnel. Compared to the delta planform results stated here, the clean delta model by Corsiglia and Koenig produced approximately 15% more lift at $\alpha = 15\ °$ (Corsiglia & Koenig, 1966). The difference in lift could be attributed to the wind tunnel model by Corsiglia and Koenig which made use of vortex lift. Vortex lift is not part of the empirical methods used here. However, the ΔC_L for the plain flap at $\delta_f = 20°$ on the study by Corsiglia and Koenig was approximately 0.24 which is 0.04

less than the results for the delta study here. This could be due to the over estimation of ΔC_L from the empirical calculations.

The following two studies examined a double slotted flap on low aspect ratio delta wings. Brown (1956) tested a 60° delta with an aspect ratio of 1.85 with a double slotted flap and Croom and Huffman (1956), tested a thin 60° delta wing with double slotted flaps. The main difference between the two studies was the size of the turning vane. Comparing the clean delta wing results obtained here and those tested by Croom and Huffman (1956) the results found here had a lift curve slope that was approximately 10% less than that found by Croom and Huffman (1956). The difference is most likely attributed to the work by Croom and Huffman (1956) being able to capture vortex lift. The two studies by Brown (1956) and Croom and Huffman (1956), resulted in similar C_L of 1.2 – 1.25 at α=15° depending on the turning vane size. The resulting C_L at α=15° are similar to the $C_{L_{MAX}}$ found here for the delta of 1.15 at α=15°. Compared to the results here of the lift curve slope for the delta planform with Fowler flaps deflected at δ = 40°, the lift curve slope of the delta planform in the study by Croom & Huffman (1956) had a 7% increase with a Fowler flap deflection of δ = 45°. This could be due to the slight increase in flap deflection angle in addition to the turning vane to help increase the flaps effectiveness. In order to obtain the $C_{L_{MAX}}$ of 1.5 found in the two studies by Brown (1956) and Croom and Huffman (1956), the angle of attack required was α = 24° with a flap deflection angle $\delta_f \approx 50°$. Overall the data from the delta planform with and without high lift devices matched consistently with previous analysis.

Unlike the highly swept delta wing, the fixed swept planform has not been the subject of studies with various mechanical high lift devices. However, since the results from the delta wing and clean swept wing match well with previous studies, it can be presumed that the results are fairly accurate for this study considering the assumptions and limitations.

5.1.1 Clean Planforms

The L/D curves of the variable geometry and the fixed swept planforms are similar. This is to be expected as the swept planform is essentially a slightly scaled version of the variable geometry planform. The aerodynamic difference between the planforms became evident at low speed, particularly with the L/D ratio. This is due to the inherent characteristics the planforms possess. While being relatively efficient at high speeds, the results show the fixed swept and delta planforms suffer significantly at low speeds.

The drag polars shown in Figure 4.14 show the large increase in drag due to the compressibility effects. That effect is evident by the roughly 0.013 or 130 drag counts increase between the respective planforms at approach and cruise conditions at α = 0. This translates to a 200% increase in drag at α = 0. In addition, the spread between the planforms is relatively small when comparing to the approach drag. This is mainly due to the similarities between the leading edge sweep angles and section airfoils. The slight decrease of cruise drag of the delta wing versus the variable geometry wing and fixed sweep wing is due to $C_{D_{LE}}$, which takes into account leading edge sweep, span, aspect ratio, and leading edge radius at the mean aerodynamic chord. The largest influence of $C_{D_{LE}}$ is the factor

aspect ratio divided by span, $\left(\frac{AR}{b}\right)$. Which, for the variable geometry is 1.5 times larger than the fixed sweep wing and 2.5 times larger than the delta wing. Besides sweeping the wing further aft, the only way to help decrease the drag is to use a sharp leading edge with a supersonic natural laminar airfoil. At higher lift coefficients, the fixed sweep and delta planforms were much further right on the drag curves compared to the variable geometry planform. This is the case because they require a larger angle of attack to achieve the same lift coefficients. Another reason why the high lift devices play such an important role in the low speed performance. These trends are even more apparent in the L/D curves.

While typical business jets may exhibit a subsonic cruise L/D approaching 19, supersonic transport designs exhibit ratios less than 10, which shows the large increase in drag in supersonic flight (Anderson, 2007). All of the L/D ratios were less than 10 at supersonic cruise. In addition, the L/D ratio for the swept and delta planform were under 19 for the approach phase for low angles of attack. The aerodynamic advantage of the unswept wing is very evident in the lift curve slope in addition to the L/D curve shown in Figure 4.15. The unswept variable geometry had an L/D_{max} ratio twice that of the delta wing and 150% that of the swept wing. This can be attributed to doubling the effective aspect ratio as the wing is unswept to $\Lambda = 20°$. During cruise, the decrease in L/D ratio for the delta shows a penalty for the large increase in area.

5.1.2 Augmented Planforms on Approach

From two-dimensional C_l to three-dimensional C_L the plain flaps lost on average 50% of their effectiveness. This figure is much worse for the slotted and Fowler flaps. The

slotted and Fowler flaps lost on average 80% of their effectiveness. The loss in effectiveness is primarily due to the high sweep angle and low aspect ratio.

One interesting note, due to the nature of the swept forward trailing edge on the delta planform, the hinge sweep line of the flaps was 18° which was significantly less than that of the fixed swept planform. The ΔC_L of the fixed swept planform is larger than that of the delta because the clean lift curve slope of the fixed swept planform is larger.

The true potential of leading edge devices is difficult to capture without use of a wind tunnel or CFD. Therefore, there exists uncertainty in the data obtained with the leading edge devices in this study. One of the main reasons for the use of slats is to mitigate flow separation at higher angles of attack. Without a wind tunnel or CFD, capturing this decrease in flow separation is difficult and use of empirical methods is unreliable. For this reason, the increase in stall angle of attack and increase in $C_{L_{MAX}}$ from the leading edge devices was not computed. Another concern with regards to the leading edge devices is the inability to properly capture the vortex lift. In particular, on the unswept and delta planforms. Whether or not this has a large impact on these planforms needs to be further investigated. With respect to the empirical calculations, the leading edge devices had larger uncertainty however, the error introduced by the leading edge empirical calculations would not have a profound impact on these results. This relatively small increase in lift from the leading edge devices is in agreement with a studies performed by Rinoie, Kwak, Miyata, and Noguchi, M. (2002), and Rinoie (2003), which studied leading vortex flaps on an SST configuration. As previously mentioned, the vortex flap is identical in shape and function to a nose flap, but used to increase vortex lift on highly swept wings. Though this study did

not deal with vortex lift, the ΔC_L results are similar to those found by Rinoie et al. (2002) and Rinoie (2003). A limited increase in C_L was observed, especially under α=10° on the sharp and rounded flap (Rinoie, 2003). The benefit of the vortex flap does not appear until the higher angles of attack where the vortex is fully formed and past the angle of attack regime that was studied here. Although the studies by Rinoie et al., (2002) and Rinoie (2003) showed little increase in lift, they showed a marked increase in L/D ratio in the lift coefficient region typically seen during landing and takeoff. This shows the effectiveness of the LEVF to create forward facing thrust vector on the forward angled flap surface decreasing overall drag of the planform.

In terms of estimated lift from leading edge devices, Torenbeek's Synthesis of Subsonic Aircraft Design (1982) states "Reliable generalized methods for predicting the effects of leading-edge devices are not known to the author…" There are not many reliable methods to predict the lift increment for leading edge flaps as there is for trailing edge flaps. For example, the $\Delta C_{L_{MAX_{wing}}}$ stated in Roskam's Aircraft Design (1990) is in Eq. 23

$$\Delta C_{L_{MAX_{wing}}} = 7.11\left(\frac{c_f}{c}\right)\left(\frac{b_{lef}}{b_e}\right)cos^2\Delta_{\frac{c}{4}} \tag{23}$$

Where:

$\frac{c_f}{c}$ = Leading edge flap chord ratio

$\frac{b_{lef}}{b_e}$ = Leading edge flap span ratio

Eq. 23 gives a fixed value for the leading edge device independent of the deflection angle and type of device. This equation was not used in this study because it did not appear to be

produce reliable results which were dependent on the type of flap used and deflection angle. The ΔC_L of a trailing edge device is far greater than that of a leading edge device. It is known that the addition of a leading edge device does not substantially increase the ΔC_L but aids primarily in flow separation at higher angles of attack with slats. For that reason the estimations of the leading edge devices have a larger chance to be more erroneous than that of the trailing edge devices.

Table 4.4 summarizes the results of the SAR calculation. Initially, it was thought that the delta wing was going to prove to be a poor aerodynamic choice, but upon estimating the SAR, it appears to be a comparable planform. The wing weight method appears to penalize higher aspect ratio wings. When compared with the delta planform, the aspect ratio of the swept wing is more than double. The delta planform therefore results in a specific range of 1% greater than the fixed swept planform but 5% less than the variable geometry planform. Even though the delta planform had an L/D_{max} almost 14% less than that of the variable geometry. The structural requirements for the higher aspect ratio and longer wings seem to mitigate the L/D advantage. With the Variable geometry wing resulting in only a 5% increase in specific air rage ratio, for a business jet that difference does not appear to be substantial. However, with the SSBJ at supersonic cruise the 5% margin would over time create a significant reduction in fuel consumption. Whether or not that difference is large enough to overcome the additional maintenance is yet to be seen. A detailed business case would need to be studied. A 5% difference for a commercial aircraft is a very large margin, especially when the aircraft would be flying multiple times a day for many years. This could be thought of as further range or to use less fuel for the same

mission which could result in tens of thousands of gallons of fuel saved per year, per aircraft flying. In terms of performance, the weight penalty for variable geometry is not as severe as initially perceived. Due to the large increase in area required by the delta planform with the addition of flaps and the decrease in L/D ratio, these penalties incurred by the delta planform outweigh that of the weight penalty of the variable geometry.

There may be a point where the flap complexity and weight is simply too great, or the flaps mechanisms cannot be completely hidden inside the wing. Therefore the addition of a Fowler flap may not be feasible with such a thin wing. The slotted flap is a very good alternative to the Fowler flap but still requires some relatively large linkages and mechanisms to operate. The plain flap while providing the lowest lift increment, is a very simple solution which is possibly one of the reasons the plain flap is found on many general aviation aircraft. The plain flap is relatively light, simply operated and inexpensive. While not providing a large increase in lift, it provides an adequate solution for those types of configurations.

Table 5.2 shows the results of the flap weight calculations. There was no method found to estimate the weight of a plain flap therefore an estimate of ⅔ of the weight of Fowler flaps was used. For reference, the slotted flap weight is close to ¾ of the weight of the Fowler flap. In the study by Rudolph (1996), it was mentioned that, plain flaps are planned for future SST configurations. With that being said, a conclusion was attempted to be drawn from a ratio of the maximum lift increment, $\Delta C_{L_{MAX}}$ to the weight of the high lift device called lift to flap weight ratio. The lighter plain flaps on fixed swept planform had a 4% decrease in lift to flap weight ratio compared to the Fowler flaps, while the slotted

flaps had only a 2% decrease. On the contrary, for the delta planform, the plain and slotted flaps had a 5% increase in lift to flap weight ratio. Overall, the range of the lift to flap ratios is rather small fluctuating by no more than ±5%. Comparing the geometry of the flaps on the delta planform with the swept planform, the delta planform flaps have a much lower "flap" aspect ratio comparing to the swept, with a shorter chord and longer flap span. This is not taken into account in the calculations. Whether or not the plain flap remains a candidate for the SST as stated by Rudolph (1996), is yet to be seen. What is clear is fitting the entirety of the high lift system inside the thin wing will be a challenge.

Table 5. 1
Comparison of Flap Data

Fixed Swept				
Trailing Edge Flap	$\Delta C_{L_{max}}$ At $\delta_{f_{max}}$	Weight of High Lift Device (lb)	$\frac{\Delta C_{L_{max}}}{W_{HLD}} * 1000$	% Difference
Plain	0.316	624	0.506	-3.9
Slotted	0.419	814	0.515	-2.3
Fowler	0.493	937	0.526	-
Delta				
Trailing Edge Flap	$\Delta C_{L_{max}}$ At $\delta_{f_{max}}$	Weight of Flap Device (lb)	$\frac{\Delta C_{L_{max}}}{W_{HLD}} * 1000$	% Difference
Plain	0.352	708	0.497	5.0
Slotted	0.459	923	0.497	5.0
Fowler	0.502	1062	0.53	-

5.2 Conclusion

The Tu-144 and the Concorde have shown that SST is possible but in order to create an economical option all of the parameters must be sufficiently satisfied. These include but are not limited to, high speed and low speed performance, mitigation of the sonic boom, environmental concerns, and lastly, the aircraft must be economically viable. Variable geometry wings are a technical engineering accomplishment that have provided an

advantageous aerodynamic solution but mechanically still face many challenges. There have been numerous research efforts with regards to variable geometry implementation to SSBJ. The delta wing is a better candidate than a simply fixed swept wing. Although the weight of the larger delta planform was significantly less than the variable geometry, the drag increase at cruise proved to be too significant to overcome the weight advantage. The weight penalty incurred by the variable geometry planform is not as detrimental as initially though when coupled with the superior cruise performance. The combinations of complexity, additional weight, and expensive operating costs have proven the downfalls in previous designs with many replacement models having fixed wings. Recent SSBJ conceptual designs tend to have fixed wings (e.g., Aerion, Spike Aerospace or Lockheed Martin's N+2). The designs appear to fall into two categories. The first having a supersonic laminar flow, low wing planform with a supersonic leading edge and the engines mounted on top of the fuselage near the empennage. The second is a highly swept delta or ogival high wing with underwing engines near the trailing edge and a third engine mounted on the fuselage.

When studying future planforms, not only are the aerodynamics important but also the mechanical and structural considerations. Though the aerodynamic solution of the variable geometry wing is promising, the results here show the SAR of the variable geometry wing to have benefit of 5% to 6% over the fixed wing counterparts. Taking into account the increase in maintenance, manufacturing and certification costs (among possibly others), the 5% margin at cruise may not be enough to overcome those additional costs. This leads to a very complicated business case. Without some suite of lift

augmentation devices a fixed wing alternative is not promising. Mechanical and augmented high lift devices have previously shown great success in commercial use, but application to a much thinner wing, like one that could be found on an SSBJ, would be difficult. Blown and or active flaps could be successful in augmenting lift, but their complex requirements and technical challenges may be too great to be feasible at this point. The most promising avenue appears to be with vortex lift and LEX as they exhibit good incremental lift in conjunction with trailing edge flaps on highly swept wings.

5.3 Recommendations and Future Research

The following are some suggested avenues for future work:

- Utilize CFD to conduct more detailed studies on the promising planforms between the natural laminar flow supersonic leading edge and the swept highly modified ogee delta.
- Modify this study to incorporate the variable geometry wing with simple high lift devices such as plain or slotted flaps with slats, similar to those found on the F-14 to test whether the possible wing area reduction would balance the high lift devices weight penalty.
- Perform a further detailed aerodynamic and structural study between the variable geometry and delta planform. Take into consideration some basic operational and maintenance costs for the two planforms to look at a possible business case study.
- Conduct further studies to validate the effectiveness trailing edge devices in conjunction with the use of leading edge vortices for a SSBJ planform.

References

Abbott, I. H., & Von Doenhoff, A. (1959). Chapter 8. *Theory of wing sections*. (2nd ed.). New York: Dover.

Anderson, J. D. (2007). Chapter 5. *Fundamentals of aerodynamics*. (4th ed.). New York: McGraw-Hill.

Analytical Methods, INC. (2007).VLAERO+©*User Manual*. (V2.2.5, pp. 7-12). Redmond, WA: Author.

Benson, L. R. (2013). *Quieting the boom: The shaped sonic boom demonstrator and the quest for quiet supersonic flight*. Washington, DC: National Aeronautics and Space Administration.

Bertin, J. J., & Cummings, R. M. (2014). *Aerodynamics for engineers*. (6th ed.). NJ: Pearson.

Brandon, J. M., Hallissy, J. B., Brown, P. W., & Lamar, J. E. (2001, May). *In-flight flow visualization results of the F-106B with a vortex flap*. Paper presented at the RTO AVT Symposium on "Advanced Flow Management: Part A – Vortex Flows and High Angle of Attack for Military Vehicles" held in Loen, Norway, 7-11 May 2001, and published in RTO-MP-069(I) Rto avt symposium.

Brown, E. A. (1956). Low-speed wind-tunnel results for a thin aspect-ratio-1.85 pointed-wing-fuselage model with double slotted flaps. *National Advisory Committee for Aeronautics Research Memorandum.*

Cessna Aircraft Company. (n.d.). *Citation X*. Retrieved from http://www.cessna.com/citation/citation-x

Chambers, J. R., (2005). *Innovation in flight*. (NASA SP-2005-4539). Retrieved from http://history.nasa. gov/monograph39/mon39_a.pdf

Clark, R. W., & Yeh, D. T. (2007, June). *Numerical study of vortex flows around a supersonic transport high-lift configuration with forebody control surfaces*. AIAA 2007-4448 25th AIAA Applied Aerodynamics Conference, Miami, FL

Corsiglia, V. R., & Koenig, D. G. (1966). Large-scale wind-tunnel tests of a low-aspect-ratio delta-winged model equipped with sharp-edged strakes. *NASA TN D-3621*

Croom, D. R., & Huffman, J. K. (1956). *Low-speed pressure-distribution investigation of a thin-delta-wing-fuselage model with double slotted flap, extended double slotted flap, and canard*. UNT Digital Library. http://digital.library.unt.edu/ark:/67531/metadc62986/.

Curry, M. (Photographer). (2003, April 10). F-18A 3-View Line Art. DFRC#:EG-0037-01 NASA Graphics Collection.

Delafosse, P. (Photographer). (2003). An air france concorde taking off [Print Photo]. Retrieved from http://arcus.centerblog.net/rub-avions--2.html).

Duchmann, A., Simon, B., Tropea, C., & Grundmann, S. (2014). Dielectric barrier discharge plasma actuators for in-flight transition delay. *AIAA Journal*, *52*, 358-367. doi: 10.2514/1.J052485

Goyer, R. (1997). Long live the jetstar. *Flying, 124(11), 36.* Retrieved from http://search.proquest.com.ezproxy.libproxy.db.erau.edu/docview/216144775?accountid=27203

Gudmundsson, S. (2014). *General aviation aircraft design: Applied methods and procedures*. (1st ed.). NY: Butterworth-Heinemann.

Gülçat, Ü. (2010). *Fundamentals of modern unsteady aerodynamics*. NY: Springer.

Evans, James R (Photographer) (2011). U.S. Navy 110606-N-DR144-314. [Print Photo]. Retrieved from http://www.navy.mil/view_image.asp?id=102135

Finck, R. D., & Hoak, D. E. (1975). Chapter 1, 2, 5, 6. *USAF stability and control datcom* (2 ed.). Irvine, CA: Global Engineering Documents.

De Saint Martin, P. (2008). HISAC - T - 6 - 26 - 1: Publishable activity report. St. Cloud, France: Dassault Aviation.. Retrieved from http://www.transport-research.info/ web /projects/project_details.cfm?id=10955

Hoerner, S. F., & Borst, H. V. (1992). *Fluid-dynamic lift*. (2nd ed.). Albuqurque, NM: Hoerner Fluid Dynamics.

Hoffler, K. D., Dhanvafa, M. R., & Frassinelli, M. C. (1986). Basic studies of delta wing flow modifications by means of apex fences. (*NASA Technical Document, 19860017727)*.

Huenecke, K. (1987). *Modern combat aircraft design*. (1st ed.). Annapolis, MD: Naval Institute Press.

Jones, M. Jr. (Photographer) 2010. C-17A externally blown Ffaps, forward view looking up and aft, left wing. Retrieved from Flickr Commons: http://www.flickr.com /photos/ 54573828 @N05/5300242640

Koklu, M. (2007). *Micro synthetic jets as effective actuator*. (Order No. 3268423, Old Dominion University). *ProQuest Dissertations and Theses*, , 276. Retrieved from http://search.proquest.com.ezproxy.libproxy.db.erau.edu/docview/304755885?accountid=27203. (304755885).

Kubota, H. (2008). Introduction: Supersonic airplane. *Journal of Aicraft*, *45*, 1473. doi: 10.2514/1.37180

European Commission. (2008). SADE: Smart high lift devices for next-generation wings. Research & Innovation: Transport. Retrieved from http://ec.europa.eu/research/transport/projects/items/sade_en.htm

Moskovitz, C. A., Vess, R. J., & Wahls, R. A. (1986). Experimental investigation of apex fence flaps on delta wings. *Journal of Aicraft*, *23*, 789-797. doi: 10.2514/3.45382

National Aeronautics and Space Administration. (Photographer). (1985). Retrieved from http://www.dfrc.nasa.gov/Gallery/Photo/FVF/index.html. [Print Photo].

Nicolai, L., & Carichner, G. (2010). *Fundamentals of aircraft and airship design*. (Vol. 1,). Reston, VA: American Institute of Aeronautics and Astronautics.

Padfield, R. R. (2008). Flying the new business class. *Barron's*, *88*(16), S9-S11. Retrieved from http://search.proquest.com.ezproxy.libproxy.db.erau.edu/docview/201058046?accountid=27203

Pappalardo, J. (2006, Sept). Swing wings. *Air & Space Magazine, Smithsonian*, Retrieved from http://www.airspacemag.com/flight-today/swing-wings-9189621/?all

Phan, L., Yamaoka, Y., & Mavris, D. (2003, Nov). *Implementation and benefits of variable geometry wings for a supersonic business jet*. AIAA's 3rd annual aviation technology, integration, and operations (ATIO) tech, Denver, Colorado.

Polhamus, E. C. (1966). A concept of the vortex lift of sharp-edged delta wings based on a leading-edge suction analogy. (*NASA Technical Note TN D-3767).*

Polhamus, E. C. (1968). Application of The Leading-Edge Suction Analogy of Vortex Lift to The Drag Due to Lift of Sharp-Edge Delta Wings. (*NASA Technical Note TN D-4739).*

Polhamus, E. C. (1971). Predictions of vortex-lift characteristics by a leading-edge suction analogy. *Journal of Aicraft*, *8*, 193-199. doi: 10.2514/3.44254

Revel, G. (2001). Giant Westland Flying Wing. *Model Airplane News, 129*, 162. Retrieved from http://search.proquest.com.ezproxy.libproxy.db.erau.edu/docview/20962 2436 ?accountid=27203

Rinoie, K. (2003). Benefit and performance of various vortex flap configurations. *Journal of Aircraft (AIAA), 40:* 1215-1218. doi: 10.2514/2.7215

Rinoie, K., Kwak, D. Y., Miyata, K., & Noguchi, M. (2002). Leading-edge vortex flaps for supersonic transport configuration Effects of flap configurations and rounded leading-edges. Tokyo, JAPAN:*ICAS 2002 Congress*, 73.1 - 73.12.

Roskam, D. J. (1990). *Airplane design*. (2nd ed., Vol. 6). KS: University of Kansas.

Rudolph, P. K. C. (1996). High-lift systems on commercial subsonic airliners. (*NASA Contractor Report , 4746)*

Sater, J. M., Crowe, C. R., Antcliff, R., & Das, A. (2000). Smart air and space structures. *Progress in astronautics and aeronautics: structures technology for future aerospace systems*, 269 - 349. doi: 10.2514/4.866593

Smart High Lift Devices for Next Generation Wings (SADE), (2012). *SADE news*. *4*. Retrieved from http://www.sade-project.eu/publications.html

Stevens, B. L., & Lewis, F. L. (2003). Modeling The Aircraft. *Aircraft control and simulation* (2nd ed.,). Hoboken, NJ: J. Wiley.

Stickley, R. (2006, Sep 22). Retiring the Tomcat. *Global News Transcripts*. Retrieved from http://search.proquest.com.ezproxy.libproxy.db.erau.edu/docview/ 190183871 ?accountid=27203

Surfaces. (2009). *Surfaces user manual*. Great OWL Publishing. Crownsville, MD

Torenbeek, E. (1982). *Synthesis of subsonic airplane design*. Hingham, MA: Delft University Press.

Warwick, G. (2012, Mar 29). Quiet, efficient supersonics within sight?. *Aviation Week*, Retrieved from http://www.aviationweek.com/Blogs.aspx?plckPostId=Blog: a68cb417-3364-4fbf-a9dd-4feda680ec9cPost:3437a2b1-f7c6-40fa-ac53-30ca71e4d263

Wickramasinghe. V, Chen, Y., Martinez, M., Wong, F., & Kernaghan, R. (2011). Design and verification of a smart wing for an extreme-agility micro-air-vehicle. *Smart Materials and Structures*, *20*, doi:10.1088/0964-1726/20/12/125007

Wilhelm, S. (2013, August 12). Latest in fuel efficiency: Split Scimitar winglet for 737s now in testing - Puget Sound Business Journal. *Widgets RSS*. Retrieved, from http://www.bizjournals.com/seattle/news/2013/08/12/split-scimitar-winglets-for-boeing.html?page=all

Yokozeki, T., & Sugiura, A. (2014). Development of variable camber morphing airfoil using corrugated structure. *Journal of Aircraft*, Manuscript in preparation. doi: 10.2514/1.C032573

APPENDIX A

Bibliography

THE ULTIMATE JET SET 10 business aircraft that changed the world. (2011, May). *Flight International, 179*, 8-I,II,III,IV,V,VI,VII,VIII. Retrieved from http://search.proquest.com.ezproxy.libproxy.db.erau.edu/docview/871910363?accountid=27203

Carlson, H. W., McElroy, M. O., Lessard, W. B., & McCullers, L. A. (1996). Improved method for prediction of attainable wing leading-edge thrust. *Nasa Technical Paper 3557*

Cook, A. M., & Jones, D. G. (1969). Large-scale wing-tunnel investigation to improve the low-speed longitudinal stability at high lift of a supersonic transport with variable-sweep wings. *NASA Technical Note TN D-5005*

Chudoba, B., Coleman, G., Huang, X., Huizenga, A., Czysz, P., & Butler, C. (2006, January). *A feasibility study of a supersonic business jet (ssbj) based on the Learjet airframe*. 44th AIAA aerospace sciences meeting and exhibit, Reno, Nevada. doi: 10.2514/6.2006-28

Daniel, L., & Traub, W. (2013). Effect of aspect ratio on gurney-flap performance. *Journal of Aircraft*, *50*(4), 1217-1225. doi: 10.2514/1.C032140

Hahne, D. E., & Glaab, L. J. (1999). Experimental and numerical optimization of a high-lift system to improve low-speed performance, stability, and control of an arrow-wing supersonic transport. *NASA Technical Paper/TP-1999-209539*

Quinto, P. F., & Paulson, Jr., J. W. (1983). Flap effectiveness on subsonic longitudinal aerodynamic characteristics of a modified arrow wing. *NASA Technical Memorandum 84582*

Wang, X. L., Wang, F. X., & Li, Y. L. (2011). Aerodynamic characteristics of high-lift devices with downward deflection of spoiler. *Journal of Aircraft*, *48*(2), 730-735. doi: 10.2514/1.C031301

APPENDIX B

B1 Typical Values

				90s	90s	1977	1977	
HISAC Low Noise Config	HISAC Long Range Config	HISAC Variable Geometry Config	HISAC Low Boom Config	Tu-444	S-21	NASA SSXJET I/II	NASA SSXJET III	**AVG**
60.70	78.74	50.5 - 67.6	62.66	53.08	65.40	42	45.5	59.04
1,615	1576.00	807	1,496	1,460		965	1,130	1,281
						0.08	0.08	
2.28	3.93	3.16 - 5.66	2.62	1.93		1.84	1.84	2.8
72.5 - 52	18.00	60 - 35	79 - 72.5 - 46		32 - 68	72 (LE)	72 (LE)	
0	1.50	0	18 - 0			0	0	
112,435	133,379	93,696	117,506	90,400	51,800	77,000	80,000	98,459
8	8	8	8	6-10	6 - 10	8	8	8
M=1.6	M=1.6	M=1.6	M=1.8	M=2				
LEX+Delta	Diamond							
69.6	84.6	116.1	78.5	61.9		79.8	70.8	79.5
1964	1967	1960	1972	1976	1975			1970
Dassault Mirage IV-A	GD F-111A	GB B-58	TU-22M	Concorde	TU-144	North American B-1B	North American XB-70A	Boeing SST
38.88	63 - 32	56.75	112.47 - 76.44	84	94.48		105.00	
840	530	1,481	1,585	3,856	4,715		6,297	9,000
0.11	0.33	0.00	0.28	0.12	0.13	0.32	0.02	0.21
1.80	7.5 - 1.93	2.20	8 - 3.69	1.70	1.90		1.80	3.40
60 (LE)	16 - 72	59 (LE)	20 - 65	Ogive	76/57		65.6 (LE)	30 -72
-1.5	0		0	0	8.3 (out)	0	-3	
73,800	100,000	176,890	273,000	412,000	455,950	477,000	542,000	675,000
				90 - 120				277
1,261	1,432	M=2+	1,446	1,259	1,350	M=2+	M=2+	1,565
36,000 ft			M=1.88	55,000 ft	50,000 ft			75,000 ft
87.9	188.7	119.4	172.2	106.8	96.7	#DIV/0!	86.1	75.0

B2 Typical Values Results

Preliminary Design Space		
	Fixed Wing	Variable Geo Wing
Wing Span (ft)	55 - 65	35 - 65
Wing Area (ft2)	1,100 - 1,400	850 - 1100
Taper Ratio (λ)	0.1 - 0.3	0.1 - 0.3
Aspect Ratio (AR)	1.5 - 3	1.5 - 3
Sweep (Λ°)	72 LE - 50	65 - 20
Dihedral (Γ°)	≈0	≈0
MTOW (lbs)	100000 - 90000	100000 - 90000
PAX	8 - 12	8 - 12
Vmax (KTS)	M=1.7 - 1.9	M=1.7 - 1.9
Wing Loading (lb/ft2)	70 - 80	90 - 110

APPENDIX C

C1 Statistical Values Used in W_x

Wing Weight Ratios	Stanford.edu http://adg.stanford.edu/aa241/structures/weightstatements.html					Roskam					
Category	Transport	Transport	Commercial	Commercial	Commercial	Jet Transport	Jet Transport	Jet Transport	Jet Transport	Supersonic Cruise	
	C-130A	C-130E	DC-9	737-200	727-100	Hawk-Siddeley 121-TC	FokkerF28-1000	BAC 1-11/300	Sud-Aero Spatiale Caravelle	Super - Cruiser	
MTOW	108,000	155,000	108000	104000	161100	115000	65000	87000	110230	47900	
W_{wing}	10,593	11,647	11391	11164	17682	12600	7330	9643	14735	3962	
W_{Empty}	60,499	68,687	44539	46288	67168	67500	31219	48722	65050	19620	
$W_{empty} - W_{wing}$	49,906	57,040	33,148	35,124	49,486	54,900	23,889	39,079	50,315	15,658	**AVG**
$(W_{empty} - W_{wing})/(W_{wing})$	0.462	0.368	0.307	0.338	0.307	0.477	0.368	0.449	0.456	0.327	**0.386**
$\mathbf{(W_{wing})/(W_{empty} - W_{wing})}$	2.16	2.72	3.26	2.96	3.26	2.09	2.72	2.23	2.19	3.06	**2.665**
	VG	Fixed Swept	Delta								
Wing weight	28,108	**12,696**	5,076			The wing planforms are most similar to the fixed sweep planform					
OEM Estimate	74,902	**33,831**	13,525								